Measurements of long-range azimuthal anisotropies and associated Fourier coefficients for pp collisions at $\sqrt{s} = 5.02$ and 13 TeV and $p + \mathrm{Pb}$ collisions at $\sqrt{s_{\mathrm{NN}}} = 5.02$ TeV with the ATLAS detector

M. Aaboud *et al.*[*]
(ATLAS Collaboration)

(Received 26 September 2016; revised manuscript received 13 June 2017; published 22 August 2017)

ATLAS measurements of two-particle correlations are presented for $\sqrt{s} = 5.02$ and 13 TeV pp collisions and for $\sqrt{s_{\mathrm{NN}}} = 5.02$ TeV $p + \mathrm{Pb}$ collisions at the LHC. The correlation functions are measured as a function of relative azimuthal angle $\Delta\phi$, and pseudorapidity separation $\Delta\eta$, using charged particles detected within the pseudorapidity interval $|\eta| < 2.5$. Azimuthal modulation in the long-range component of the correlation function, with $|\Delta\eta| > 2$, is studied using a template fitting procedure to remove a "back-to-back" contribution to the correlation function that primarily arises from hard-scattering processes. In addition to the elliptic, $\cos(2\Delta\phi)$, modulation observed in a previous measurement, the pp correlation functions exhibit significant $\cos(3\Delta\phi)$ and $\cos(4\Delta\phi)$ modulation. The Fourier coefficients $v_{n,n}$ associated with the $\cos(n\Delta\phi)$ modulation of the correlation functions for $n = 2$–4 are measured as a function of charged-particle multiplicity and charged-particle transverse momentum. The Fourier coefficients are observed to be compatible with $\cos(n\phi)$ modulation of per-event single-particle azimuthal angle distributions. The single-particle Fourier coefficients v_n are measured as a function of charged-particle multiplicity, and charged-particle transverse momentum for $n = 2$–4. The integrated luminosities used in this analysis are, 64 nb^{-1} for the $\sqrt{s} = 13$ TeV pp data, 170 nb^{-1} for the $\sqrt{s} = 5.02$ TeV pp data, and 28 nb^{-1} for the $\sqrt{s_{\mathrm{NN}}} = 5.02$ TeV $p + \mathrm{Pb}$ data.

DOI: 10.1103/PhysRevC.96.024908

I. INTRODUCTION

Observations of azimuthal anisotropies in the angular distributions of particles produced in proton-lead ($p + \mathrm{Pb}$) collisions at the LHC [1–5] and in deuteron-gold ($d + \mathrm{Au}$) [6–8] and $^3\mathrm{He} + \mathrm{Au}$ [9] collisions at RHIC have garnered much interest due to the remarkable similarities between the phenomena observed in those colliding systems and the effects of collective expansion seen in the $\mathrm{Pb} + \mathrm{Pb}$ and $\mathrm{Au} + \mathrm{Au}$ collisions [3,10–13].[1] The most intriguing feature of the azimuthal anisotropies is the "ridge": an enhancement in the production of particles with small azimuthal angle (ϕ) separation which extends over a large range of pseudorapidity (η) separation [1,2,14,15]. In $\mathrm{Pb} + \mathrm{Pb}$ [3,10–13] and $p + \mathrm{Pb}$ [1–3] collisions, the ridge is understood to result from sinusoidal modulation of the single-particle azimuthal angle distributions, and the characteristics of the modulation, for example the p_{T} dependence [16], are remarkably similar in the two systems [4].

While the modulation of the azimuthal angle distributions in $\mathrm{Pb} + \mathrm{Pb}$ collisions is understood to result from the geometry of the initial state and the imprinting of that geometry on the angular distributions of the particles by the collective expansion (see, e.g., [17–19] and references therein), there is, as yet, no consensus that the modulation observed in $p + \mathrm{Pb}$ collisions results from the same mechanism. Indeed, an alternative explanation for the modulation using perturbative QCD and assuming saturated parton distributions in the lead nucleus is capable of reproducing many features of the $p + \mathrm{Pb}$ data [20–29]. Nonetheless, because of the many similarities between the $p + \mathrm{Pb}$ and $\mathrm{Pb} + \mathrm{Pb}$ observations, extensive theoretical and experimental effort has been devoted to address the question of whether the strong-coupling physics understood to be responsible for the collective dynamics in $A + A$ collisions may persist in smaller systems [30–40].

A recent study by the ATLAS Collaboration of two-particle angular correlations in proton–proton (pp) collisions at center-of-mass energies of $\sqrt{s} = 13$ and 2.76 TeV obtained results that are consistent with the presence of an elliptic or $\cos(2\phi)$ modulation of the per-event single particle azimuthal angle distributions [41]. This result suggests that the ridge previously observed in $\sqrt{s} = 7$ TeV pp collisions [14] results from modulation of the single-particle azimuthal angle distributions similar to that seen in $\mathrm{Pb} + \mathrm{Pb}$ and $p + \mathrm{Pb}$ collisions. Indeed, the p_{T} dependence of the modulation was similar to that observed in the other systems. Unexpectedly, the amplitude of the modulation relative to the average differential particle yield $\langle dN/d\phi \rangle$, was observed to be constant, within uncertainties, as a function of the charged particle multiplicity of the pp events and to be consistent between the two energies, suggesting that the modulation is an intrinsic feature of high-energy pp collisions. These results provide further urgency to address the question of whether strong coupling and collective dynamics play a significant role in small systems, including the smallest systems accessible at collider energies—pp collisions. Since the elliptic modulation observed in the pp data is qualitatively

[*]Full author list given at the end of the article.

[1]However, Ref. [8] argues that the observed correlations may be due to poorly understood hard-scattering contributions.

similar to that seen in $p+\mathrm{Pb}$ collisions, a direct, quantitative comparison of pp and $p+\mathrm{Pb}$ measurements is necessary for evaluating whether the phenomena are related.

The modulation of the single-particle azimuthal angle distributions in $A+A$, $p/d+A$, and, most recently, pp collisions is usually characterized using a set of Fourier coefficients v_n, that describe the relative amplitudes of the sinusoidal components of the single-particle distributions. More explicitly, the azimuthal angle distributions of the particles are parameterized according to

$$\frac{dN}{d\phi} = \left\langle \frac{dN}{d\phi} \right\rangle \left(1 + \sum_n 2v_n \cos[n(\phi - \Psi_n)] \right), \tag{1}$$

where the average in the equation indicates an average over azimuthal angle. Here, Ψ_n represents one of the n angles at which the nth-order harmonic is maximum; it is frequently referred to as the event-plane angle for the nth harmonic. In $\mathrm{Pb}+\mathrm{Pb}$ collisions, $n=2$ modulation is understood to primarily result from an elliptic anisotropy of the initial state for collisions with nonzero impact parameter; that anisotropy is subsequently imprinted onto the angular distributions of the produced particles by the collective evolution of the medium, producing an elliptic modulation of the produced particle azimuthal angle distributions in each event [17,42,43]. The higher ($n>2$) harmonics are understood to result from position-dependent fluctuations in the initial-state energy density which produce higher-order spatial eccentricities that similarly get converted into sinusoidal modulation of the single-particle $dN/d\phi$ distribution by the collective dynamics [44–51]. Significant v_n values have been observed in $\mathrm{Pb}+\mathrm{Pb}$ ($p+\mathrm{Pb}$) collisions up to $n=6$ [13] ($n=5$ [4]). An important, outstanding question is whether $n>2$ modulation is present in pp collisions.

The $v_{n,n}$ coefficients can be measured using two-particle angular correlation functions, which, when evaluated as a function of $\Delta\phi \equiv \phi^a - \phi^b$, where a and b represent the two particles used to construct the correlation function, have an expansion similar to that in Eq. (1):

$$\frac{dN_{\mathrm{pair}}}{d\Delta\phi} = \left\langle \frac{dN_{\mathrm{pair}}}{d\Delta\phi} \right\rangle \left[1 + \sum_n 2v_{n,n} \cos(n\Delta\phi) \right]. \tag{2}$$

If the modulation of the two-particle correlation function arises solely from the modulation of the single-particle distributions, then $v_{n,n} = v_n^2$. Often, the two-particle correlations are measured using different transverse momentum (p_{T}) ranges for particles a and b. Since the modulation is observed to vary with p_{T}, then

$$v_{n,n}\left(p_{\mathrm{T}}^{\mathrm{a}}, p_{\mathrm{T}}^{\mathrm{b}}\right) = v_n\left(p_{\mathrm{T}}^{\mathrm{a}}\right) v_n\left(p_{\mathrm{T}}^{\mathrm{b}}\right) \tag{3}$$

if the modulation of the correlation function results solely from single-particle modulation.[2] This "factorization" hypothesis can be tested experimentally by measuring $v_{n,n}(p_{\mathrm{T}}^{\mathrm{a}}, p_{\mathrm{T}}^{\mathrm{b}})$ for different ranges of $p_{\mathrm{T}}^{\mathrm{b}}$ and estimating $v_n(p_{\mathrm{T}}^{\mathrm{a}})$ using

$$v_n\left(p_{\mathrm{T}}^{\mathrm{a}}\right) = v_{n,n}\left(p_{\mathrm{T}}^{\mathrm{a}}, p_{\mathrm{T}}^{\mathrm{b}}\right) \Big/ \sqrt{v_{n,n}\left(p_{\mathrm{T}}^{\mathrm{b}}, p_{\mathrm{T}}^{\mathrm{b}}\right)} \tag{4}$$

and evaluating whether $v_n(p_{\mathrm{T}}^{\mathrm{a}})$ depends on the choice of $p_{\mathrm{T}}^{\mathrm{b}}$.

In addition to the sinusoidal modulation, the two-particle correlation functions include contributions from hard-scattering processes that produce a jet peak centered at $\Delta\phi = \Delta\eta = 0$ and a dijet enhancement at $\Delta\phi = \pi$ that extends over a wide range of $\Delta\eta$. The jet peak can be avoided by studying the long-range part of the correlation function, which is typically chosen to be $|\Delta\eta| > 2$. Because the dijet contribution to the two-particle correlation function is not localized in $\Delta\eta$, that contribution has to be subtracted from the measured correlation function, typically using the correlation function measured in low-multiplicity ("peripheral") events. Different peripheral subtraction methods have been applied for the $p+\mathrm{Pb}$ measurements in the literature [2,4]; all of them relied on the "zero yield at minimum" (ZYAM) [2,4] hypothesis to subtract an assumed flat combinatoric component from the peripheral reference correlation function. These methods were found to be inadequate for pp collisions, where the amplitude of the dijet enhancement at $\Delta\phi = \pi$ is much larger than the (absolute) amplitude of the sinusoidal modulation. For the measurements in Ref. [41], a template fitting method, described below, was developed which is better suited for extracting a small sinusoidal modulation from the data. Application of the template fitting method to the pp data provided an excellent description of the measured correlation functions. It also indicated substantial bias resulting from the application of the ZYAM-subtraction procedure to the peripheral reference correlation function due to the nonzero $v_{2,2}$ in low-multiplicity events. As a result, the measurements presented in Ref. [41] were obtained without using ZYAM subtraction. However, the previously published $p+\mathrm{Pb}$ data [4] may be susceptible to an unknown bias due to the use of the ZYAM method. Thus, a reanalysis of the $p+\mathrm{Pb}$ data is both warranted and helpful in making comparisons between pp and $p+\mathrm{Pb}$ data.

To address the points raised above, this paper extends previous measurements of two-particle correlations in pp collisions at $\sqrt{s} = 13$ TeV using additional data acquired by ATLAS subsequent to the measurements in Ref. [41] and provides new measurements of such correlations in pp collisions at $\sqrt{s} = 5.02$ TeV. It also presents a reanalysis of two-particle correlations in 5.02 TeV $p+\mathrm{Pb}$ collisions and presents a direct comparison between the pp and $p+\mathrm{Pb}$ data at the same per-nucleon center-of-mass energy as well as a comparison between the pp data at the two energies. Two-particle Fourier coefficients $v_{n,n}$ are measured, where statistical precision allows, for $n=2$, 3, and 4 as a function of charged-particle multiplicity and transverse energy. Measurements are performed for different $p_{\mathrm{T}}^{\mathrm{a}}$ and $p_{\mathrm{T}}^{\mathrm{b}}$ intervals and the factorization of the resulting $v_{n,n}$ values is tested.

This paper is organized as follows. Section II gives a brief overview of the ATLAS detector subsystems and triggers used in this analysis. Section III describes the data sets and the offline selection criteria used to select events and reconstruct charged-particle tracks. The variables used to characterize the "event activity" of the pp and $p+\mathrm{Pb}$ collisions are also described. Section IV gives details of the two-particle correlation method. Section V describes the template fitting of the two-particle correlations, which was originally developed

[2] See Refs. [52,53] for analyses of the breakdown of factorization.

TABLE I. The list of L1 and $N_{\rm trk}^{\rm HLT}$ requirements for the pp and $p+$Pb HMT triggers used in this analysis. For the pp HMT triggers, the L1 requirement is on the $E_{\rm T}$ over the entire ATLAS calorimetry ($E_{\rm T}^{\rm L1}$) or hits in the MBTS. For the $p+$Pb HMT triggers, the L1 requirement is on the $E_{\rm T}$ restricted to the FCal ($E_{\rm T}^{\rm L1,FCal}$).

pp 13 TeV		pp 5.02 TeV		p+Pb	
L1	HLT	L1	HLT	L1	HLT
MBTS	$N_{\rm trk}^{\rm HLT} \geqslant 60$	$E_{\rm T}^{\rm L1} > 5$ GeV	$N_{\rm trk}^{\rm HLT} \geqslant 60$	$E_{\rm T}^{\rm L1,FCal} > 10$ GeV	$N_{\rm trk}^{\rm HLT} \geqslant 100$
$E_{\rm T}^{\rm L1} > 10$ GeV	$N_{\rm trk}^{\rm HLT} \geqslant 90$	$E_{\rm T}^{\rm L1} > 10$ GeV	$N_{\rm trk}^{\rm HLT} \geqslant 90$	$E_{\rm T}^{\rm L1,FCal} > 10$ GeV	$N_{\rm trk}^{\rm HLT} \geqslant 130$
		$E_{\rm T}^{\rm L1} > 20$ GeV	$N_{\rm trk}^{\rm HLT} \geqslant 90$	$E_{\rm T}^{\rm L1,FCal} > 50$ GeV	$N_{\rm trk}^{\rm HLT} \geqslant 150$
				$E_{\rm T}^{\rm L1,FCal} > 50$ GeV	$N_{\rm trk}^{\rm HLT} \geqslant 180$
				$E_{\rm T}^{\rm L1,FCal} > 65$ GeV	$N_{\rm trk}^{\rm HLT} \geqslant 200$
				$E_{\rm T}^{\rm L1,FCal} > 65$ GeV	$N_{\rm trk}^{\rm HLT} \geqslant 225$

in Ref. [41]. The template fits are used to extract the Fourier harmonics $v_{n,n}$ [Eq. (2)] of the long-range correlation, and the factorization of the $v_{n,n}$ into single-particle harmonics v_n [Eq. (3)] is studied. The stability of the $v_{n,n}$ as a function of the pseudorapidity separation between the charged-particle pairs is also checked. Section VI describes the systematic uncertainties associated with the measured $v_{n,n}$. Section VII presents the main results of the analysis, which are the $p_{\rm T}$ and event-activity dependence of the single-particle harmonics, v_n. Detailed comparisons of the v_n between the three data sets, 13 TeV pp, 5.02 TeV pp, and 5.02 TeV $p+$Pb, are also shown. Section VIII gives a summary of the main results and observations.

II. EXPERIMENT

A. ATLAS detector

The measurements presented in this paper were performed using the ATLAS [54] inner detector (ID), minimum-bias trigger scintillators (MBTS), calorimeter, zero-degree calorimeters (ZDC), and the trigger and data acquisition systems. The ID detects charged particles within the pseudorapidity range[3] $|\eta| < 2.5$ using a combination of silicon pixel detectors including the "insertable B-layer" (IBL) [55,56] that was installed between run 1 (2009–2013) and run 2, silicon microstrip detectors (SCTs), and a straw-tube transition radiation tracker (TRT), all immersed in a 2 T axial magnetic field [57]. The MBTS system detects charged particles over $2.07 < |\eta| < 3.86$ using two hodoscopes on each side of the detector, positioned at $z = \pm 3.6$ m. These hodoscopes were rebuilt between run 1 and run 2. The ATLAS calorimeter system consists of a liquid argon (LAr) electromagnetic (EM) calorimeter covering $|\eta| < 3.2$, a steel–scintillator sampling hadronic calorimeter covering $|\eta| < 1.7$, a LAr hadronic calorimeter covering $1.5 < |\eta| < 3.2$, and two LAr electromagnetic and hadronic forward calorimeters (FCal) covering $3.2 < |\eta| < 4.9$. The ZDCs, situated $\approx \pm 140$ m from the nominal IP, detect neutral particles, mostly neutrons and photons, with $|\eta| > 8.3$. The ZDCs use tungsten plates as absorbers, and quartz rods sandwiched between the tungsten plates as the active medium.

B. Trigger

The ATLAS trigger system [58] consists of a level-1 (L1) trigger implemented using a combination of dedicated electronics and programmable logic, and a software-based high-level trigger (HLT). Due to the large interaction rates, only a small fraction of minimum-bias events could be recorded for all three data sets. The configuration of the minimum-bias (MB) triggers varied between the different data sets. Minimum-bias $p+$Pb events were selected by requiring a hit in at least one MBTS counter on each side (MBTS_1_1) or a signal in the ZDC on the Pb-fragmentation side with the trigger threshold set just below the peak corresponding to a single neutron. In the 13 TeV pp data, MB events were selected by a L1 trigger that requires a signal in at least one MBTS counter (MBTS_1). In the 5.02 TeV pp data, MB events were selected using the logical OR of the MBTS_1, MBTS_1_1, and a third trigger that required at least one reconstructed track at the HLT. In order to increase the number of events having high charged-particle multiplicity, several high-multiplicity (HMT) triggers were implemented. These apply a L1 requirement on either the transverse energy ($E_{\rm T}$) in the calorimeters or on the number of hits in the MBTS, and an HLT requirement on the multiplicity of HLT-reconstructed charged-particle tracks. That multiplicity, $N_{\rm trk}^{\rm HLT}$, is evaluated for tracks having $p_{\rm T} > 0.4$ GeV that are associated with the reconstructed vertex with the highest multiplicity in the event. This last requirement suppresses the selection of events with multiple collisions (pileup), as long as the collision vertices are not so close as to be indistinguishable. The HMT trigger configurations used in this analysis are summarized in Table I.

III. DATA SETS

The $\sqrt{s} = 13$ and 5.02 TeV pp data were collected during run 2 of the LHC. The 13 TeV pp data were recorded over

[3] ATLAS uses a right-handed coordinate system with its origin at the nominal interaction point (IP) in the center of the detector and the z axis along the beam pipe. The x axis points from the IP to the center of the LHC ring, and the y axis points upward. Cylindrical coordinates (r,ϕ) are used in the transverse plane, ϕ being the azimuthal angle around the z axis. The pseudorapidity is defined in terms of the polar angle θ as $\eta = -\ln\tan(\theta/2)$.

two periods: a set of low-luminosity runs in June 2015 (used in Ref. [41]) for which the number of collisions per bunch crossing, μ, varied between 0.002 and 0.04, and a set of intermediate-luminosity runs in August 2015 where μ varied between 0.05 and 0.6. The 5.02 TeV pp data were recorded during November 2015 in a set of intermediate-luminosity runs with μ of $\sim$1.5. The $p+\mathrm{Pb}$ data were recorded in run 1 during $p+\mathrm{Pb}$ operation of the LHC in January 2013. During that period, the LHC was configured with a 4 TeV proton beam and a 1.57 TeV per-nucleon Pb beam that together produced collisions at $\sqrt{s_{\mathrm{NN}}} = 5.02$ TeV. The higher energy of the proton beam produces a net rapidity shift of the nucleon-nucleon center-of-mass frame by 0.47 units in the proton-going direction, relative to the ATLAS reference system. The $p+\mathrm{Pb}$ data were collected in two periods between which the directions of the proton and lead beams were reversed. The integrated luminosities for the three datasets are as follows: 75 nb^{-1} for the $\sqrt{s} = 13$ TeV pp data, 26 pb^{-1} for the $\sqrt{s} = 5.02$ TeV pp data, and 28 nb^{-1} for the $\sqrt{s_{\mathrm{NN}}} = 5.02$ TeV $p+\mathrm{Pb}$ data. However, due to the large interaction rates, the full luminosities could not be sampled by the various HMT triggers listed in Table I. In the $\sqrt{s} = 13$ TeV and $\sqrt{s} = 5.02$ TeV pp data, the luminosity sampled by the HMT trigger with the highest $E_{\mathrm{T}}^{\mathrm{L1}}$ and $N_{\mathrm{trk}}^{\mathrm{HLT}}$ thresholds were 64 nb^{-1} and 170 nb^{-1}, respectively. In the $\sqrt{s_{\mathrm{NN}}} = 5.02$ TeV $p+\mathrm{Pb}$ data, the $N_{\mathrm{trk}}^{\mathrm{HLT}} \geqslant 225$ trigger sampled the entire 28 nb^{-1} luminosity.

A. Event and track selection

In the offline analysis, additional requirements are imposed on the events selected by the MB and HMT triggers. The events are required to have a reconstructed vertex with the z position of the vertex restricted to ± 150 mm. In the $p+\mathrm{Pb}$ data, noncollision backgrounds are suppressed by requiring at least one hit in a MBTS counter on each side of the interaction point, and the time difference measured between the two sides of the MBTS to be less than 10 ns. In the 2013 $p+\mathrm{Pb}$ run, the luminosity conditions provided by the LHC resulted in an average probability of 3% for pileup events. The pileup events are suppressed by rejecting events containing more than one good reconstructed vertex. The remaining pileup events are further suppressed using the number of detected neutrons, N_n, measured in the ZDC on the Pb-fragmentation side. The distribution of N_n in events with pileup is broader than that for the events without pileup. Hence, rejecting events at the high tail end of the ZDC signal distribution further suppresses the pileup, while retaining more than 98% of the events without pileup. In the pp data, pileup is suppressed by only using tracks associated with the vertex having the largest $\sum p_{\mathrm{T}}^2$, where the sum is over all tracks associated with the vertex. Systematic uncertainties in the measured v_n associated with the residual pileup are estimated in Sec. VI.

In the $p+\mathrm{Pb}$ analysis, charged-particle tracks are reconstructed in the ID using an algorithm optimized for pp minimum-bias measurements [59]. The tracks are required to have $p_{\mathrm{T}} > 0.4$ GeV and $|\eta| < 2.5$, at least one pixel hit, with the additional requirement of a hit in the first pixel layer when one is expected,[4] and at least six SCT hits. In addition, the transverse (d_0) and longitudinal [$z_0 \sin(\theta)$] impact parameters of the track relative to the vertex are required to be less than 1.5 mm. They are also required to satisfy $|d_0|/\sigma_{d_0} < 3$ and $|z_0 \sin(\theta)|/\sigma_{z_0 \sin(\theta)} < 3$, where σ_{d_0} and $\sigma_{z_0 \sin(\theta)}$ are uncertainties in d_0 and $z_0 \sin(\theta)$, respectively.

In the pp analysis, charged-particle tracks and primary vertices are reconstructed in the ID using an algorithm similar to that used in run 1, but substantially modified to improve performance [60,61]. The reconstructed tracks are required to satisfy the following selection criteria: $p_{\mathrm{T}} > 0.4$ GeV and $|\eta| < 2.5$; at least one pixel hit, with the additional requirement of a hit in the IBL if one is expected (if a hit is not expected in the IBL, a hit in the next pixel layer is required if such a hit is expected); a minimum of six hits in the SCTs; $|d_0| < 1.5$ mm and $|z_0 \sin(\theta)| < 1.5$ mm.[5] Finally, in order to remove tracks with mismeasured p_{T} due to interactions with the material or other effects, the track-fit χ^2 probability is required to be larger than 0.01 for tracks having $p_{\mathrm{T}} > 10$ GeV.

The efficiencies $\epsilon(p_{\mathrm{T}}, \eta)$ of track reconstruction for the above track selection cuts are obtained using Monte Carlo (MC) generated events that are passed through a GEANT4 [62] simulation [63] of the ATLAS detector response and reconstructed using the algorithms applied to the data. For determining the $p+\mathrm{Pb}$ efficiencies, the events are generated with version 1.38b of the HIJING event generator [64] with a center-of-mass boost matching the beam conditions. For determining the pp efficiencies, nondiffractive 13 TeV pp events obtained from the PYTHIA8 [65] event generator (with the A2 set of tuned parameters [66] and the MSTW2008LO PDFs [67]) are used. Both the pp and $p+\mathrm{Pb}$ efficiencies increase by $\sim$3% from 0.4 to 0.6 GeV and vary only weakly with p_{T} for $p_{\mathrm{T}} > 0.6$ GeV. In the $p+\mathrm{Pb}$ case, the efficiency at $p_{\mathrm{T}} \sim 0.6$ GeV ranges from 81% at $\eta = 0$ to 73% at $|\eta| = 1.5$ and 65% at $|\eta| > 2.0$. The efficiency is also found to vary by less than 2% over the multiplicity range used in the analysis. In the pp case, the efficiency at $p_{\mathrm{T}} \sim 0.6$ GeV ranges from 87% at $\eta = 0$ to 76% at $|\eta| = 1.5$ and 69% for $|\eta| > 2.0$.

B. Event-activity classes

As in previous ATLAS analyses of long-range correlations in $p+\mathrm{Pb}$ [2,4] and pp [41] collisions, the event activity is quantified by $N_{\mathrm{ch}}^{\mathrm{rec}}$: the total number of reconstructed charged-particle tracks with $p_{\mathrm{T}} > 0.4$ GeV, passing the track selections discussed in Sec. III A. From the simulated events (Sec. III A), it is determined that the tracking efficiency reduces the measured $N_{\mathrm{ch}}^{\mathrm{rec}}$ relative to the event generator multiplicity for $p_{\mathrm{T}} > 0.4$ GeV primary charged particles[6] by

[4] A hit is expected if the extrapolated track crosses an active region of a pixel module that has not been disabled.

[5] In the pp analysis the transverse impact parameter d_0 is calculated with respect to the average beam position, and not with respect to the vertex.

[6] For the $p+\mathrm{Pb}$ simulation, the event generator multiplicity includes charged particles that originate directly from the collision or result from decays of particles with $c\tau < 10$ mm. The definition for

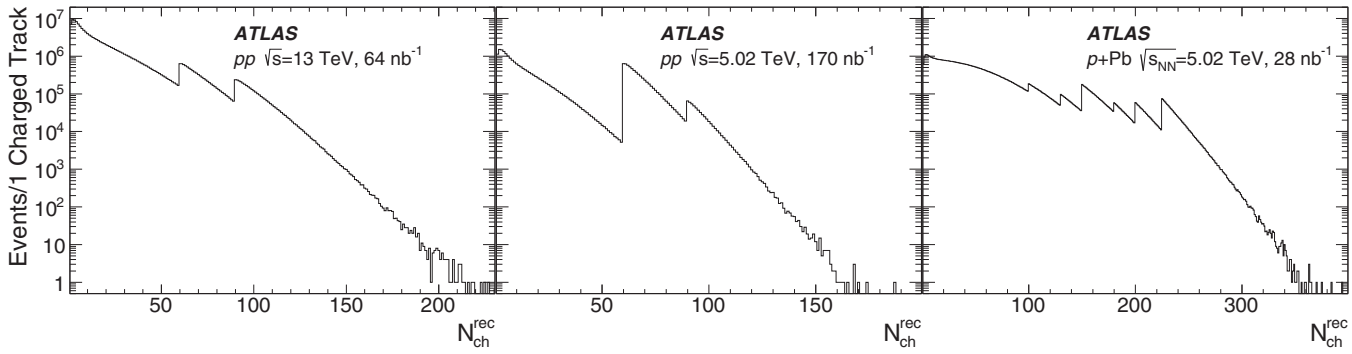

FIG. 1. Distributions of the multiplicity, $N_{\rm ch}^{\rm rec}$, of reconstructed charged particles having $p_{\rm T} > 0.4$ GeV in the 13 TeV pp (left), 5.02 TeV pp (middle), and 5.02 TeV $p+{\rm Pb}$ (right) data used in this analysis. The discontinuities in the distributions correspond to different high-multiplicity trigger thresholds.

approximately multiplicity-independent factors. The reduction factors and their uncertainties are 1.29 ± 0.05 and 1.18 ± 0.05 for the $p+{\rm Pb}$ and pp collisions, respectively.

For $p+{\rm Pb}$ collisions there is a direct correlation between $N_{\rm ch}^{\rm rec}$ and the number of participating nucleons in the Pb nucleus: events with larger $N_{\rm ch}^{\rm rec}$ values have, on average, a larger number of participating nucleons in the Pb nucleus and a smaller impact parameter. In this case, the concept of centrality used in $A+A$ collisions is applicable, and in this paper the terms "central" and "peripheral" are used to refer to events with large and small values of $N_{\rm ch}^{\rm rec}$, respectively. For pp collisions there may not be a correlation between $N_{\rm ch}^{\rm rec}$ and impact parameter. However, for convenience, the pp events with large and small $N_{\rm ch}^{\rm rec}$ are also termed as "central" and "peripheral", respectively.

Figure 1 shows the $N_{\rm ch}^{\rm rec}$ distributions for the three data sets used in this paper. The discontinuities in the distributions result from the different HMT triggers, for which an offline requirement of $N_{\rm ch}^{\rm rec} > N_{\rm trk}^{\rm HLT}$ is applied. This requirement ensures that the HMT triggered events are used only where the HLT trigger is almost fully efficient.

The pp event activity can also be quantified using the total transverse energy deposited in the FCal ($E_{\rm T}^{\rm FCal}$). This quantity has been used to determine the centrality in all ATLAS heavy-ion analyses. Using the $E_{\rm T}^{\rm FCal}$ to characterize the event activity has the advantage that independent sets of particles are used to determine the event activity and to measure the long-range correlations. Similarly in the $p+{\rm Pb}$ case, the event activity can be characterized by the sum of transverse energy measured on the Pb-fragmentation side of the FCal ($E_{\rm T}^{\rm FCal,Pb}$) [2,4]. Results presented in this paper use both $N_{\rm ch}^{\rm rec}$ and the $E_{\rm T}^{\rm FCal}$ (or $E_{\rm T}^{\rm FCal,Pb}$) to quantify the event activity.

IV. TWO-PARTICLE CORRELATION ANALYSIS

The study of two-particle correlations in this paper follows previous ATLAS measurements in Pb + Pb [13,69,70], $p+$ Pb [2,4], and pp [41] collisions. For a given event class, the two-particle correlations are measured as a function of the relative azimuthal angle $\Delta\phi \equiv \phi^a - \phi^b$ and pseudorapidity $\Delta\eta \equiv \eta^a - \eta^b$ separation. The labels a and b denote the two particles in the pair, which may be selected from different $p_{\rm T}$ intervals. The particles a and b are conventionally referred to as the "trigger" and "associated" particles, respectively. The correlation function is defined as

$$C(\Delta\eta, \Delta\phi) = \frac{S(\Delta\eta, \Delta\phi)}{B(\Delta\eta, \Delta\phi)}, \tag{5}$$

where S and B represent pair distributions constructed from the same event and from "mixed events" [71], respectively. The same-event distribution S is constructed using all particle pairs that can be formed in each event from tracks that have passed the selections described in Sec. III A. The S distribution contains both the physical correlations between particle pairs and correlations arising from detector acceptance effects. The mixed-event distribution $B(\Delta\eta, \Delta\phi)$ is similarly constructed by choosing the two particles in the pair from different events. The B distribution does not contain physical correlations, but has detector acceptance effects similar to those in S. In taking the ratio, S/B in Eq. (5), the detector acceptance effects largely cancel, and the resulting $C(\Delta\eta, \Delta\phi)$ contains physical correlations only. The pair of events used in the mixing are required to have similar $N_{\rm ch}^{\rm rec}$ ($|\Delta N_{\rm ch}^{\rm rec}| < 10$) and similar $z_{\rm vtx}$ ($|\Delta z_{\rm vtx}| < 10$ mm), so that acceptance effects in $S(\Delta\eta, \Delta\phi)$ are properly reflected in, and compensated by, corresponding variations in $B(\Delta\eta, \Delta\phi)$. To correct $S(\Delta\eta, \Delta\phi)$ and $B(\Delta\eta, \Delta\phi)$ for the individual ϕ-averaged inefficiencies of particles a and b, the pairs are weighted by the inverse product of their tracking efficiencies $1/(\epsilon_a \epsilon_b)$. Statistical uncertainties are calculated for $C(\Delta\eta, \Delta\phi)$ using standard error-propagation procedures assuming no correlation between S and B, and with the statistical variance of S and B in each $\Delta\eta$ and $\Delta\phi$ bin taken to be $\sum 1/(\epsilon_a \epsilon_b)^2$ where the sum runs over all of the pairs included in the bin. Typically, the two-particle correlations are used only to study the shape of the correlations in $\Delta\phi$, and are conveniently normalized. In this paper, the normalization of $C(\Delta\eta, \Delta\phi)$ is chosen such that the $\Delta\phi$-averaged value of $C(\Delta\eta, \Delta\phi)$ is unity for $|\Delta\eta| > 2$.

Examples of correlation functions are shown in Fig. 2 for $0.5 < p_{\rm T}^{\rm a,b} < 5$ GeV and for two different $N_{\rm ch}^{\rm rec}$ ranges for each

primary charged particles is somewhat tighter in the pp simulation [68].

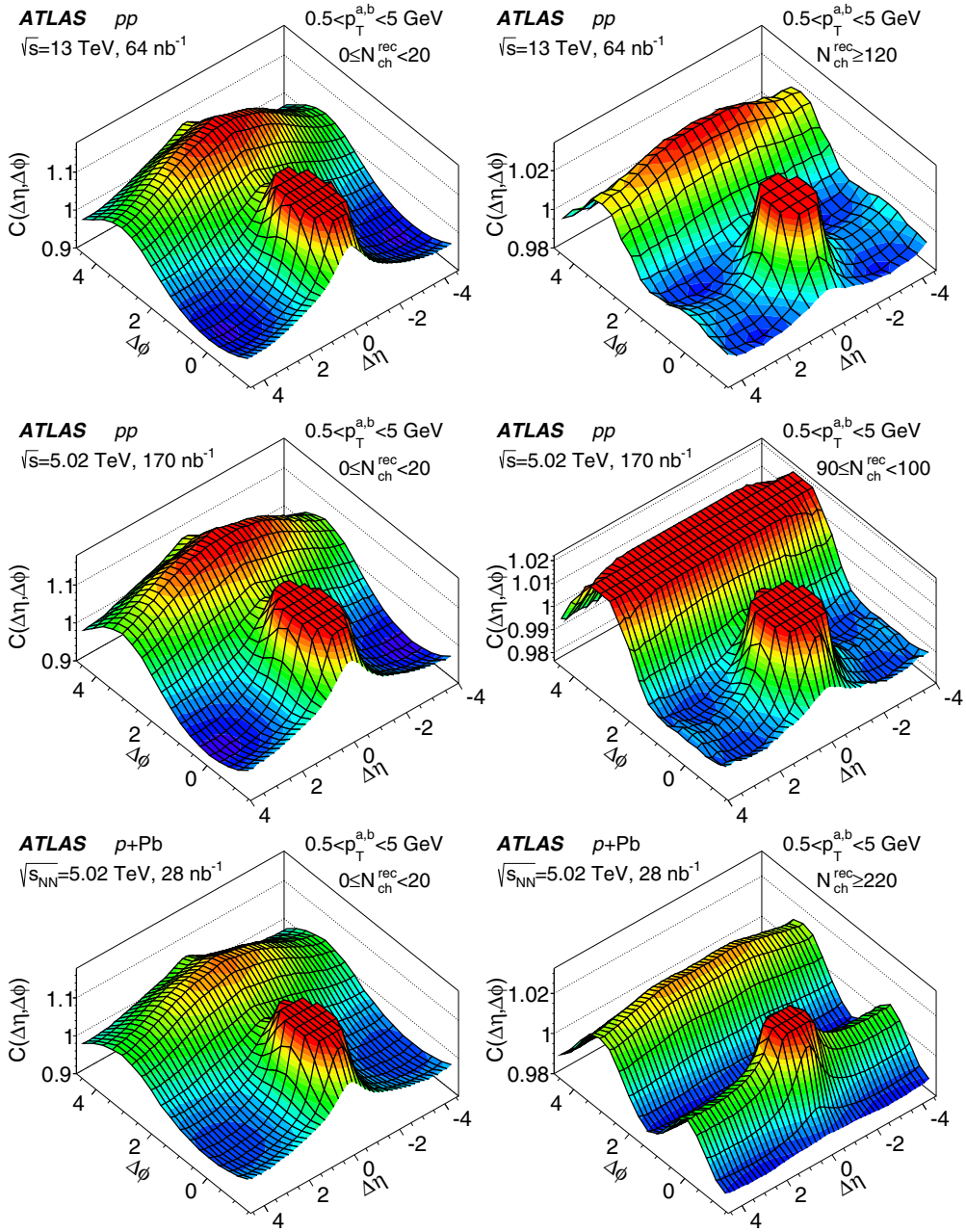

FIG. 2. Two-particle correlation functions $C(\Delta\eta,\Delta\phi)$ in 13 TeV pp collisions (top panels), 5.02 TeV pp collisions (middle panels), and in 5.02 TeV $p+\mathrm{Pb}$ collisions (bottom panels). The left panels correspond to a lower-multiplicity range of $0 \leqslant N_{\mathrm{ch}}^{\mathrm{rec}} < 20$. The right panels correspond to higher multiplicity ranges of $N_{\mathrm{ch}}^{\mathrm{rec}} \geqslant 120$ for 13 TeV pp, $90 \leqslant N_{\mathrm{ch}}^{\mathrm{rec}} < 100$ for the 5.02 TeV pp, and $N_{\mathrm{ch}}^{\mathrm{rec}} \geqslant 220$ for the 5.02 TeV $p+\mathrm{Pb}$. The plots are for charged particles having $0.5 < p_{\mathrm{T}}^{\mathrm{a,b}} < 5$ GeV. The distributions have been truncated to suppress the peak at $\Delta\eta = \Delta\phi = 0$ and are plotted over $|\Delta\eta| < 4.6$ ($|\Delta\eta| < 4.0$ for middle row) to avoid statistical fluctuations at larger $|\Delta\eta|$. For the middle-right panel, the peak at $\Delta\phi = \pi$ has also been truncated.

of the three data sets: 13 TeV pp (top), 5.02 TeV pp (middle), and 5.02 TeV $p+\mathrm{Pb}$ (bottom). The left panels show results for $0 \leqslant N_{\mathrm{ch}}^{\mathrm{rec}} < 20$ while the right panels show representative high-multiplicity ranges of $N_{\mathrm{ch}}^{\mathrm{rec}} \geqslant 120$ for the 13 TeV pp data, $90 \leqslant N_{\mathrm{ch}}^{\mathrm{rec}} < 100$ for the 5.02 TeV pp data, and $N_{\mathrm{ch}}^{\mathrm{rec}} \geqslant 220$ for the 5.02 TeV $p+\mathrm{Pb}$ data. The correlation functions are plotted over the range $-\pi/2 < \Delta\phi < 3\pi/2$; the periodicity of the measurement requires that $C(\Delta\eta,3\pi/2) = C(\Delta\eta,-\pi/2)$. The low-multiplicity correlation functions exhibit features that are understood to result primarily from hard-scattering processes: a peak centered at $\Delta\eta = \Delta\phi = 0$ that arises primarily from jets and an enhancement centered at $\Delta\phi = \pi$ and extending over the full $\Delta\eta$ range which results from dijets. These features also dominate the high-multiplicity correlation functions.

Additionally, in the high-multiplicity correlation functions, each of the three systems exhibit a ridge—an enhancement centered at $\Delta\phi = 0$ that extends over the entire measured $\Delta\eta$ range.

One-dimensional correlation functions $C(\Delta\phi)$ are obtained by integrating the numerator and denominator of Eq. (5) over $2 < |\Delta\eta| < 5$ prior to taking the ratio

$$C(\Delta\phi) = \frac{\int_2^5 d|\Delta\eta|\ S(|\Delta\eta|,\Delta\phi)}{\int_2^5 d|\Delta\eta|\ B(|\Delta\eta|,\Delta\phi)} \equiv \frac{S(\Delta\phi)}{B(\Delta\phi)}. \quad (6)$$

This $|\Delta\eta|$ range is chosen to focus on the long-range features of the correlation functions. From the one-dimensional correlation functions, "per-trigger-particle yields," $Y(\Delta\phi)$ are calculated [2,4,71]:

$$Y(\Delta\phi) = \left(\frac{\int_{-\pi/2}^{3\pi/2} B(\Delta\phi)d\Delta\phi}{N^a \int_{-\pi/2}^{3\pi/2} d\Delta\phi}\right) C(\Delta\phi), \quad (7)$$

where N^a denotes the total number of trigger particles, corrected to account for the tracking efficiency. The $Y(\Delta\phi)$ distribution is identical in shape to $C(\Delta\phi)$, but has a physically relevant normalization: it represents the average number of associated particles per trigger particle in a given $\Delta\phi$ interval. This allows operations, such as subtraction of the $Y(\Delta\phi)$ distribution in one event-activity class from the $Y(\Delta\phi)$ distribution in another, which have been used in studying the $p+$Pb ridge [2,4].

V. TEMPLATE FITTING

In order to separate the ridge from other sources of angular correlation, such as dijets, the ATLAS Collaboration developed a template fitting procedure described in Ref. [41]. In this procedure, the measured $Y(\Delta\phi)$ distributions are assumed to result from a superposition of a "peripheral" $Y(\Delta\phi)$ distribution, $Y^{\rm periph}(\Delta\phi)$, scaled up by a multiplicative factor and a constant modulated by $\cos(n\Delta\phi)$ for $n \geqslant 2$. The resulting template fit function,

$$Y^{\rm templ}(\Delta\phi) = Y^{\rm ridge}(\Delta\phi) + F\,Y^{\rm periph}(\Delta\phi)\,, \quad (8)$$

where

$$Y^{\rm ridge}(\Delta\phi) = G\left(1 + \sum_{n=2}^{\infty} 2v_{n,n}\cos(n\Delta\phi)\right), \quad (9)$$

has free parameters F and $v_{n,n}$. A $v_{1,1}$ term is not included in $Y^{\rm ridge}(\Delta\phi)$ [Eq. (9)] as the presence of a $v_{1,1}$ component in the measured $Y(\Delta\phi)$ is accounted for by the $FY^{\rm periph}(\Delta\phi)$ term. The parameter F is the multiplicative factor by which the $Y^{\rm periph}(\Delta\phi)$ is scaled. The coefficient G, which represents the magnitude of the combinatoric component of $Y^{\rm ridge}(\Delta\phi)$, is fixed by requiring that the integral of $Y^{\rm templ}(\Delta\phi)$ be equal to the integral of the measured $Y(\Delta\phi)$: $\int_0^\pi d\Delta\phi\ Y^{\rm templ}(\Delta\phi) = \int_0^\pi d\Delta\phi\ Y(\Delta\phi)$. In this paper, when studying the $N_{\rm ch}^{\rm rec}$ dependence of the long-range correlation, the $0 \leqslant N_{\rm ch}^{\rm rec} < 20$ multiplicity interval is used to produce $Y^{\rm periph}(\Delta\phi)$. When studying the $E_{\rm T}^{\rm FCal}$ ($E_{\rm T}^{\rm FCal,Pb}$) dependence, the $E_{\rm T}^{\rm FCal} < 10$ GeV ($E_{\rm T}^{\rm FCal,Pb} < 10$ GeV) interval is used to produce $Y^{\rm periph}(\Delta\phi)$.

The template fitting procedure is similar to the peripheral subtraction procedure used in previous ATLAS $p+$Pb ridge analyses [4]. In those analyses, the scale factor for the peripheral reference, analogous to F in Eq. (8), was determined by matching the near-side jet peaks between the peripheral and central samples. A more important difference, however, lies in the treatment of the peripheral bin. In the earlier analyses, a ZYAM procedure was performed on the peripheral reference, and only the modulated part of $Y^{\rm periph}(\Delta\phi)$, $Y^{\rm periph}(\Delta\phi) - Y^{\rm periph}(0)$, was used in the peripheral subtraction.[7] The ZYAM procedure makes several assumptions, the most relevant of which for the present analysis is that there is no long-range correlation in the peripheral bin. As pointed out in Ref. [41], neglecting the nonzero modulation present in $Y^{\rm periph}(\Delta\phi)$ significantly biases the measured $v_{n,n}$ values. Results from an alternative version of the template fitting, where a ZYAM procedure is performed on the peripheral reference, by using $Y^{\rm periph}(\Delta\phi) - Y^{\rm periph}(0)$ in place of $Y^{\rm periph}(\Delta\phi)$ in Eq. (8), are also presented in this paper. This ZYAM-based template fit is similar to the $p+$Pb peripheral subtraction procedure. These results are included mainly to compare with previous measurements and to demonstrate the improvements obtained using the present method.

In Ref. [41] the template fitting procedure only included the second-order harmonic $v_{2,2}$, but was able to reproduce the $N_{\rm ch}^{\rm rec}$-dependent evolution of $Y(\Delta\phi)$ on both the near and away sides. The left panel of Fig. 3 shows such a template fit, in the 13 TeV pp data, that only includes $v_{2,2}$. The right panel shows the difference between the $Y(\Delta\phi)$ and the $Y^{\rm templ}(\Delta\phi)$ distributions demonstrating the presence of small (compared to $v_{2,2}$), but significant residual $v_{3,3}$ and $v_{4,4}$ components. While it is possible that $\cos3\Delta\phi$ and $\cos4\Delta\phi$ contributions could arise in the template fitting method due to small multiplicity-dependent changes in the shape of the dijet component of the correlation function, such effects would not produce the excess at $\Delta\phi \sim 0$ observed in the right-hand panel in Fig. 3. That excess and the fact that its magnitude is compatible with the remainder of the distribution indicates that there is real $\cos3\Delta\phi$ and $\cos4\Delta\phi$ modulation in the two-particle correlation functions. Thus this paper extends the $v_{2,2}$ results in Ref. [41] by including $v_{3,3}$ and $v_{4,4}$ as well. A study of these higher-order harmonics, including their $N_{\rm ch}^{\rm rec}$ and $p_{\rm T}$ dependence and factorization [Eq. (4)], can help in better understanding the origin of the long-range correlations.

Figure 4 shows template fits to the 13 TeV (left panels) and 5.02 TeV pp data (right panels), for $0.5 < p_{\rm T}^{\rm a,b} < 5$ GeV. From top to bottom, each panel represents a different $N_{\rm ch}^{\rm rec}$ range. The template fits [Eq. (9)] include harmonics 2–4. Visually, a ridge, i.e., a peak on the near side, cannot be seen in the top two rows, which correspond to low and intermediate $N_{\rm ch}^{\rm rec}$ intervals, respectively. However, the template fits indicate the presence of a large modulated component of $Y^{\rm ridge}(\Delta\phi)$ even in these $N_{\rm ch}^{\rm rec}$ intervals. Several prior pp ridge measurements rely on the ZYAM method [71,72] to extract yields on the near side [14,15]. In these analyses, the yield of excess pairs in the ridge above the minimum of the $Y(\Delta\phi)$ distribution is considered to be the strength of the ridge. Figure 4 shows that such a procedure would give zero yields in low- and intermediate-multiplicity collisions where the minimum of $Y(\Delta\phi)$ occurs at

[7] The minimum of $Y^{\rm periph}(\Delta\phi)$ is at $\Delta\phi = 0$ and is thus equal to $Y^{\rm periph}(0)$, which the ZYAM procedure subtracts out.

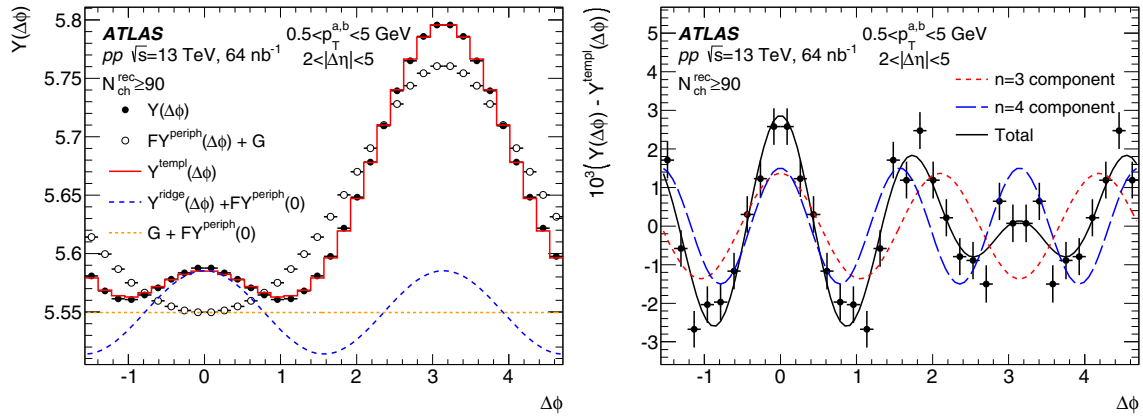

FIG. 3. Left panel: template fit to the per-trigger particle yields $Y(\Delta\phi)$ in 13 TeV pp collisions for charged-particle pairs with $0.5 < p_{\mathrm{T}}^{\mathrm{a,b}} < 5$ GeV and $2 < |\Delta\eta| < 5$. This plot corresponds to the $N_{\mathrm{ch}}^{\mathrm{rec}} \geqslant 90$ multiplicity range. The template fitting includes only the second-order harmonic, $v_{2,2}$. The solid points indicate the measured $Y(\Delta\phi)$, the open points and curves show different components of the template (see legend) that are shifted along the y axis by G or by $FY^{\mathrm{periph}}(0)$, where necessary, for presentation. Right panel: The difference between the $Y(\Delta\phi)$ and the template fit, showing the presence of $v_{3,3}$ and $v_{4,4}$ components. The vertical error bars indicate statistical uncertainties.

$\Delta\phi \sim 0$. In high-multiplicity events the ZYAM-based yields, while nonzero, are still underestimated.

Figure 5 shows the template fits to the $p+\mathrm{Pb}$ data in a format similar to Fig. 4. The template fits describe the data well across the entire $N_{\mathrm{ch}}^{\mathrm{rec}}$ range used in this paper. Previous $p+\mathrm{Pb}$ ridge analyses used a peripheral subtraction procedure to remove the jet component from $Y(\Delta\phi)$ [1–5]. That procedure is similar to the ZYAM-based template fitting procedure, in that it assumes absence of any long-range correlations in the peripheral events. In the following sections, comparisons between the $v_{n,n}$ obtained from these two methods are shown.

A. Fourier coefficients

Figure 6 shows the $v_{n,n}$ obtained from the template fits in the 13 TeV pp data, as a function of $N_{\mathrm{ch}}^{\mathrm{rec}}$ and $E_{\mathrm{T}}^{\mathrm{FCal}}$. The $v_{n,n}$ from the ZYAM-based template fits as well as the coefficients obtained from a direct Fourier transform of $Y(\Delta\phi)$,

$$\text{Fourier-}v_{n,n} \equiv \frac{\int Y(\Delta\phi)\cos(n\Delta\phi)d\Delta\phi}{\int Y(\Delta\phi)d\Delta\phi}, \tag{10}$$

are also shown for comparison. While the template $v_{n,n}$ are the most physically meaningful quantities, the Fourier $v_{n,n}$ are also included to demonstrate how the template fitting removes the hard contribution. Similarly, the ZYAM-based template $v_{n,n}$ are also included, as the ZYAM-based fitting is similar to the peripheral subtraction procedure used in prior $p+\mathrm{Pb}$ analyses [2,4], and comparing with the ZYAM-based results illustrates the improvement brought about in the template fitting procedure.

The $v_{2,2}$ values are nearly independent of $N_{\mathrm{ch}}^{\mathrm{rec}}$ throughout the measured range. As concluded in Ref. [41], this implies that the long-range correlation is not unique to high-multiplicity events, but is in fact present even at very low multiplicities. In the $E_{\mathrm{T}}^{\mathrm{FCal}}$ dependence, however, $v_{2,2}$ shows a systematic decrease at low $E_{\mathrm{T}}^{\mathrm{FCal}}$. Further, the asymptotic value of the template $v_{2,2}$ at large $N_{\mathrm{ch}}^{\mathrm{rec}}$ is also observed to be ∼10% larger than the asymptotic value at large $E_{\mathrm{T}}^{\mathrm{FCal}}$. This might indicate that the $v_{2,2}$ at a given rapidity is more correlated with the local multiplicity than the global multiplicity.

The removal of the hard-process contribution to $v_{2,2}$ in the template fitting can be seen by comparing to the Fourier-$v_{2,2}$ values. The Fourier-$v_{2,2}$ values are always larger than the template $v_{2,2}$ and show a systematic increase at small $N_{\mathrm{ch}}^{\mathrm{rec}}$ ($E_{\mathrm{T}}^{\mathrm{FCal}}$). This indicates the presence of a relatively large contribution from back-to-back dijets over this range. Asymptotically, at large $N_{\mathrm{ch}}^{\mathrm{rec}}$ the Fourier-$v_{2,2}$ values become stable, but show a small decreasing trend in the $E_{\mathrm{T}}^{\mathrm{FCal}}$ dependence. The ZYAM-based $v_{2,2}$ values are smaller than the template-$v_{2,2}$ values for all $N_{\mathrm{ch}}^{\mathrm{rec}}$ ($E_{\mathrm{T}}^{\mathrm{FCal}}$), and by construction systematically decrease to zero for the lower $N_{\mathrm{ch}}^{\mathrm{rec}}$ ($E_{\mathrm{T}}^{\mathrm{FCal}}$) intervals. However, at larger $N_{\mathrm{ch}}^{\mathrm{rec}}$ ($E_{\mathrm{T}}^{\mathrm{FCal}}$) they also show only a weak dependence on $N_{\mathrm{ch}}^{\mathrm{rec}}$ ($E_{\mathrm{T}}^{\mathrm{FCal}}$). Asymptotically, at large $N_{\mathrm{ch}}^{\mathrm{rec}}$ the $v_{2,2}$ values from the Fourier transform and the default template fits match to within ∼10% (relative). In general, the $v_{2,2}$ values from all three methods agree within ±15% at large $N_{\mathrm{ch}}^{\mathrm{rec}}$ or $E_{\mathrm{T}}^{\mathrm{FCal}}$. This implies that at very high multiplicities, $N_{\mathrm{ch}}^{\mathrm{rec}} \sim 120$, the ridge signal is sufficiently strong that the assumptions made in removing the hard contributions to $Y(\Delta\phi)$ do not make a large difference. However, for the highest p_{T} values used in this analysis, $p_{\mathrm{T}}^{\mathrm{a}} > 7$ GeV, it is observed that the width of the dijet peak in the pp correlation functions broadens with increasing multiplicity. This change is opposite to that seen at lower p_{T} where $v_{2,2}$ causes the dijet peak to become narrower. As a result, the measured $v_{2,2}$ values become negative. This bias from the multiplicity dependence of the hard-scattering contribution likely affects the correlation functions at lower $p_{\mathrm{T}}^{\mathrm{a,b}}$ values and its potential impact is discussed below.

The $v_{2,2}$ component is dominant, with a magnitude approximately 30 times larger than $v_{3,3}$ and $v_{4,4}$, which are comparable to each other. This is in stark contrast to $\mathrm{Pb}+\mathrm{Pb}$ collisions where in the most central events, where the average geometry has less influence, the $v_{n,n}$ have comparable magnitudes [13]. The Fourier $v_{3,3}$ shows considerable $N_{\mathrm{ch}}^{\mathrm{rec}}$ ($E_{\mathrm{T}}^{\mathrm{FCal}}$) dependence and is negative almost everywhere. However, the $v_{3,3}$ values from the template fits are mostly positive. As the factorization

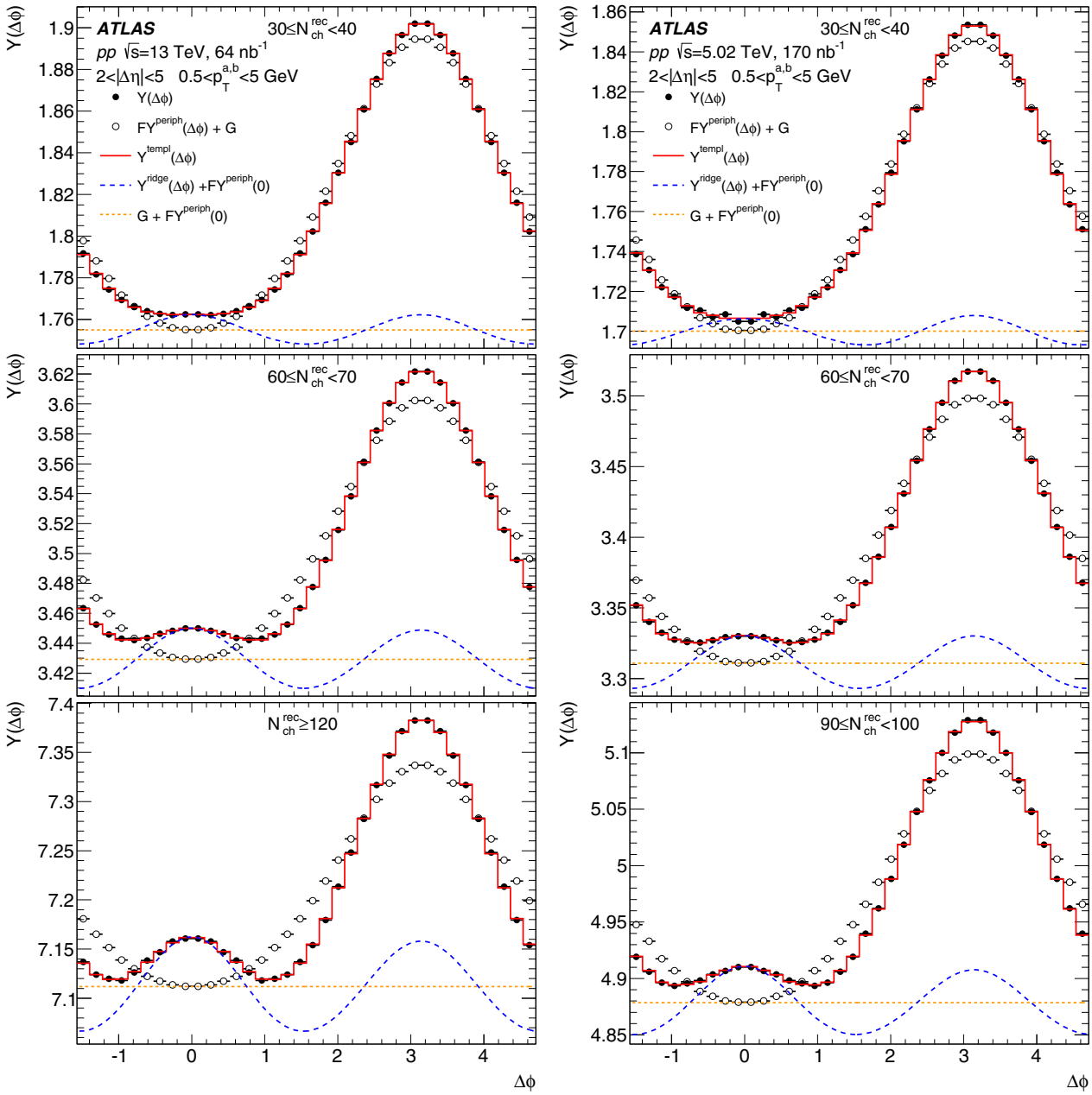

FIG. 4. Template fits to the per-trigger particle yields $Y(\Delta\phi)$, in 13 TeV (left panels) and in 5.02 TeV (right panels) pp collisions for charged-particle pairs with $0.5 < p_{\mathrm{T}}^{\mathrm{a,b}} < 5$ GeV and $2 < |\Delta\eta| < 5$. The template fitting includes second-order, third-order, and fourth-order harmonics. From top to bottom, each panel represents a different $N_{\mathrm{ch}}^{\mathrm{rec}}$ range. The solid points indicate the measured $Y(\Delta\phi)$, the open points and curves show different components of the template (see legend) that are shifted along the y axis by G or by $FY^{\mathrm{periph}}(0)$, where necessary, for presentation.

of the $v_{n,n}$ requires that the $v_{n,n}$ be positive [Eq. (3)], the negative Fourier $v_{3,3}$ clearly does not arise from single-particle modulation. However, because the template $v_{3,3}$ is positive, its origin from single-particle modulation cannot be ruled out. Within statistical uncertainties, the $v_{4,4}$ values from all three methods are positive throughout the measured $N_{\mathrm{ch}}^{\mathrm{rec}}$ range. Within statistical uncertainties, the $v_{4,4}$ values are consistent with no $N_{\mathrm{ch}}^{\mathrm{rec}}$ or $E_{\mathrm{T}}^{\mathrm{FCal}}$ dependence.

Figure 7 shows the $v_{n,n}$ values from the 5.02 TeV pp data as a function of $N_{\mathrm{ch}}^{\mathrm{rec}}$ for a higher $p_{\mathrm{T}}^{\mathrm{a,b}}$ bin of 1–5 GeV. The same trends seen in the 13 TeV data (Fig. 6) are observed here, and the conclusions are identical to those made in the 13 TeV case.

Figure 8 shows the $v_{n,n}$ for the $p+\mathrm{Pb}$ data. The results are plotted both as a function of $N_{\mathrm{ch}}^{\mathrm{rec}}$ (left panels) and $E_{\mathrm{T}}^{\mathrm{FCal,Pb}}$ (right panels). The $v_{2,2}$ values obtained from the template fits show a systematic increase with $N_{\mathrm{ch}}^{\mathrm{rec}}$ over $N_{\mathrm{ch}}^{\mathrm{rec}} \lesssim 150$, unlike the pp case where $v_{2,2}$ is nearly independent of $N_{\mathrm{ch}}^{\mathrm{rec}}$. This increase is much larger compared to the systematic uncertainties in the $v_{2,2}$ values (discussed later in Sec. VI). This is possibly indicative of a systematic change in the average

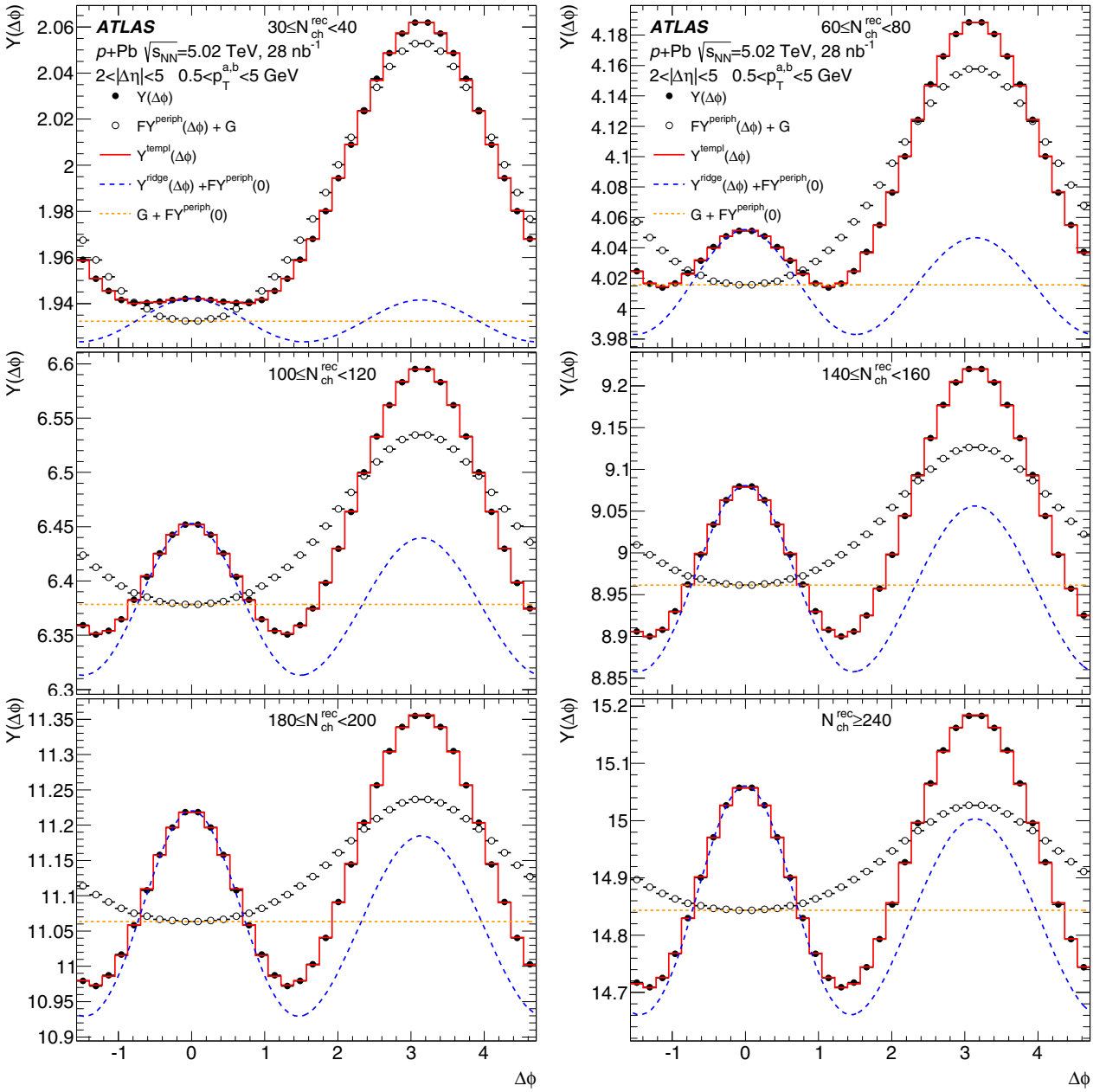

FIG. 5. Template fits to the per-trigger particle yields $Y(\Delta\phi)$ in 5.02 TeV $p+\mathrm{Pb}$ collisions for charged-particle pairs with $0.5 < p_{\mathrm{T}}^{\mathrm{a,b}} < 5$ GeV and $2 < |\Delta\eta| < 5$. The template fitting includes second-order, third-order, and fourth-order harmonics. Each panel represents a different $N_{\mathrm{ch}}^{\mathrm{rec}}$ range. The solid points indicate the measured $Y(\Delta\phi)$, the open points and curves show different components of the template (see legend) that are shifted along the y axis by G or by $FY^{\mathrm{periph}}(0)$, where necessary, for presentation.

collision geometry which is present in $p+\mathrm{Pb}$ but not in pp collisions. A similar increase of the $v_{2,2}$ values is also observed in the $E_{\mathrm{T}}^{\mathrm{FCal,Pb}}$ dependence. The higher-order harmonics $v_{3,3}$ and $v_{4,4}$ show a stronger relative increase with increasing $N_{\mathrm{ch}}^{\mathrm{rec}}$ and $E_{\mathrm{T}}^{\mathrm{FCal,Pb}}$. This also implies that the assumption made in the template fitting, regarding the independence or weak dependence of the $v_{n,n}$ on $N_{\mathrm{ch}}^{\mathrm{rec}}$, is not strictly correct for $v_{3,3}$ and $v_{4,4}$.

Figure 8 also compares the Fourier and ZYAM-based template-$v_{n,n}$ values. The $v_{n,n}$ from the peripheral subtraction procedure used in a previous ATLAS $p+\mathrm{Pb}$ long-range correlation analysis [4] are also shown. The peripheral-subtracted $v_{n,n}$ values are nearly identical to the values obtained from the ZYAM-based template fits. This is expected, as the treatment of the peripheral bin is identical in both cases: both use the ZYAM-subtracted $Y^{\mathrm{periph}}(\Delta\phi)$ as the peripheral reference. What differs procedurally between the two methods is determination of the scale factor by which $Y^{\mathrm{periph}}(\Delta\phi)$ is scaled up when subtracting it from $Y(\Delta\phi)$. In the peripheral subtraction case, this scale factor, analogous to the parameter F in Eq. (8), is determined by matching the near-side jet peaks over the region $|\Delta\eta| < 1$ and $|\Delta\phi| < 1$. In the template-fitting

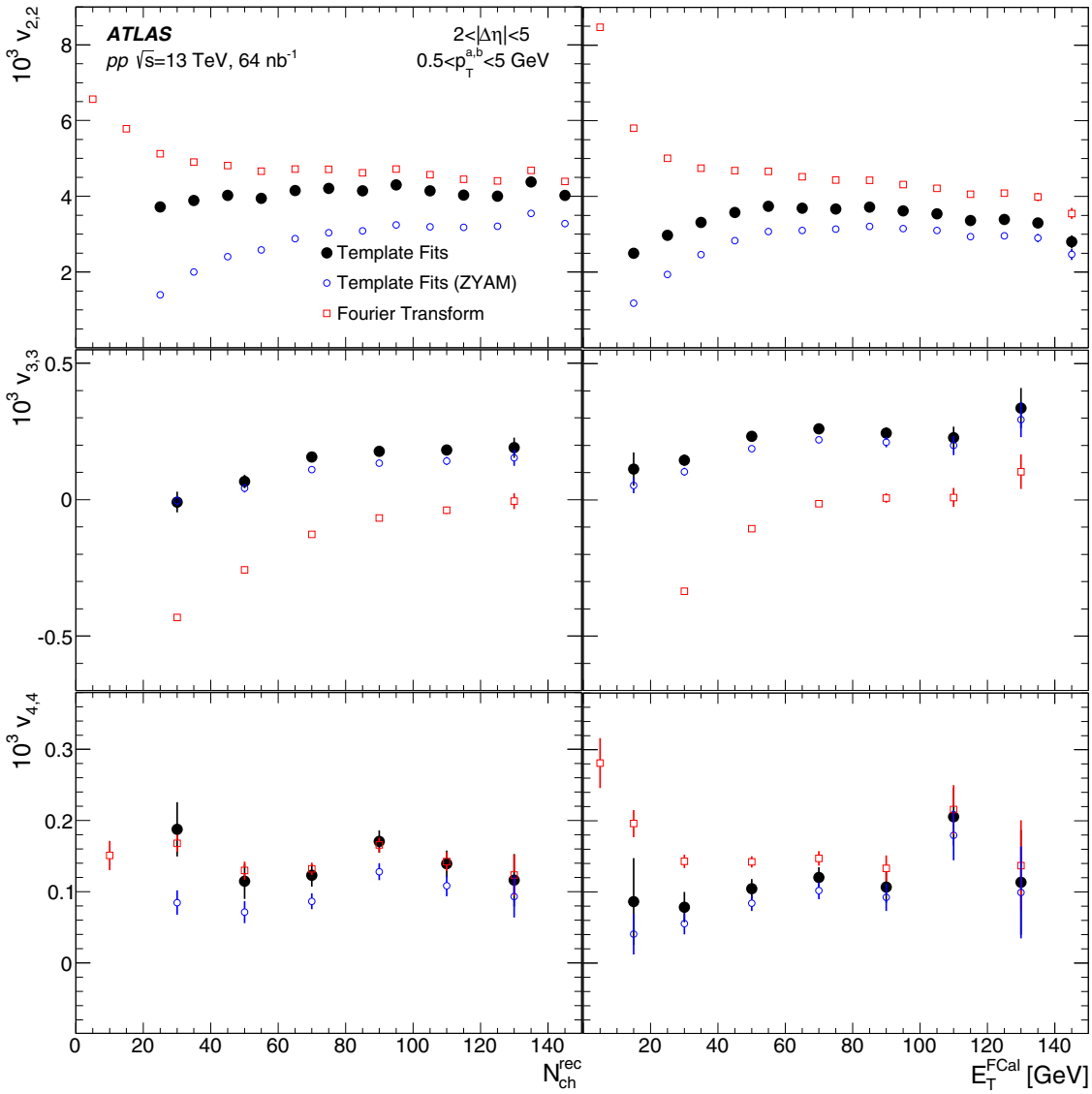

FIG. 6. The $v_{n,n}$ obtained from the template fitting procedure in the 13 TeV pp data, as a function of $N_{\mathrm{ch}}^{\mathrm{rec}}$ (left panels), and as a function of $E_{\mathrm{T}}^{\mathrm{FCal}}$ (right panels). The top, middle, and bottom panels correspond to $v_{2,2}$, $v_{3,3}$, and $v_{4,4}$, respectively. The results are for $0.5 < p_{\mathrm{T}}^{\mathrm{a,b}} < 5$ GeV. The error bars indicate statistical uncertainties. The $v_{n,n}$ obtained from a direct Fourier transform of $Y(\Delta\phi)$ and from the ZYAM-based template fits are also shown for comparison.

case, the parameter F is determined by the jet contribution to the away-side peak. The similarity of the $v_{2,2}$ values from the two procedures implies that whether the matching is done in the near-side jet peak or over the away-side peak, identical values of the scale factor are obtained. The Fourier-$v_{2,2}$ and template-$v_{2,2}$ values are surprisingly similar except at very low $N_{\mathrm{ch}}^{\mathrm{rec}}$ or $E_{\mathrm{T}}^{\mathrm{FCal,Pb}}$. This is unlike the pp case (Figs. 6 and 7), where the values differed by ∼15% (relative) at large $N_{\mathrm{ch}}^{\mathrm{rec}}$. This similarity does not hold for $v_{3,3}$ where the values from the template fit are systematically larger than the values obtained from Fourier decomposition. For all harmonics, the relative difference in the $v_{n,n}$ decreases with increasing event activity. Like in the pp case (Fig. 6), this implies that at large enough event activity, the $v_{n,n}$ are less sensitive to the assumptions made in removing the hard contributions.

B. Test of factorization in template fits

If the $v_{n,n}$ obtained from the template fits are the result of single-particle modulations, then the $v_{n,n}$ should factorize as in Eq. (3), and the $v_n(p_{\mathrm{T}}^{\mathrm{a}})$ obtained by correlating trigger particles at a given $p_{\mathrm{T}}^{\mathrm{a}}$ with associated particles in several different intervals of $p_{\mathrm{T}}^{\mathrm{b}}$ [Eq. (4)] should be independent of the choice of the $p_{\mathrm{T}}^{\mathrm{b}}$ interval. Figure 9 demonstrates the factorization of the $v_{2,2}$ in the 13 TeV pp data, as a function of $N_{\mathrm{ch}}^{\mathrm{rec}}$. The left panel shows the $v_{2,2}$ values for $0.5 < p_{\mathrm{T}}^{\mathrm{a}} < 5$ GeV and for four different choices of the associated particle p_{T}: 0.5–5, 0.5–1, 1–2, and 2–3 GeV. The right panel shows the corresponding $v_2(p_{\mathrm{T}}^{\mathrm{a}})$ obtained using Eq. (4). While the $v_{2,2}(p_{\mathrm{T}}^{\mathrm{a}}, p_{\mathrm{T}}^{\mathrm{b}})$ values vary by a factor of ∼2 between the different choices of the $p_{\mathrm{T}}^{\mathrm{b}}$ interval, the corresponding $v_2(p_{\mathrm{T}}^{\mathrm{a}})$ values agree quite well. Similar plots for the p + Pb data are shown in Fig. 10. Here

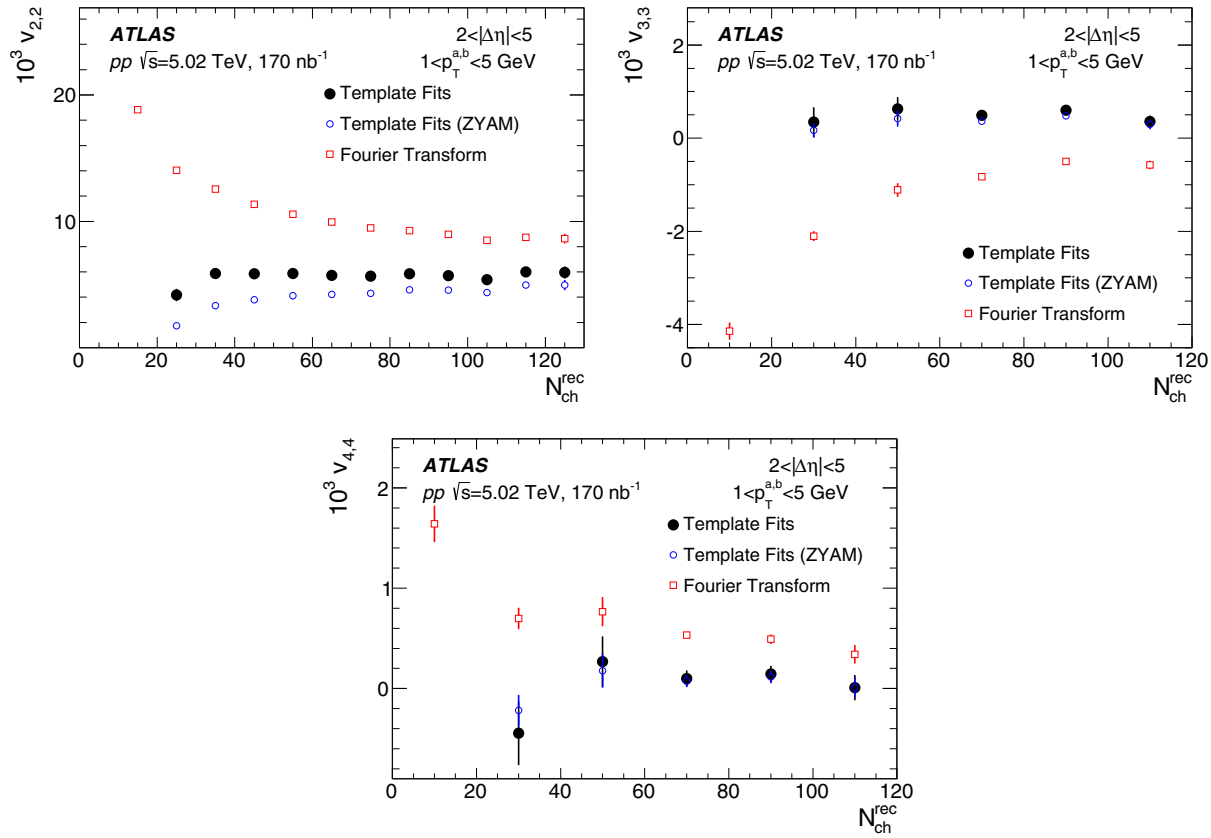

FIG. 7. The $v_{n,n}$ obtained from the template fitting procedure in the 5.02 TeV pp data, as a function of $N_{\mathrm{ch}}^{\mathrm{rec}}$. The three panels correspond to $n = 2$, 3, and 4, respectively. The results are for $1 < p_{\mathrm{T}}^{\mathrm{a,b}} < 5$ GeV. The error bars indicate statistical uncertainties. The $v_{n,n}$ obtained from a direct Fourier transform of $Y(\Delta\phi)$ and from the ZYAM-based template fits are also shown for comparison.

due to higher statistical precision in the data, the factorization is tested for both $v_{2,2}$ and $v_{3,3}$. The variation of $v_{2,2}(p_{\mathrm{T}}^{\mathrm{a}}, p_{\mathrm{T}}^{\mathrm{b}})$ between the four $p_{\mathrm{T}}^{\mathrm{b}}$ intervals is a factor of $\sim$2 while the variation of $v_{3,3}(p_{\mathrm{T}}^{\mathrm{a}}, p_{\mathrm{T}}^{\mathrm{b}})$ is more than a factor of 3. However, the corresponding $v_n(p_{\mathrm{T}}^{\mathrm{a}})$ values are in good agreement with each other, with the only exception being the $v_{2,2}$ values for $2 < p_{\mathrm{T}}^{\mathrm{b}} < 3$ GeV where some deviation from this behavior is seen for $N_{\mathrm{ch}}^{\mathrm{rec}} \lesssim 60$.

Figure 11 studies the $p_{\mathrm{T}}^{\mathrm{a}}$ dependence of the factorization in the 13 TeV pp data for $v_{2,2}$ (top panels) and $v_{3,3}$ (bottom panels). The results are shown for the $N_{\mathrm{ch}}^{\mathrm{rec}} \geqslant 90$ multiplicity range. The left panels show the $v_{n,n}$ as a function of $p_{\mathrm{T}}^{\mathrm{a}}$ for four different choices of the associated particle p_{T}: 0.5–5, 0.5–1, 1–2, and 2–3 GeV. The right panels show the corresponding v_n $(p_{\mathrm{T}}^{\mathrm{a}})$ obtained using Eq. (4). In the $v_{2,2}$ case, factorization holds reasonably well for $p_{\mathrm{T}}^{\mathrm{a}} \leqslant 3$ GeV, and becomes worse at higher p_{T}. This breakdown at higher p_{T} is likely caused by the above-discussed multiplicity-dependent distortions of the dijet component of the correlation function which are not accounted for in the template fitting procedure. For $v_{3,3}$, the factorization holds reasonably well for $p_{\mathrm{T}}^{\mathrm{b}} > 1$ GeV. The $0.5 < p_{\mathrm{T}}^{\mathrm{b}} < 1$ GeV case shows a larger deviation in the factorization, but has much larger associated statistical uncertainties. Similar plots for the p + Pb case are shown in Fig. 12. Here the factorization holds for $v_{2,2}$, $v_{3,3}$, and $v_{4,4}$ up to $p_{\mathrm{T}}^{\mathrm{b}} \sim 5$ GeV.

C. Dependence of $v_{n,n}$ on $\Delta\eta$ gap

A systematic study of the $\Delta\eta$ dependence of the $v_{n,n}$ can also help in determining the origin of the long-range correlation. If it arises from mechanisms that only correlate a few particles in an event, such as jets, then a strong dependence of the correlation on the $\Delta\eta$ gap between particle pairs is expected. Figure 13 shows the measured $v_{n,n}$ (left panels) and $v_n = \sqrt{v_{n,n}}$ (right panels), as a function of $|\Delta\eta|$ for $|\Delta\eta| > 1$ in the 13 TeV pp data. Also shown for comparison are the Fourier and ZYAM-based template $v_{n,n}$. The template $v_{2,2}$ (top left panel) and v_2 (top right panel) are quite stable, especially for $|\Delta\eta| > 1.5$, where the influence of the near-side jet is diminished. In contrast, the Fourier $v_{2,2}$ show a strong $|\Delta\eta|$ dependence. The $\Delta\eta$ dependence is largest at small $|\Delta\eta|$ because of the presence of the sharply peaked near-side jet, but is considerable even for $|\Delta\eta| > 2$. Similarly, the Fourier-$v_{3,3}$ shows large $|\Delta\eta|$ dependence, going from positive values at $|\Delta\eta| \sim 1$ to negative values at large $|\Delta\eta|$, while the template $v_{3,3}$ change only weakly in comparison. The Fourier $v_{3,3}$ is often negative, ruling out the possibility of it being generated by single-particle anisotropies, which require that $v_{n,n} = v_n^2$ be positive. For points where $v_{3,3}$ is negative, v_3 is not defined and hence not plotted. The template $v_{3,3}$ is, however, positive and, therefore, consistent with a single-particle anisotropy as its origin, except for the highest $|\Delta\eta|$ interval where it is consistent with zero. The $v_{4,4}$ values, like the $v_{2,2}$ and $v_{3,3}$

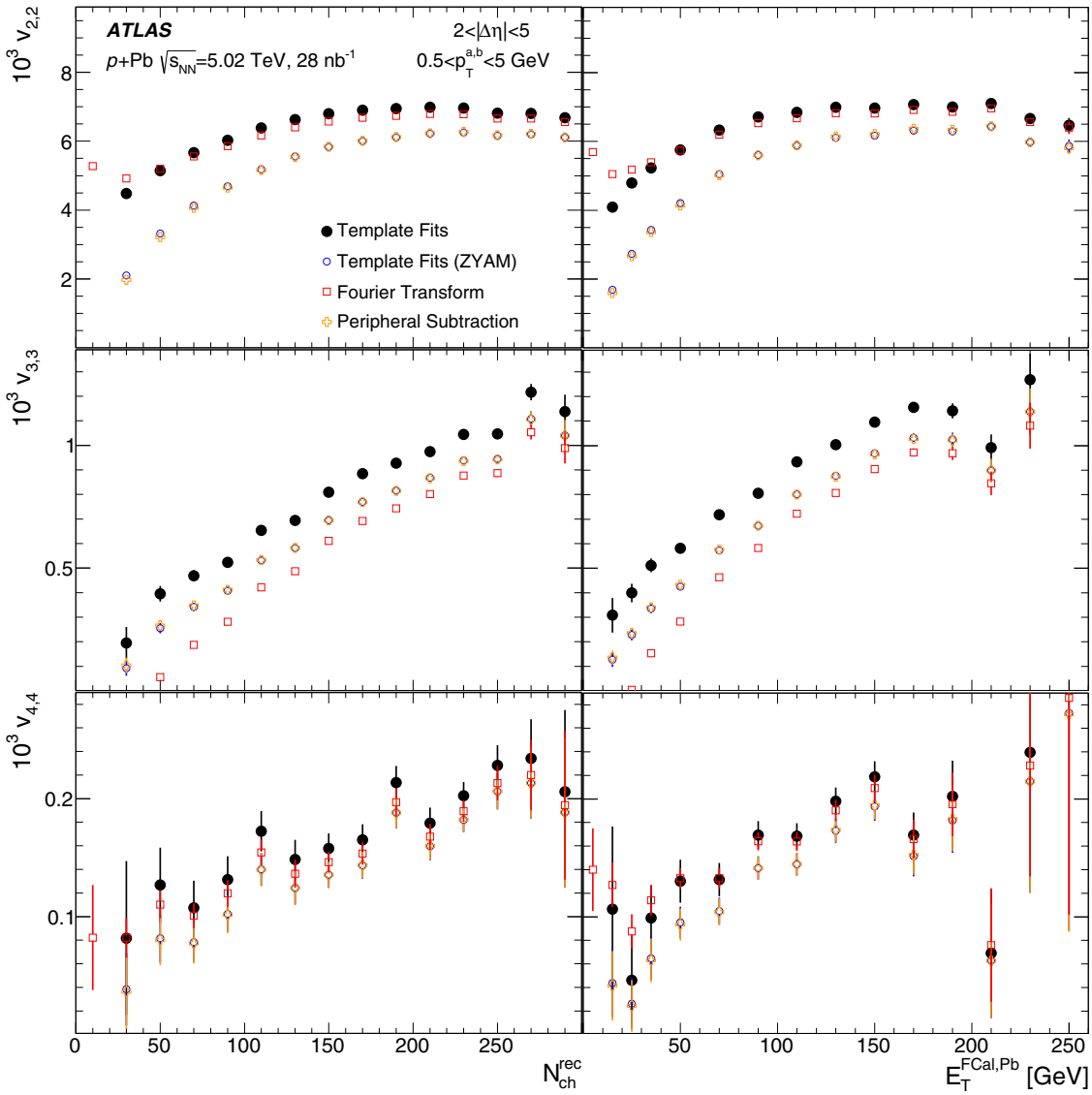

FIG. 8. The $v_{n,n}$ obtained from the template fitting procedure in the 5.02 TeV $p+\mathrm{Pb}$ data, as a function of $N_{\mathrm{ch}}^{\mathrm{rec}}$ (left panels), and as a function of the Pb-fragmentation side FCal-E_{T}(right panels). The top, middle, and bottom panels correspond to $v_{2,2}$, $v_{3,3}$, and $v_{4,4}$, respectively. The results are for $0.5 < p_{\mathrm{T}}^{\mathrm{a,b}} < 5$ GeV. The error bars indicate statistical uncertainties. The $v_{n,n}$ obtained from a direct Fourier transform of $Y(\Delta\phi)$, the peripheral subtraction procedure, and from the ZYAM-based template fits are also shown for comparison.

values, vary only weakly with $|\Delta\eta|$. These observations further support the conclusion that the template $v_{n,n}$ are coefficients of genuine long-range correlations.

VI. SYSTEMATIC UNCERTAINTIES AND CROSS CHECKS

The systematic uncertainties in this analysis arise from choosing the peripheral bin used in the template fits, pileup, tracking efficiency, pair acceptance, and Monte Carlo consistency. Each source is discussed separately below.

Peripheral interval. As explained in Sec. V, the template fitting procedure makes two assumptions. First it assumes that the contributions to $Y(\Delta\phi)$ from hard processes have identical shape across all event activity ranges, and only change in overall scale. Second, it assumes that the $v_{n,n}$ are only weakly dependent on the event activity. The assumptions are self-consistent for the $N_{\mathrm{ch}}^{\mathrm{rec}}$ dependence of the $v_{n,n}$ in the 5.02 and 13 TeV pp data (Figs. 6 and 7), where the measured template-$v_{n,n}$ values do turn out to be nearly independent of $N_{\mathrm{ch}}^{\mathrm{rec}}$. However, for the $E_{\mathrm{T}}^{\mathrm{FCal}}$ dependence in the pp data, and for both the $N_{\mathrm{ch}}^{\mathrm{rec}}$ and $E_{\mathrm{T}}^{\mathrm{FCal,Pb}}$ dependence in the $p+\mathrm{Pb}$ data, a systematic increase of the template $v_{2,2}$ with event activity is seen at small event activity. This indicates the breakdown of one of the above two assumptions. To test the sensitivity of the measured $v_{n,n}$ to any residual changes in the width of the away-side jet peak and to the $v_{n,n}$ present in the peripheral reference, the analysis is repeated using $0 \leqslant N_{\mathrm{ch}}^{\mathrm{rec}} < 10$ and $10 \leqslant N_{\mathrm{ch}}^{\mathrm{rec}} < 20$ intervals to form $Y^{\mathrm{periph}}(\Delta\phi)$. The variations in the $v_{n,n}$ for the different chosen peripheral intervals are taken to be a systematic uncertainty. For a given dataset,

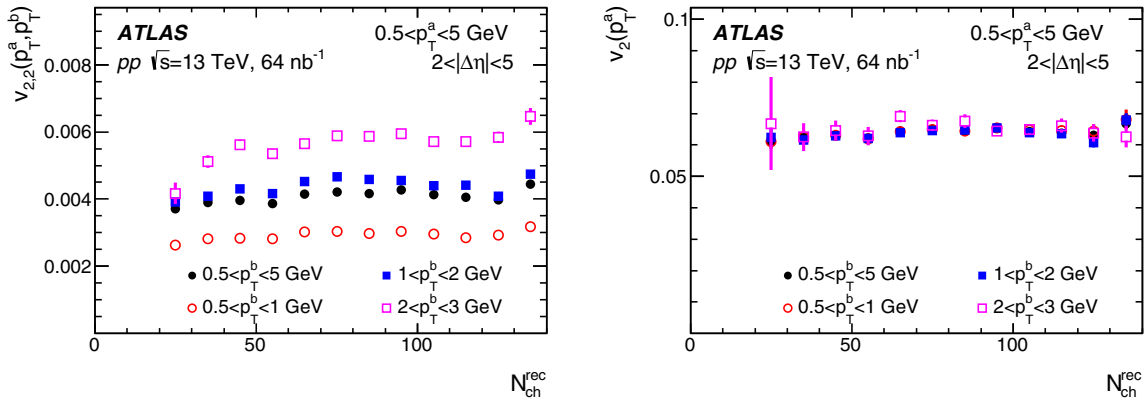

FIG. 9. The left panel shows $v_{2,2}$ as a function of $N_{\mathrm{ch}}^{\mathrm{rec}}$ in the 13 TeV pp data, for $0.5 < p_{\mathrm{T}}^{\mathrm{a}} < 5$ GeV and for different choices of the $p_{\mathrm{T}}^{\mathrm{b}}$ interval. The right panel shows the corresponding v_2 values obtained using Eq. (4). The error bars indicate statistical uncertainties only.

this uncertainty is strongly correlated across all multiplicity intervals. Choosing a peripheral interval with larger mean multiplicity typically decreases the measured $v_{n,n}$.

The sensitivity of the template v_2 to which peripheral interval is chosen is demonstrated in the left panels of Fig. 14, where v_2 is shown for three different peripheral $N_{\mathrm{ch}}^{\mathrm{rec}}$ interval choices: $0 \leqslant N_{\mathrm{ch}}^{\mathrm{rec,periph}} < 5$, $0 \leqslant N_{\mathrm{ch}}^{\mathrm{rec,periph}} < 10$, and $0 \leqslant N_{\mathrm{ch}}^{\mathrm{rec,periph}} < 20$. In both the 13 and 5.02 TeV pp data, except at very low $N_{\mathrm{ch}}^{\mathrm{rec}}$, the v_2 values are nearly independent of the chosen peripheral reference. In the 13 TeV pp case, the variation is ∼6% at $N_{\mathrm{ch}}^{\mathrm{rec}} \sim 30$ and decreases to ∼1% for $N_{\mathrm{ch}}^{\mathrm{rec}} \geqslant 60$. Even in the $p+\mathrm{Pb}$ case, where the measured template $v_{2,2}$ exhibits some dependence on $N_{\mathrm{ch}}^{\mathrm{rec}}$, the dependence of the template v_2 on the choice of peripheral bin is quite small: ∼6% at $N_{\mathrm{ch}}^{\mathrm{rec}} \sim 30$ and decreases to ∼2% for $N_{\mathrm{ch}}^{\mathrm{rec}} \sim 60$. Also shown for comparison are the corresponding v_2 values obtained from the ZYAM-based template fitting method (right panels of Fig. 14). These exhibit considerable dependence on the peripheral reference. For the 13 TeV pp case, the variation in the ZYAM-based v_2 is ∼40% at $N_{\mathrm{ch}}^{\mathrm{rec}} \sim 30$, and decreases to ∼12% at $N_{\mathrm{ch}}^{\mathrm{rec}} \sim 60$ and asymptotically at large $N_{\mathrm{ch}}^{\mathrm{rec}}$ is ∼7%. For the $p+\mathrm{Pb}$ case, the variation is even larger: ∼35% at $N_{\mathrm{ch}}^{\mathrm{rec}} \sim 30$ and ∼14% for $N_{\mathrm{ch}}^{\mathrm{rec}} \sim 60$. These results show that the template v_2 is quite stable as the peripheral interval is

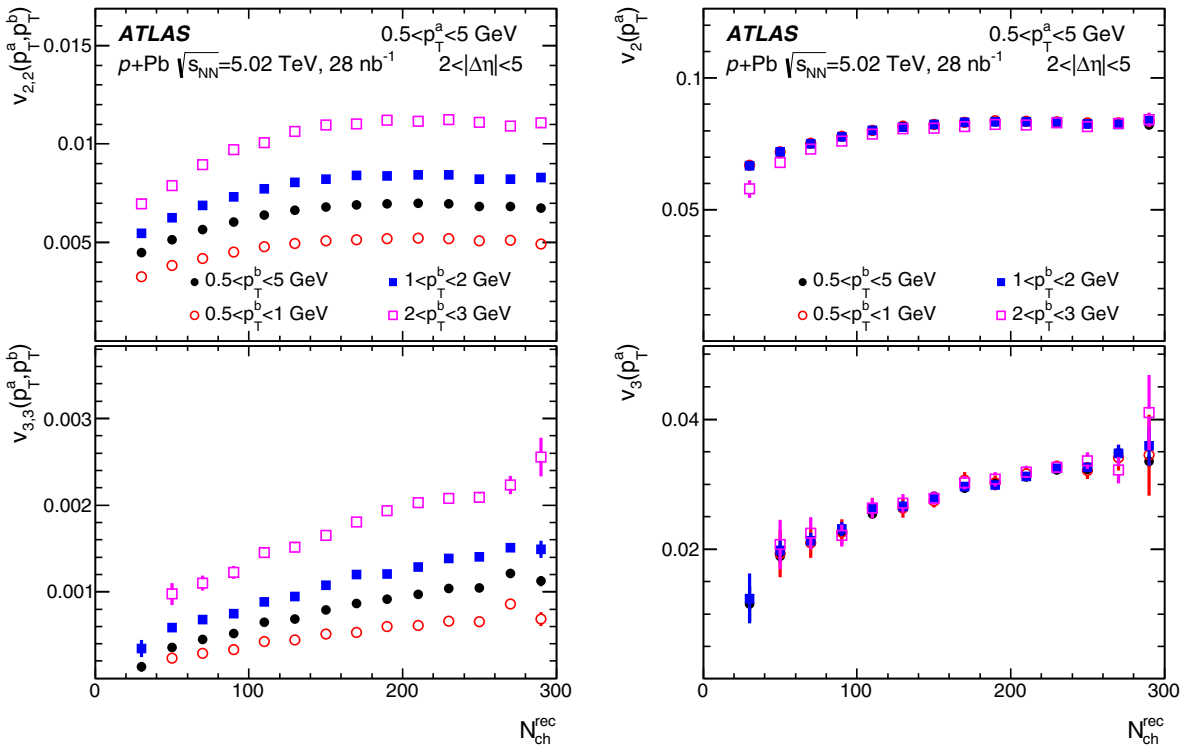

FIG. 10. The left panels show $v_{2,2}$ (top) and $v_{3,3}$ (bottom) as a function of $N_{\mathrm{ch}}^{\mathrm{rec}}$ in the 5.02 TeV $p+\mathrm{Pb}$ data, for $0.5 < p_{\mathrm{T}}^{\mathrm{a}} < 5$ GeV and for different choices of the $p_{\mathrm{T}}^{\mathrm{b}}$ interval. The right panels shows the corresponding v_2 (top) and v_3 (bottom) values obtained using Eq. (4). The error bars indicate statistical uncertainties only.

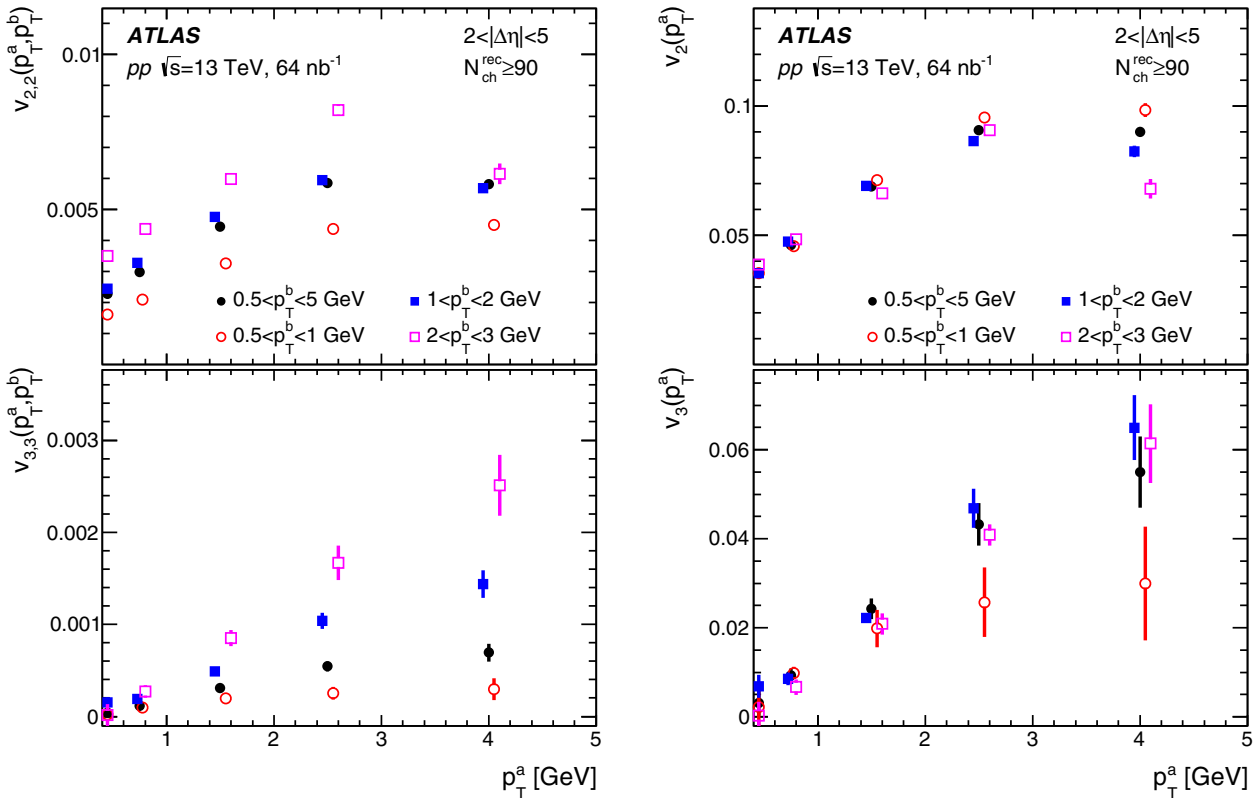

FIG. 11. The left panels show $v_{2,2}$ (top) and $v_{3,3}$ (bottom) as a function of $p_{\mathrm{T}}^{\mathrm{a}}$ in the 13 TeV pp data, for $N_{\mathrm{ch}}^{\mathrm{rec}} \geqslant 90$ and for different choices of the $p_{\mathrm{T}}^{\mathrm{b}}$ interval. The right panels shows the corresponding v_2 (top) and v_3 (bottom) values obtained using Eq. (4). The error bars indicate statistical uncertainties only. The $p_{\mathrm{T}}^{\mathrm{a}}$ intervals plotted are 0.4–0.5, 0.5–1, 1–2, 2–3, and 3–5 GeV. In some cases, the data points have been slightly shifted along the x axis, for clarity.

varied, while the ZYAM-based result is very sensitive. This is one of the advantages of the new method. For the ZYAM-based results, as the upper edge of the peripheral interval is moved to lower multiplicities, the measured v_2 becomes less and less dependent on $N_{\mathrm{ch}}^{\mathrm{rec}}$. Qualitatively, it seems that in the limit of $N_{\mathrm{ch}}^{\mathrm{rec,periph}} \to 0$ the ZYAM-based pp-v_2 would be nearly independent of $N_{\mathrm{ch}}^{\mathrm{rec}}$, thus contradicting the assumption of zero v_2 made in the ZYAM method, and supporting the flat-v_2 assumption made in the new method.

Pileup. Pileup events, when included in the two-particle correlation measurement, dilute the $v_{n,n}$ signal since they produce pairs where the trigger and associated particle are from different collisions and thus have no physical correlations. The maximal fractional dilution in the $v_{n,n}$ is equal to the pileup rate. In the $p+\mathrm{Pb}$ data, nearly all of the events containing pileup are removed by the procedure described in Sec. III. The influence of the residual pileup is evaluated by relaxing the pileup rejection criteria and then calculating the change in the $Y(\Delta\phi)$ and v_n values. The differences are taken as an estimate of the uncertainty for the $v_{n,n}$, and are found to be negligible in low event activity classes, and increase to 4% for events with $N_{\mathrm{ch}}^{\mathrm{rec}} \sim 300$.

In the pp data, for events containing multiple vertices, only tracks associated with the vertex having the largest $\sum p_{\mathrm{T}}^2$, where the sum is over all tracks associated with the vertex, are used in the analysis. Events with multiple unresolved vertices affect the results by increasing the combinatoric pedestal in $Y(\Delta\phi)$. The fraction of events with merged vertices is estimated and taken as the relative uncertainty associated with pileup in the pp analysis. The merged-vertex rate in the 13 TeV pp data is 0–3% over the 0–150 $N_{\mathrm{ch}}^{\mathrm{rec}}$ range. In the 5.02 TeV pp data, it is 0–4% over the 0–120 $N_{\mathrm{ch}}^{\mathrm{rec}}$ range.

Track reconstruction efficiency. In evaluating $Y(\Delta\phi)$, each particle is weighted by $1/\epsilon(p_{\mathrm{T}},\eta)$ to account for the tracking efficiency. The systematic uncertainties in the efficiency $\epsilon(p_{\mathrm{T}},\eta)$ thus need to be propagated into $Y(\Delta\phi)$ and the final $v_{n,n}$ measurements. Unlike $Y(\Delta\phi)$, which is strongly affected by the efficiency, the $v_{n,n}$ are mostly insensitive to the tracking efficiency. This is because the $v_{n,n}$ measure the relative variation of the yields in $\Delta\phi$; an overall increase or decrease in the efficiency changes the yields but does not affect the $v_{n,n}$. However, as the tracking efficiency and its uncertainties have p_{T} and η dependence, there is some residual effect on the $v_{n,n}$. The corresponding uncertainty in the $v_{n,n}$ is estimated by repeating the analysis while varying the efficiency to its upper and lower extremes. In the pp analysis, this uncertainty is estimated to be 0.5% for $v_{2,2}$ and 2.5% for $v_{3,3}$ and $v_{4,4}$. The corresponding uncertainties in the $p+\mathrm{Pb}$ data are 0.8%, 1.6%, and 2.4% for $v_{2,2}$, $v_{3,3}$, and $v_{4,4}$, respectively.

Pair acceptance. As described in Sec. IV, this analysis uses the mixed-event distributions $B(\Delta\eta,\Delta\phi)$ and $B(\Delta\phi)$ to estimate and correct for the pair acceptance of the detector.

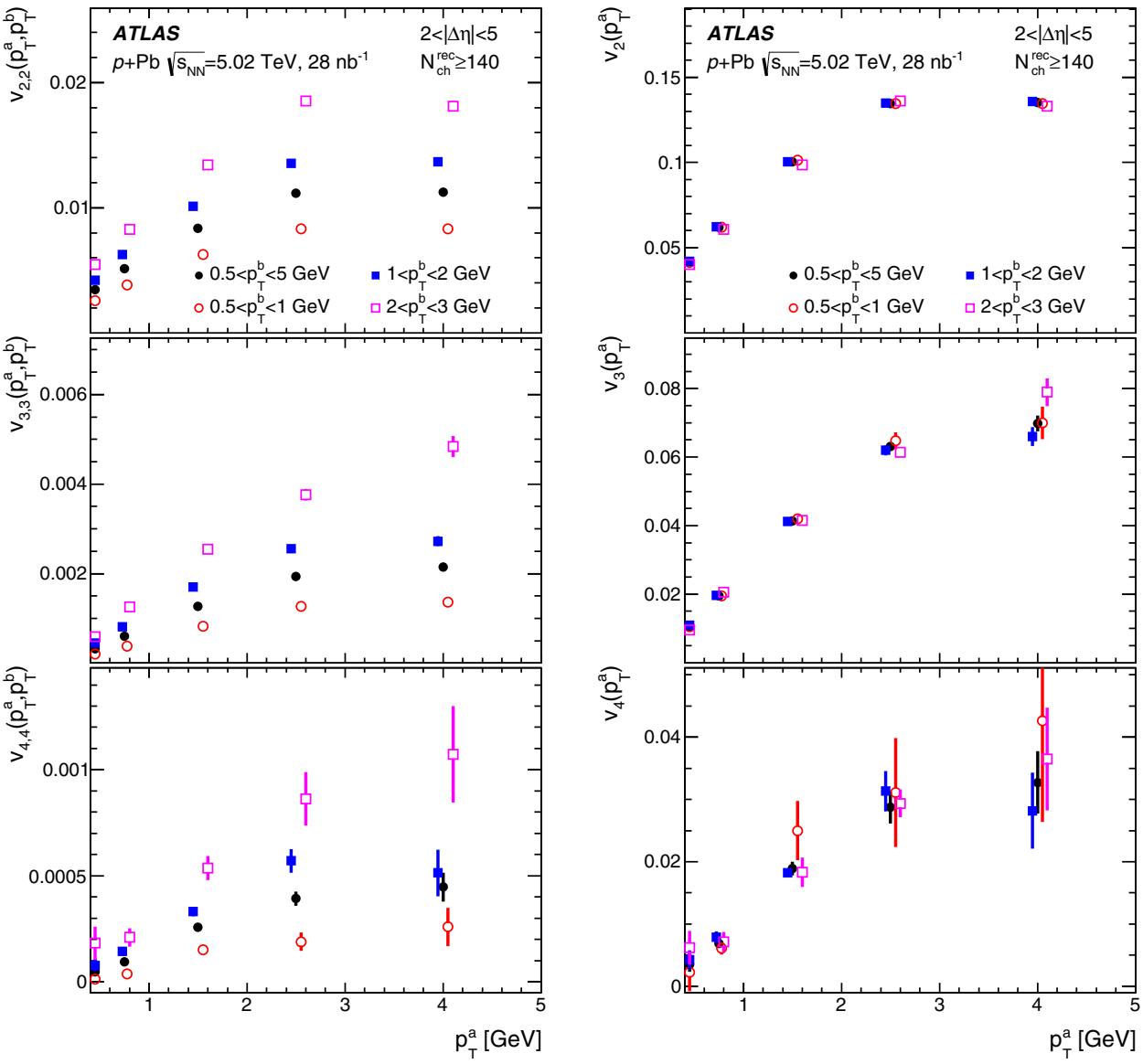

FIG. 12. The left panels show the $v_{n,n}$ as a function of $p_{\mathrm{T}}^{\mathrm{a}}$ in the 5.02 TeV $p+\mathrm{Pb}$ data, for $N_{\mathrm{ch}}^{\mathrm{rec}} \geqslant 140$ and for different choices of the $p_{\mathrm{T}}^{\mathrm{b}}$ interval. From top to bottom, the three rows correspond to $n = 2$, 3, and 4. The right panels shows the corresponding v_n values obtained using Eq. (4). The error bars indicate statistical uncertainties only. The $p_{\mathrm{T}}^{\mathrm{a}}$ intervals plotted are 0.4–0.5, 0.5–1, 1–2, 2–3, and 3–5 GeV. In some cases, the data points have been slightly shifted along the x axis, for clarity.

The mixed-event distributions are in general quite flat in $\Delta\phi$. The Fourier coefficients of the mixed-event distributions $v_{n,n}^{\mathrm{det}}$, which quantify the magnitude of the corrections, are $\sim 10^{-4}$ in the $p+\mathrm{Pb}$ data, and $\sim 2\times 10^{-5}$ in the pp data. In the $p+\mathrm{Pb}$ analysis, potential systematic uncertainties in the $v_{n,n}$ due to residual pair-acceptance effects not corrected by the mixed events are evaluated following Ref. [13]. This uncertainty is found to be smaller than $\sim 10^{-5}$. In the pp analysis, since the mixed-event corrections are themselves quite small, the entire correction is conservatively taken as the systematic uncertainty.

MC closure. The analysis procedure is validated by measuring the $v_{n,n}$ of reconstructed particles in fully simulated PYTHIA8 and HIJING events and comparing them to those obtained using the generated particles. The difference between the generated and reconstructed $v_{n,n}$ varies between 10^{-5} and 10^{-4} (absolute) in the pp case and between 2% and 8% (relative) in the $p+\mathrm{Pb}$ case, for the different harmonics. This difference is an estimate of possible systematic effects that are not accounted for in the measurement, such as a mismatch between the true and reconstructed momentum for charged particles, and is included as a systematic uncertainty.

As a cross-check, the dependence of the long-range correlations on the relative charge of the two particles used in the correlation is studied. If the long-range correlations arise from phenomena that correlate only a few particles in an event, such as jets or decays, then a dependence of the correlation on the relative sign of the particles making

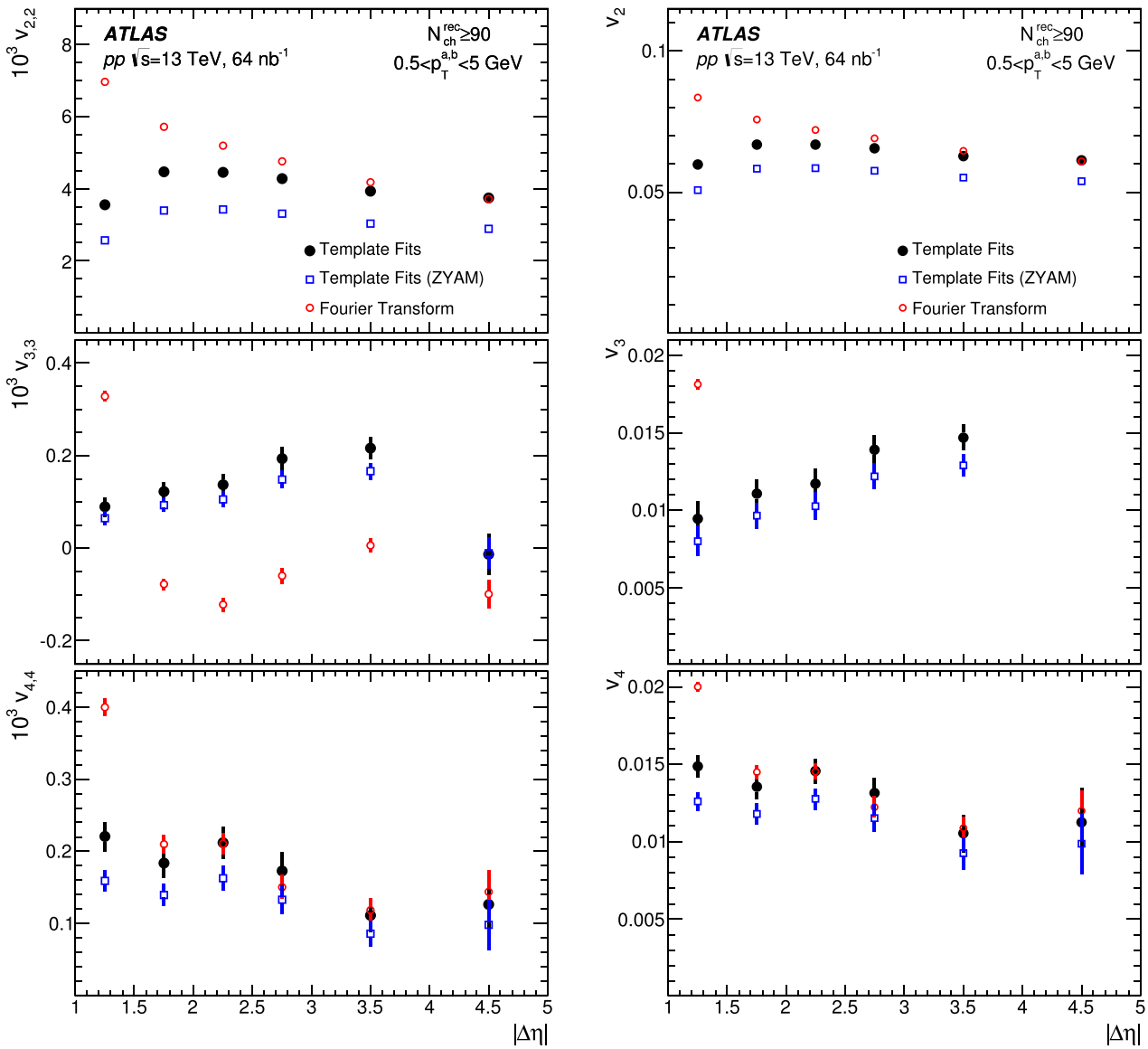

FIG. 13. The $|\Delta\eta|$ dependence of the $v_{n,n}$ (left panels) and v_n (right panels) in the 13 TeV pp data. From top to bottom the rows correspond to $n = 2$, 3, and 4, respectively. The ZYAM-template and Fourier-$v_{n,n}$ values are also shown for comparison. Only the range $|\Delta\eta| > 1$ is shown to suppress the large Fourier $v_{n,n}$ at $|\Delta\eta| \sim 0$ that arise due to the near-side jet peak. Plots are for the $N_{\rm ch}^{\rm rec} \geqslant 90$ multiplicity range and for $0.5 < p_{\rm T}^{\rm a,b} < 5$ GeV. The error bars indicate statistical uncertainties only. For points where $v_{3,3}$ is negative, v_3 is not defined and hence not plotted.

up the pair is expected. Figure 15 shows the measured v_2 from the template fits for both the same-charge and opposite-charge pairs. No systematic difference between the two is observed.

Tables II and III list the systematic uncertainties in the $v_{n,n}$ for the 13 TeV and 5.02 TeV pp data, respectively. Most uncertainties are listed as relative uncertainties (in percentages of the $v_{n,n}$), while some are listed as absolute uncertainties. Uncertainties for the $p+$Pb data are listed in Table IV. The corresponding uncertainties in the v_n are obtained by propagating the uncertainties in the $v_{n,n}$ when using Eq. (3) to obtain the v_n. In some cases the systematic uncertainties in the $v_{n,n}$ are larger than 100%. In these cases the corresponding uncertainties in the v_n cannot be calculated, as the v_n are only defined for $v_{n,n} > 0$. Such cases are excluded from the v_n results presented in Sec. VII below.

VII. RESULTS

Figure 16 provides a summary of the main results of this paper in the inclusive $p_{\rm T}$ interval $0.5 < p_{\rm T} < 5$ GeV. It compares the v_n obtained from the 5.02 TeV, 13 TeV pp, and 5.02 TeV $p+$Pb template fits. The left panels show v_2, v_3, and v_4 as a function of $N_{\rm ch}^{\rm rec}$ while the right panels show the results as a function of $p_{\rm T}^{\rm a}$ for the $N_{\rm ch}^{\rm rec} \geqslant 60$ multiplicity range. The measured v_3 and v_4 in the 5.02 TeV pp data for $0.5 < p_{\rm T}^{\rm a,b} < 5$ GeV have large systematic uncertainties associated with the choice of peripheral reference and are not

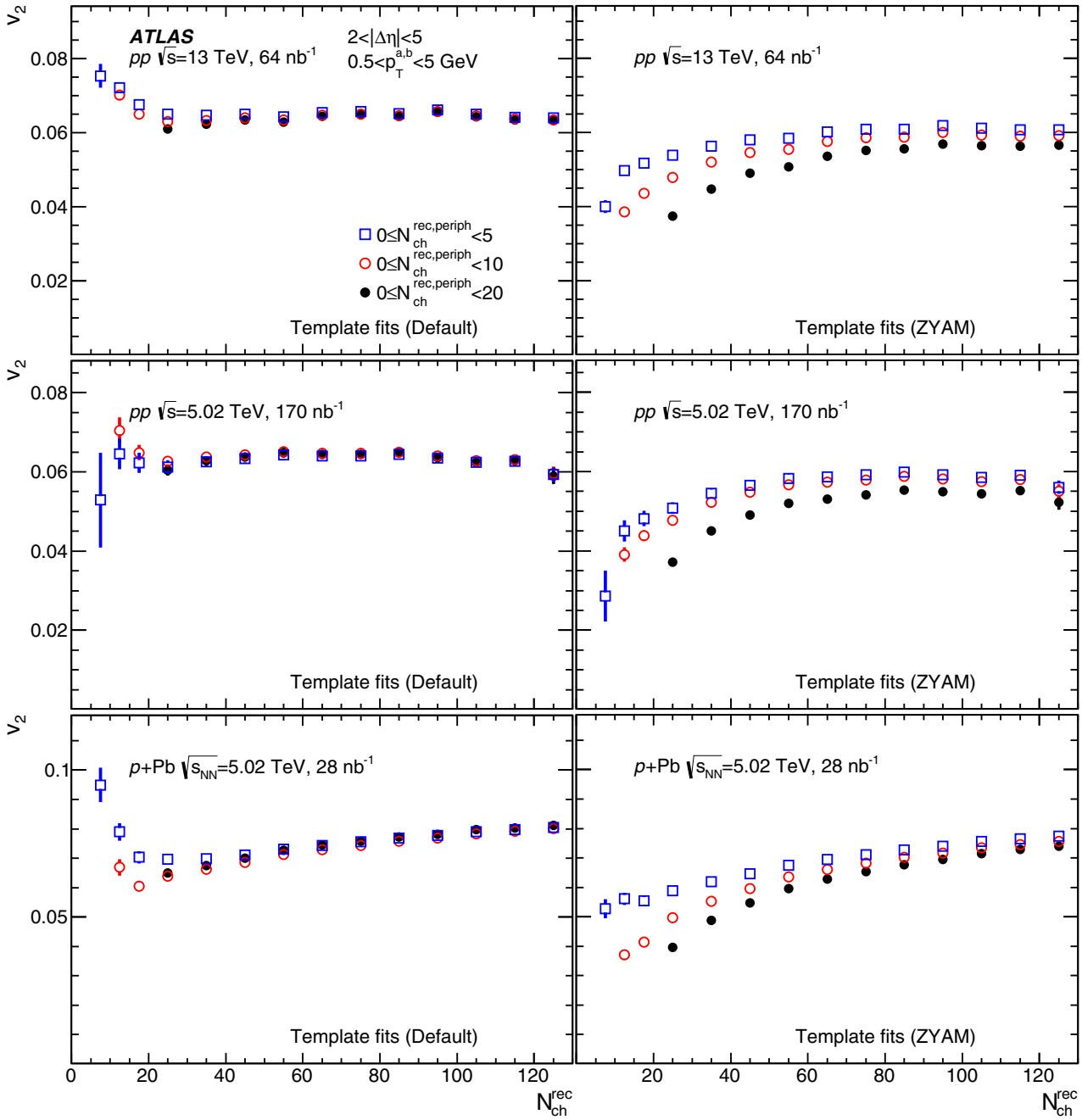

FIG. 14. Dependence of v_2 on the peripheral bin chosen for the default (left panels) and ZYAM-based (right panels) template fitting methods. The top panels correspond to 13 TeV pp collisions, middle panels correspond to 5.02 TeV pp collisions, and the lower panels correspond to 5.02 TeV $p+\mathrm{Pb}$ collisions. The results are plotted as a function of $N_{\mathrm{ch}}^{\mathrm{rec}}$ and for $0.5 < p_{\mathrm{T}}^{\mathrm{a,b}} < 5$ GeV. The error bars indicate statistical uncertainties.

shown in Fig. 16. They are shown in Fig. 18 for a different p_{T} interval of $1 < p_{\mathrm{T}}^{\mathrm{a,b}} < 5$ GeV. Figure 16 shows that the $p+\mathrm{Pb}$ v_2 increases with increasing $N_{\mathrm{ch}}^{\mathrm{rec}}$ as previously observed [4] while the pp v_2 is $N_{\mathrm{ch}}^{\mathrm{rec}}$-independent within uncertainties. The $p+\mathrm{Pb}$ v_3 is significantly larger than the pp v_3 and also shows a systematic increase with $N_{\mathrm{ch}}^{\mathrm{rec}}$, while the pp v_3 is consistent with being $N_{\mathrm{ch}}^{\mathrm{rec}}$-independent. The pp and $p+\mathrm{Pb}$ v_4 are consistent within large uncertainties, and the $p+\mathrm{Pb}$ v_4 increases weakly with increasing $N_{\mathrm{ch}}^{\mathrm{rec}}$.

The difference between the pp and $p+\mathrm{Pb}$ results for the $N_{\mathrm{ch}}^{\mathrm{rec}}$ dependence of the v_n is expected. Studies of the centrality dependence of the multiplicity distributions in $p+\mathrm{Pb}$ collisions show a strong correlation between the multiplicity and the number of participants, or equivalently, the number of scatterings of the proton in the nucleus [73]. Regardless of the interpretation of the results, a dependence of the v_n on the geometry of the $p+\mathrm{Pb}$ collisions is expected [74]. In contrast, the relationship between multiplicity and

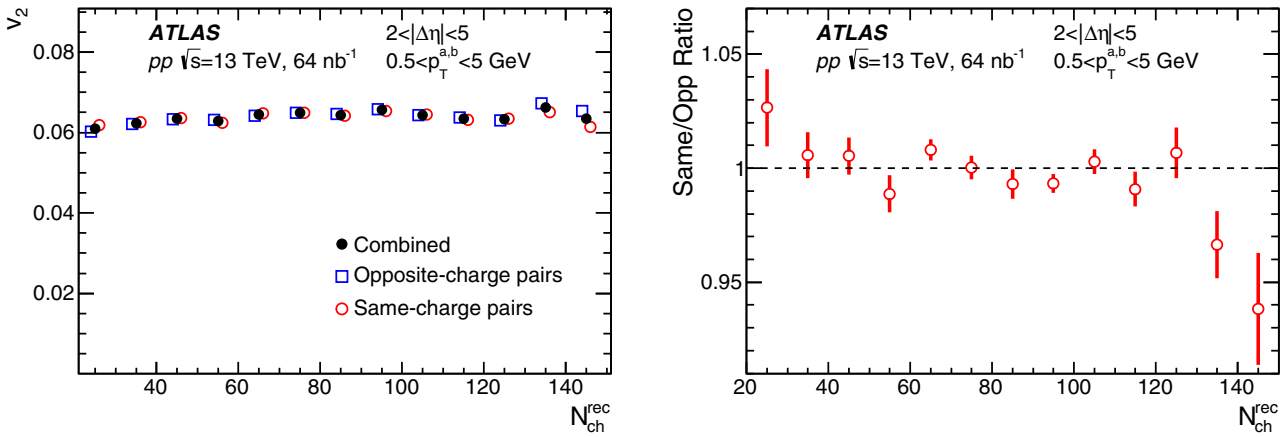

FIG. 15. Left panel: comparison of the v_2 for same-charge and opposite-charge pairs in the 13 TeV pp data. Also shown are the v_2 values for the two types of pairs combined. Right panel: ratio of the same-charge to the opposite-charge v_2. The results are for $0.5 < p_{\mathrm{T}}^{\mathrm{a,b}} < 5$ GeV. For clarity, the data points for the same-charge and opposite-charge v_n are slightly shifted along the x axis. The error bars indicate statistical uncertainties.

geometry in pp collisions is poorly understood and necessarily different as there are, by definition, only two colliding nucleons. However, an early study of this problem accounting for perturbative evolution did predict a weak dependence of v_2 on multiplicity, as observed in this measurement [75]. A more recent study that models the proton substructure and fluctuations in the multiplicity of the final particles showed that the eccentricities ϵ_2 and ϵ_3 of the initial entropy-density distributions in pp collisions have no correlation with the final particle multiplicity [76]. If the v_n in pp collisions are directly related to the ϵ_n, then the calculations in Ref. [76] are consistent with the trends observed in the measured v_n.

The pp and $p+\mathrm{Pb}$ $v_2(p_{\mathrm{T}})$ shown in Fig. 16 display similar trends with both increasing with p_{T} at low p_{T}, reaching a maximum near 3 GeV and decreasing at higher p_{T}. The $v_2(p_{\mathrm{T}})$ values for the 5.02 and 13 TeV pp data agree within uncertainties. The p_{T} dependence of the v_3 and v_4 values is similar to that of v_2 at low p_{T}, where the $p+\mathrm{Pb}$ results increase more rapidly with increasing p_{T}. However, unlike for v_2, the values of v_3 and v_4 are similar at high p_{T} for the pp and $p+\mathrm{Pb}$ data. A direct test of the similarity of the p_{T} dependence of the Fourier coefficients in pp and $p+\mathrm{Pb}$ collisions is provided in Fig. 17 for $n=2$. The pp v_2 values have been multiplied by 1.51, the ratio ($p+\mathrm{Pb}$ to pp) of the maximum v_2 in the top right panel in Fig. 16. The resulting $v_2(p_{\mathrm{T}}^{\mathrm{a}})$ values for (scaled) pp and $p+\mathrm{Pb}$ agree well for $p_{\mathrm{T}}^{\mathrm{a}}$ up to 5 GeV. At higher $p_{\mathrm{T}}^{\mathrm{a}}$ the pp v_2 decreases more rapidly due to the above-described multiplicity-dependent change in the shape of the dijet peak in the two-particle correlation function at high p_{T}. After the scaling, the pp $v_2(p_{\mathrm{T}}^{\mathrm{a}})$ are slightly higher than the $p+\mathrm{Pb}$ at low $p_{\mathrm{T}}^{\mathrm{a}}$, but the similarity of the shapes of the p_{T} dependence is, nonetheless, striking.

A separate evaluation of the $N_{\mathrm{ch}}^{\mathrm{rec}}$ dependence of the v_2, v_3, and v_4 values is shown in Fig. 18 for the $1 < p_{\mathrm{T}}^{\mathrm{a,b}} < 5$ GeV interval, where the 5.02 TeV pp measurements yield meaningful v_3 and v_4 results. The figure shows agreement between the 5.02 and 13 TeV pp data for all three Fourier coefficients. It also shows that the $p+\mathrm{Pb}$ v_2, v_3, and v_4 rise

TABLE II. Systematic uncertainties for the $v_{n,n}$ obtained from the template analysis in the 13 TeV pp data. Where ranges are provided for both multiplicity and the uncertainty, the uncertainty varies from the first value to the second value as the multiplicity varies from the lower to upper limits of the range. Where no multiplicity range is provided the uncertainty is multiplicity independent.

Source	$v_{2,2}$		$v_{3,3}$		$v_{4,4}$	
	$N_{\mathrm{ch}}^{\mathrm{rec}}$ range	syst. unc.	$N_{\mathrm{ch}}^{\mathrm{rec}}$ range	syst. unc.	$N_{\mathrm{ch}}^{\mathrm{rec}}$ range	syst. unc.
Choice of peripheral bin (%)	20–30	7	20–50	>100	20–50	30
$0.5 < p_{\mathrm{T}}^{\mathrm{a,b}} < 5$ GeV	30–60	7–2	50–100	100–40	50–100	30–10
	>60	2	>100	40	>100	10
Choice of peripheral bin (%)	20–30	6	20–60	40–20		
$1 < p_{\mathrm{T}}^{\mathrm{a,b}} < 5$ GeV	30–60	6–2	60–100	20–10		5
	>80	2	>100	10		
Pileup (%)	0–150	0–3	0–150	0–3	0–150	0–3
Tracking efficiency (%)		0.5		2.5		2.5
Pair acceptance (absolute)		2×10^{-5}		2×10^{-5}		2×10^{-5}
MC closure (absolute)		1×10^{-4}		2×10^{-5}		2×10^{-5}

TABLE III. Systematic uncertainties for the $v_{n,n}$ obtained from the template analysis in the 5.02 TeV pp data. Where ranges are provided for both multiplicity and the uncertainty, the uncertainty varies from the first value to the second value as the multiplicity varies from the lower to upper limits of the range. Where no multiplicity range is provided the uncertainty is multiplicity independent.

Source	$v_{2,2}$		$v_{3,3}$		$v_{4,4}$	
	$N_{\mathrm{ch}}^{\mathrm{rec}}$ range	syst. unc.	$N_{\mathrm{ch}}^{\mathrm{rec}}$ range	syst. unc.	$N_{\mathrm{ch}}^{\mathrm{rec}}$ range	syst. unc.
Choice of peripheral bin (%)	20–30	8	20–30	55	20–30	>100
$1 < p_{\mathrm{T}}^{\mathrm{a,b}} < 5$ GeV	30–70	8–2	30–50	55–12	>30	50
	>70	2	>50	12		
Pileup (%)	0–120	0–4	0–120	0–4	0–120	0–4
Tracking efficiency (%)		0.5		2.5		2.5
Pair acceptance (absolute)		2×10^{-5}		2×10^{-5}		2×10^{-5}
MC closure (absolute)		1×10^{-4}		2×10^{-5}		2×10^{-5}

monotonically with increasing $N_{\mathrm{ch}}^{\mathrm{rec}}$ while the pp results are generally $N_{\mathrm{ch}}^{\mathrm{rec}}$ independent. One possible exception to this statement is that the 13 TeV data indicate a small (∼15%) decrease in v_2 in the two lowest $N_{\mathrm{ch}}^{\mathrm{rec}}$ intervals. The pp and $p+\mathrm{Pb}$ v_3 and v_4 agree at low $N_{\mathrm{ch}}^{\mathrm{rec}}$ while v_2 still differs significantly, although by a smaller amount than at larger $N_{\mathrm{ch}}^{\mathrm{rec}}$. This behavior is different from that observed in the inclusive p_{T} interval, which may, in turn, reflect the convergence of the $v_2(p_{\mathrm{T}})$ between the pp and $p+\mathrm{Pb}$ data shown in the top right panel of Fig. 16.

Measurements [70,77] and theoretical analyses [78–82] of the correlations between the Fourier coefficients and event-plane angles of different flow harmonics in $\mathrm{Pb}+\mathrm{Pb}$ collisions have indicated significant "nonlinearity" resulting from collective expansion such that the response of the medium to an initial elliptic eccentricity can contribute to $\cos(4\phi)$ modulation of the produced particles. In $\mathrm{Pb}+\mathrm{Pb}$ collisions, the nonlinear contribution to v_4 is found to dominate over the geometric contribution except for the most central collisions where the initial-state fluctuations have the greatest impact. The nonlinear contribution to v_4 is expected to be proportional to v_2^2 so a comparison of the measured v_4 to v_2^2 in pp and $p+\mathrm{Pb}$ collisions may be of interest. The results are presented in Fig. 19, which shows v_4/v_2^2 versus $N_{\mathrm{ch}}^{\mathrm{rec}}$ for the 13 TeV pp and the $p+\mathrm{Pb}$ data. In the ratio, the correlated systematic uncertainties between the measured v_4 and v_2^2 cancel. The ratio is observed to be constant as a function of $N_{\mathrm{ch}}^{\mathrm{rec}}$ for both data sets even though the $p+\mathrm{Pb}$ v_2 and v_4 increase with $N_{\mathrm{ch}}^{\mathrm{rec}}$. The v_4/v_2^2 ratio is observed to be 50% larger in the pp data than in the $p+\mathrm{Pb}$ data. Naively, this would indicate a larger nonlinear contribution to v_4 in pp collisions compared to $p+\mathrm{Pb}$ collisions.

VIII. CONCLUSION

In summary, this paper presents results of two-charged-particle correlation measurements made by ATLAS in $\sqrt{s} =$ 13 and 5.02 TeV pp collisions and in 5.02 TeV $p+\mathrm{Pb}$ collisions at the LHC. This measurement uses integrated luminosities of 64 nb^{-1} for the $\sqrt{s} = 13$ TeV pp data, 170 nb^{-1} for the $\sqrt{s} = 5.02$ TeV pp data, and 28 nb^{-1} for the $\sqrt{s_{\mathrm{NN}}} = 5.02$ TeV $p+\mathrm{Pb}$ data. The 13 TeV measurements represent an extension of results presented in Ref. [41] using a larger data sample. The $p+\mathrm{Pb}$ results are obtained from a

TABLE IV. Systematic uncertainties for the $v_{n,n}$ obtained from the template analysis in the 5.02 TeV $p+\mathrm{Pb}$ data. Where ranges are provided for both multiplicity and the uncertainty, the uncertainty varies from the first value to the second value as the multiplicity varies from the lower to upper limits of the range. Where no multiplicity range is provided the uncertainty is multiplicity independent.

Source	$v_{2,2}$		$v_{3,3}$		$v_{4,4}$	
	$N_{\mathrm{ch}}^{\mathrm{rec}}$ range	syst. unc.	$N_{\mathrm{ch}}^{\mathrm{rec}}$ range	syst. unc.	$N_{\mathrm{ch}}^{\mathrm{rec}}$ range	syst. unc.
Choice of peripheral bin (%)	20–30	5	20–30	>100	20–30	>100
$0.5 < p_{\mathrm{T}}^{\mathrm{a,b}} < 5$ GeV	30–250	5–2	30–50	100–40	30–50	100–20
			50–250	40–5	50–250	20–2
Choice of peripheral bin (%)	20–30	12	20–50	55–20	20–50	70–10
$1 < p_{\mathrm{T}}^{\mathrm{a,b}} < 5$ GeV	30–50	12–6	50–100	20–10	50–250	10–5
	50–250	6–2	100–250	10–5		
Pileup (%)	0–300	0–4	0–300	0–4	0–300	0–4
Tracking efficiency (%)		0.8		1.6		2.4
Pair acceptance (absolute)		10^{-5}		10^{-5}		10^{-5}
MC closure (%)		2		4		8

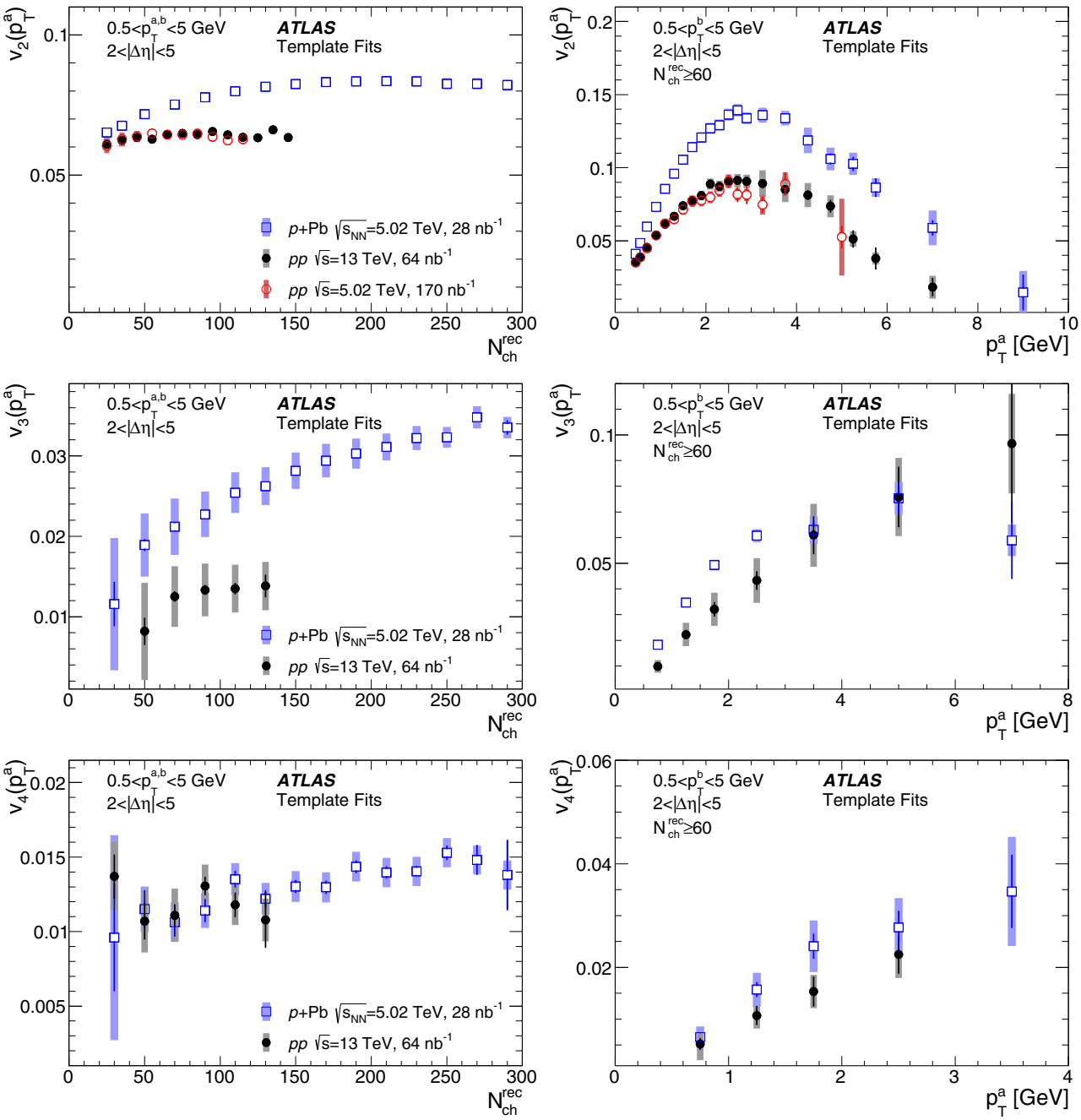

FIG. 16. Left panels: comparison of the v_n obtained from the template fitting procedure in the 13 TeV pp, 5.02 TeV pp, and 5.02 TeV $p+\mathrm{Pb}$ data, as a function of $N_{\mathrm{ch}}^{\mathrm{rec}}$. The results are for $0.5 < p_{\mathrm{T}}^{\mathrm{a,b}} < 5$ GeV. Right panels: the p_{T} dependence of the v_n for the $N_{\mathrm{ch}}^{\mathrm{rec}} \geqslant 60$ multiplicity range. From top to bottom the rows correspond to $n = 2$, 3, and 4, respectively. The error bars and shaded bands indicate statistical and systematic uncertainties, respectively.

reanalysis of run 1 data presented in Ref. [4] using a template fitting procedure developed for pp collisions and applied in Ref. [41]. The correlation functions are measured for different intervals of measured charged-particle multiplicity and FCal transverse energy and for different intervals of charged-particle transverse momentum; many of the results are presented for an "inclusive" p_{T} interval $0.5 < p_{\mathrm{T}} < 5$ GeV.

One-dimensional distributions of per-trigger-particle yields as a function of azimuthal angle separation, $Y(\Delta\phi)$, are obtained from the long-range ($|\Delta\eta| > 2$) component of the correlation functions. A template fitting procedure is applied to the $Y(\Delta\phi)$ distributions to remove the contributions from hard-scattering processes and to measure the relative amplitudes $v_{n,n}$ of the sinusoidal modulation of the soft underlying event. Results for $v_{2,2}$, $v_{3,3}$, and $v_{4,4}$ are obtained for all three colliding systems. An analysis of the factorizability of the $v_{n,n}$ shows good factorization for most of the measured $N_{\mathrm{ch}}^{\mathrm{rec}}$ and p_{T} intervals although factorization is observed to break

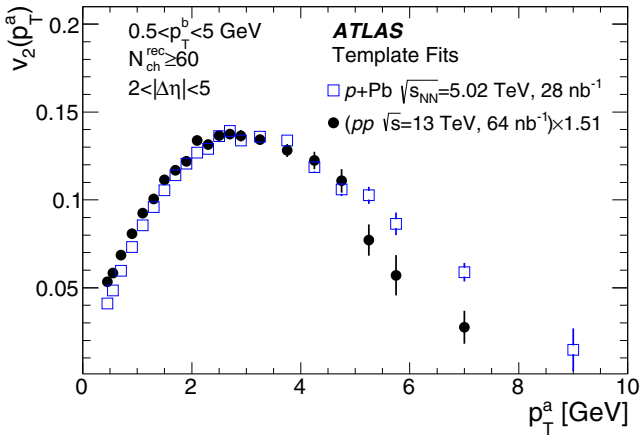

FIG. 17. Comparison of the shapes of the $v_2(p_T)$ in the 13 TeV pp and 5.02 TeV $p+\mathrm{Pb}$ data. The pp v_2 has been scaled by a factor of 1.51 along the y axis in order to match the maximum of the v_2 in the two data sets. The results are for $0.5 < p_T^b < 5$ GeV and $N_{ch}^{rec} \geqslant 60$. The error bars indicate statistical uncertainties.

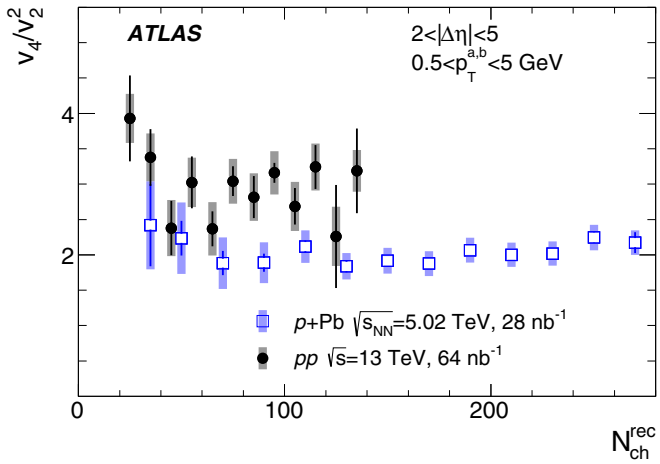

FIG. 19. Ratio of v_4 to v_2^2 as a function of N_{ch}^{rec} in the 13 TeV pp and 5.02 TeV $p+\mathrm{Pb}$ data. The results are for $0.5 < p_T^{a,b} < 5$ GeV. The error bars and shaded bands indicate statistical and systematic uncertainties, respectively.

down for the most extreme combinations of p_T^a and p_T^b in the lowest and highest multiplicity or transverse energy intervals. Since the $v_{n,n}$ results are observed to be consistent with the presence of single-particle modulation of the per-event $dN/d\phi$ distributions, single-particle v_n values are extracted and plotted versus N_{ch}^{rec} and p_T.

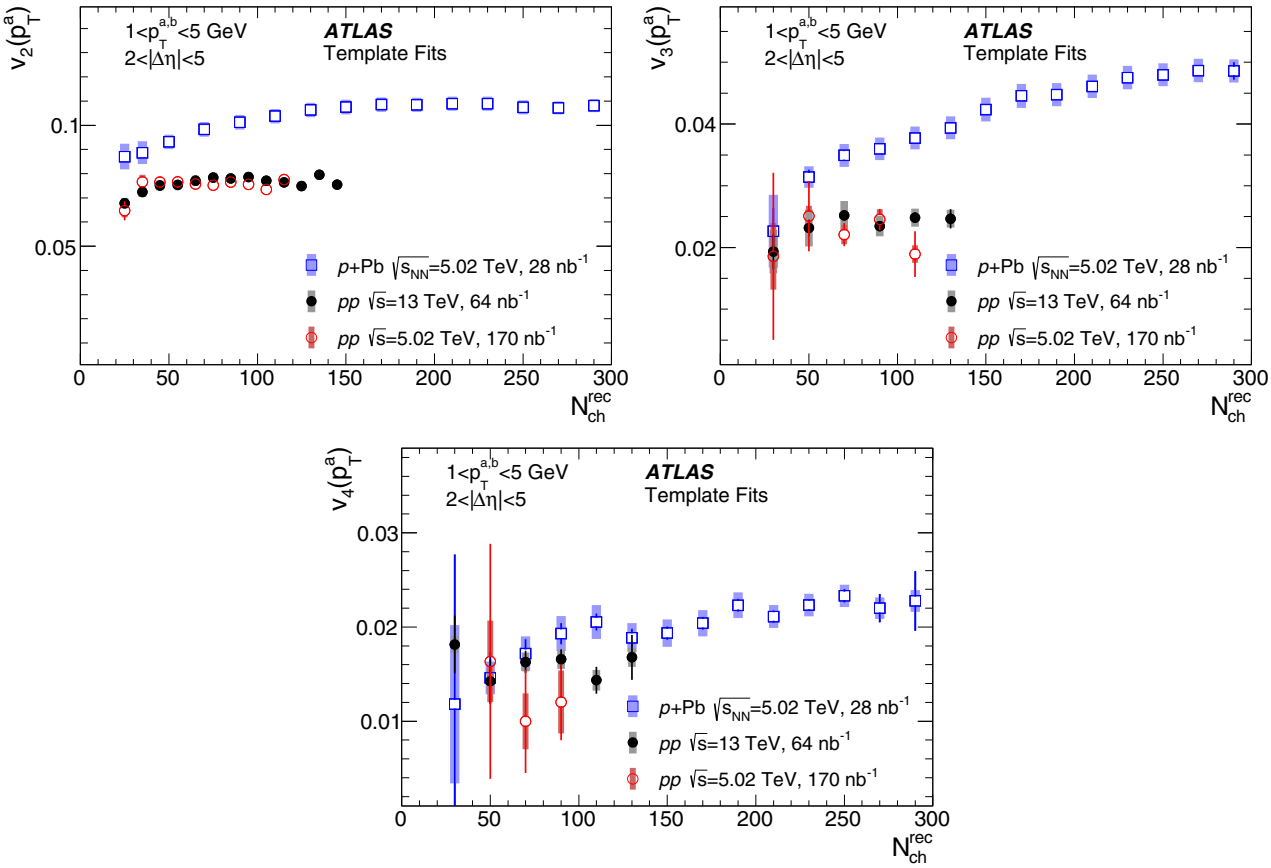

FIG. 18. Comparison of the v_n obtained from the template fitting procedure in the 13 TeV pp, 5.02 TeV pp, and 5.02 TeV $p+\mathrm{Pb}$ data, as a function of N_{ch}^{rec}. The results are for $1 < p_T^{a,b} < 5$ GeV. The three panels correspond to $n = 2$, 3, and 4. The error bars and shaded bands indicate statistical and systematic uncertainties, respectively.

Comparisons of the v_2, v_3, and v_4 values between 13 and 5.02 TeV pp collisions show no significant variation in these quantities with center-of-mass energy. As observed in Ref. [41], the v_2 values obtained in pp collisions at both energies are observed to be independent of $N_{\rm ch}^{\rm rec}$ within uncertainties for the inclusive $p_{\rm T}$ interval. However, for the $1 < p_{\rm T} < 5$ GeV interval a ~15% decrease in v_2 is seen in the lowest $N_{\rm ch}^{\rm rec}$ intervals. The $p+{\rm Pb}$ v_2 values are larger than the pp v_2 values for all multiplicities and are observed to increase slowly with $N_{\rm ch}^{\rm rec}$. However, the $p+{\rm Pb}$ trend appears to converge with the pp values for the lowest multiplicities, at least in the inclusive $p_{\rm T}$ interval. For the $1 < p_{\rm T} < 5$ GeV interval, the $v_2(p_{\rm T})$ trends do not show the same convergence between pp and $p+{\rm Pb}$ results. Similar to the results for v_2, the pp v_3 and v_4 values are consistent with being independent of $N_{\rm ch}^{\rm rec}$ within uncertainties and the $p+{\rm Pb}$ values are observed to increase with $N_{\rm ch}^{\rm rec}$. The pp and $p+{\rm Pb}$ v_3 and v_4 values are consistent within uncertainties in the lowest measured $N_{\rm ch}^{\rm rec}$ intervals.

The $p_{\rm T}$ dependence of the pp and $p+{\rm Pb}$ v_2 values is similar: both rise approximately linearly with $p_{\rm T}$ and reach a maximum near 3 GeV. The maximum $p+{\rm Pb}$ v_2 value is approximately 50% larger than the maximum v_2 values for the 13 and 5.02 TeV pp data, which are consistent within uncertainties. The $p+{\rm Pb}$ v_3 and v_4 values also increase more rapidly with increasing $p_{\rm T}$ than the corresponding pp values for $p_{\rm T} < 2$ GeV, but the $p+{\rm Pb}$ v_3 values saturate above 3 GeV while the measured 13 TeV pp v_3 values continue to increase with increasing $p_{\rm T}$ over the full range of the measurement. A test of the similarity of the $p_{\rm T}$ dependence of the pp and $p+{\rm Pb}$ v_2 values rescaling pp v_2 values shows that the pp and $p+{\rm Pb}$ $v_2(p_{\rm T}^{\rm a})$ distributions are remarkably similar in shape for $p_{\rm T}^{\rm a} < 5$ GeV.

An evaluation of the v_4/v_2^2 ratio in the inclusive $p_{\rm T}$ interval shows results that are $N_{\rm ch}^{\rm rec}$ independent for both the 13 TeV pp data and the $p+{\rm Pb}$ data. This ratio is observed to be 50% larger for the pp data than for the $p+{\rm Pb}$ data.

The similarities between the pp and $p+{\rm Pb}$ results presented here suggest a common physical origin for the azimuthal anisotropies. The difference in the observed multiplicity dependence of the Fourier coefficients likely arises from the different geometry of the pp and $p+{\rm Pb}$ collisions.

ACKNOWLEDGMENTS

We thank CERN for the very successful operation of the LHC, as well as the support staff from our institutions without whom ATLAS could not be operated efficiently. We acknowledge the support of ANPCyT, Argentina; YerPhI, Armenia; ARC, Australia; BMWFW and FWF, Austria; ANAS, Azerbaijan; SSTC, Belarus; CNPq and FAPESP, Brazil; NSERC, NRC and CFI, Canada; CERN; CONICYT, Chile; CAS, MOST and NSFC, China; COLCIENCIAS, Colombia; MSMT CR, MPO CR and VSC CR, Czech Republic; DNRF and DNSRC, Denmark; IN2P3-CNRS, CEA-DSM/IRFU, France; SRNSF, Georgia; BMBF, HGF, and MPG, Germany; GSRT, Greece; RGC, Hong Kong SAR, China; ISF, I-CORE and Benoziyo Center, Israel; INFN, Italy; MEXT and JSPS, Japan; CNRST, Morocco; NWO, Netherlands; RCN, Norway; MNiSW and NCN, Poland; FCT, Portugal; MNE/IFA, Romania; MES of Russia and NRC KI, Russian Federation; JINR; MESTD, Serbia; MSSR, Slovakia; ARRS and MIZŠ, Slovenia; DST/NRF, South Africa; MINECO, Spain; SRC and Wallenberg Foundation, Sweden; SERI, SNSF and Cantons of Bern and Geneva, Switzerland; MOST, Taiwan; TAEK, Turkey; STFC, United Kingdom; DOE and NSF, United States of America. In addition, individual groups and members have received support from BCKDF, the Canada Council, CANARIE, CRC, Compute Canada, FQRNT, and the Ontario Innovation Trust, Canada; EPLANET, ERC, ERDF, FP7, Horizon 2020 and Marie Skłodowska-Curie Actions, European Union; Investissements d'Avenir Labex and Idex, ANR, Région Auvergne and Fondation Partager le Savoir, France; DFG and AvH Foundation, Germany; Herakleitos, Thales, and Aristeia programs co-financed by EU-ESF and the Greek NSRF; BSF, GIF and Minerva, Israel; BRF, Norway; CERCA Programme Generalitat de Catalunya, Generalitat Valenciana, Spain; the Royal Society and Leverhulme Trust, United Kingdom. The crucial computing support from all WLCG partners is acknowledged gratefully, in particular from CERN, the ATLAS Tier-1 facilities at TRIUMF (Canada), NDGF (Denmark, Norway, Sweden), CC-IN2P3 (France), KIT/GridKA (Germany), INFN-CNAF (Italy), NL-T1 (Netherlands), PIC (Spain), ASGC (Taiwan), RAL (UK) and BNL (USA), the Tier-2 facilities worldwide, and large non-WLCG resource providers. Major contributors of computing resources are listed in Ref. [83].

[1] B. Abelev *et al.* (ALICE Collaboration), Long-range angular correlations on the near and away side in $p-{\rm Pb}$ collisions at $\sqrt{s_{NN}} = 5.02$ TeV, Phys. Lett. B **719**, 29 (2013).

[2] ATLAS Collaboration, Observation of Associated Near-Side and Away-Side Long-Range Correlations in $\sqrt{s_{\rm NN}} = 5.02$ TeV Proton–Lead Collisions with the ATLAS Detector, Phys. Rev. Lett. **110**, 182302 (2013).

[3] CMS Collaboration, Multiplicity and transverse momentum dependence of two- and four-particle correlations in pPb and PbPb collisions, Phys. Lett. B **724**, 213 (2013).

[4] ATLAS Collaboration, Measurement of long-range pseudorapidity correlations and azimuthal harmonics in $\sqrt{s_{\rm NN}} =$ 5.02 TeV proton–lead collisions with the ATLAS detector, Phys. Rev. C **90**, 044906 (2014).

[5] CMS Collaboration, Evidence for Collective Multi-Particle Correlations in pPb Collisions, Phys. Rev. Lett. **115**, 012301 (2015).

[6] A. Adare *et al.* (PHENIX Collaboration), Quadrupole Anisotropy in Dihadron Azimuthal Correlations in Central $d+{\rm Au}$ Collisions at $\sqrt{s_{\rm NN}} = 200$ GeV, Phys. Rev. Lett. **111**, 212301 (2013).

[7] A. Adare *et al.* (PHENIX Collaboration), Measurement of Long-Range Angular Correlation and Quadrupole Anisotropy of Pions and (anti)protons in Central $d+{\rm Au}$

Collisions at $\sqrt{s_{\rm NN}} = 200$ GeV, Phys. Rev. Lett. **114**, 192301 (2015).
[8] L. Adamczyk *et al.* (STAR Collaboration), Long-range pseudorapidity dihadron correlations in $d+$Au collisions at $\sqrt{s_{\rm NN}} =$ 200 GeV, Phys. Lett. B **747**, 265 (2015).
[9] A. Adare *et al.* (PHENIX Collaboration), Measurements of Elliptic and Triangular Flow in High-Multiplicity ^{3}He + Au Collisions at $\sqrt{s_{NN}} = 200$ GeV, Phys. Rev. Lett. **115**, 142301 (2015).
[10] K. Aamodt *et al.* (ALICE Collaboration), Higher Harmonic Anisotropic Flow Measurements of Charged Particles in Pb-Pb Collisions at $\sqrt{s_{\rm NN}} = 2.76$ TeV, Phys. Rev. Lett. **107**, 032301 (2011).
[11] K. Aamodt *et al.* (ALICE Collaboration), Harmonic decomposition of two-particle angular correlations in Pb-Pb collisions at $\sqrt{s_{\rm NN}} = 2.76$ TeV, Phys. Lett. B **708**, 249 (2012).
[12] CMS Collaboration, Centrality dependence of dihadron correlations and azimuthal anisotropy harmonics in PbPb collisions at $\sqrt{s_{\rm NN}} = 2.76$ TeV, Eur. Phys. J. C **72**, 2012 (2012).
[13] ATLAS Collaboration, Measurement of the azimuthal anisotropy for charged particle production in $\sqrt{s_{\rm NN}} = 2.76$ TeV lead-lead collisions with the ATLAS detector, Phys. Rev. C **86**, 014907 (2012).
[14] CMS Collaboration, Observation of long-range, near-side angular correlations in proton–proton collisions at the LHC, J. High Energy Phys. 09 (2010) 091.
[15] CMS Collaboration, Observation of long-range, near-side angular correlations in pPb collisions at the LHC, Phys. Lett. B **718**, 795 (2013).
[16] I. Kozlov, M. Luzum, G. Denicol, S. Jeon, and C. Gale, Transverse momentum structure of pair correlations as a signature of collective behavior in small collision systems, arXiv:1405.3976.
[17] P. Huovinen, P. F. Kolb, U. W. Heinz, P. V. Ruuskanen, and S. A. Voloshin, Radial and elliptic flow at RHIC: Further predictions, Phys. Lett. B **503**, 58 (2001).
[18] P. Romatschke and M. Strickland, Collective modes of an anisotropic quark gluon plasma, Phys. Rev. D **68**, 036004 (2003).
[19] U. Heinz and R. Snellings, Collective flow and viscosity in relativistic heavy-ion collisions, Annu. Rev. Nucl. Part. Sci. **63**, 123 (2013).
[20] A. Dumitru, K. Dusling, F. Gelis, J. Jalilian-Marian, T. Lappi, and R. Venugopalan, The Ridge in proton-proton collisions at the LHC, Phys. Lett. B **697**, 21 (2011).
[21] M. G. Ryskin, A. D. Martin, and V. A. Khoze, Probes of multiparticle production at the LHC, J. Phys. G **38**, 085006 (2011).
[22] K. Dusling and R. Venugopalan, Azimuthal Collimation of Long Range Rapidity Correlations by Strong Color Fields in High Multiplicity Hadron-Hadron Collisions, Phys. Rev. Lett. **108**, 262001 (2012).
[23] P. Tribedy and R. Venugopalan, QCD saturation at the LHC: Comparisons of models to p + p and A + A data and predictions for p + Pb collisions, Phys. Lett. B **710**, 125 (2012); **718**, 1154(E) (2013).
[24] K. Dusling and R. Venugopalan, Explanation of systematics of CMS p+Pb high multiplicity di-hadron data at $\sqrt{s}_{\rm NN} =$ 5.02 TeV, Phys. Rev. D **87**, 054014 (2013).
[25] K. Dusling and R. Venugopalan, Comparison of the color glass condensate to dihadron correlations in proton-proton and proton-nucleus collisions, Phys. Rev. D **87**, 094034 (2013).
[26] A. Dumitru and V. Skokov, Anisotropy of the semiclassical gluon field of a large nucleus at high energy, Phys. Rev. D **91**, 074006 (2015).
[27] J. Noronha and A. Dumitru, Azimuthal asymmetries in high-energy collisions of protonswith holographic shockwaves, Phys. Rev. D **89**, 094008 (2014).
[28] A. Dumitru, A. V. Giannini, and V. Skokov, Anisotropic particle production and azimuthal correlationsin high-energy pA collisions, arXiv:1503.03897.
[29] T. Lappi, Azimuthal harmonics of color fields in a high energynucleus, Phys. Lett. B **744**, 315 (2015).
[30] P. Bozek, Collective flow in p-Pb and d-Pd collisions at TeVenergies, Phys. Rev. C **85**, 014911 (2012).
[31] P. Bozek and W. Broniowski, Correlations from hydrodynamic flow in p-Pb collisions, Phys. Lett. B **718**, 1557 (2013).
[32] A. Bzdak, B. Schenke, P. Tribedy, and R. Venugopalan, Initial state geometry and the role of hydrodynamics inproton-proton, proton-nucleus and deuteron-nucleus collisions, Phys. Rev. C **87**, 064906 (2013).
[33] P. Bozek and W. Broniowski, Collective dynamics in high-energy proton-nucleuscollisions, Phys. Rev. C **88**, 014903 (2013).
[34] E. Shuryak and I. Zahed, High-multiplicity pp and pA collisions: Hydrodynamics at itsedge, Phys. Rev. C **88**, 044915 (2013).
[35] P. Bozek, W. Broniowski, and G. Torrieri, Mass Hierarchy in Identified Particle Distributions Inproton-Lead Collisions, Phys. Rev. Lett. **111**, 172303 (2013).
[36] G. Y. Qin and B. Müller, Elliptic and triangular flow anisotropy in deuteron-goldcollisions at $\sqrt{s_{\rm NN}} = 200$ GeV at RHIC and in proton-leadcollisions at $\sqrt{s_{\rm NN}} = 5.02$ TeV at the LHC, Phys. Rev. C **89**, 044902 (2014).
[37] G. Başar and D. Teaney, Scaling relation between pA and AA collisions, Phys. Rev. C **90**, 054903 (2014).
[38] M. Habich, G. A. Miller, P. Romatschke, and W. Xiang, Testing hydrodynamic descriptions of p+p collisions at $\sqrt{s} = 7$ TeV, Eur. Phys. J. C **76**, 408 (2016).
[39] P. M. Chesler, Colliding Shock Waves and Hydrodynamics in Small Systems, Phys. Rev. Lett. **115**, 241602 (2015).
[40] P. M. Chesler, How Big are the Smallest Drops of Quark-Gluon Plasma? J. High Energy Phys. 03 (2016) 146.
[41] ATLAS Collaboration, Observation of Long-Range Elliptic Anisotropies in $\sqrt{s} = 13$ and 2.76 TeV pp Collisions with the ATLAS Detector, Phys. Rev. Lett. **116**, 172301 (2016).
[42] H. Sorge, Elliptical Flow: A Signature for Early Pressure Inultrarelativistic Nucleus-Nucleus Collisions, Phys. Rev. Lett. **78**, 2309 (1997).
[43] P. F. Kolb, U. W. Heinz, P. Huovinen, K. J. Eskola, and K. Tuominen, Centrality dependence of multiplicity, transverse energy,and elliptic flow from hydrodynamics, Nucl. Phys. A **696**, 197 (2001).
[44] B. Alver and G. Roland, Collision geometry fluctuations and triangular flow inheavy-ion collisions, Phys. Rev. C **81**, 054905 (2010); **82**, 039903(E) (2010).
[45] B. Schenke, S. Jeon, and C. Gale, Elliptic and Triangular Flow in Event-By-Event (3+1)Dviscous Hydrodynamics, Phys. Rev. Lett. **106**, 042301 (2011).
[46] H. Holopainen, H. Niemi, and K. J. Eskola, Event-by-event hydrodynamics and elliptic flow fromfluctuating initial state, Phys. Rev. C **83**, 034901 (2011).

[47] B. H. Alver, C. Gombeaud, M. Luzum, and J. Y. Ollitrault, Triangular flow in hydrodynamics and transport theory, Phys. Rev. C **82**, 034913 (2010).
[48] H. Petersen, G. Y. Qin, S. A. Bass, and B. Muller, Triangular flow in event-by-event ideal hydrodynamics in Au+Au collisions at $\sqrt{s_{NN}} = 200A$ GeV, Phys. Rev. C **82**, 041901 (2010).
[49] G. Y. Qin, H. Petersen, S. A. Bass, and B. Muller, Translation of collision geometry fluctuations into momentumanisotropies in relativistic heavy-ion collisions, Phys. Rev. C **82**, 064903 (2010).
[50] F. G. Gardim, F. Grassi, M. Luzum, and J. Y. Ollitrault, Mapping the hydrodynamic response to the initial geometry inheavy-ion collisions, Phys. Rev. C **85**, 024908 (2012).
[51] B. Schenke, P. Tribedy, and R. Venugopalan, Fluctuating Glasma Initial Conditions and Flow in Heavy Ioncollisions, Phys. Rev. Lett. **108**, 252301 (2012).
[52] F. G. Gardim, F. Grassi, M. Luzum, and J.-Y. Ollitrault, Breaking of factorization of two-particle correlations inhydrodynamics, Phys. Rev. C **87**, 031901 (2013).
[53] CMS Collaboration, Evidence for transverse momentum and pseudorapiditydependent event plane fluctuations in PbPb and *p*Pb collisions, Phys. Rev. C **92**, 034911 (2015).
[54] ATLAS Collaboration, The ATLAS Experiment at the CERN Large Hadron Collider, JINST **3**, S08003 (2008).
[55] ATLAS Collaboration, ATLAS Insertable B-Layer Technical Design Report, CERN-LHCC-2010-013. ATLAS-TDR-19, 2010, http://cds.cern.ch/record/1291633
[56] ATLAS Collaboration, ATLAS Insertable B-Layer Technical Design Report Addendum, CERN-LHCC-2012-009. ATLAS-TDR-19-ADD-1, Addendum to CERN-LHCC-2010-013, ATLAS-TDR-019, 2012, http://cds.cern.ch/record/1451888
[57] ATLAS Collaboration, The ATLAS Inner Detector commissioning and calibration, Eur. Phys. J. C **70**, 787 (2010).
[58] ATLAS Collaboration, Performance of the ATLAS Trigger System in 2010, Eur. Phys. J. C **72**, 1849 (2012).
[59] ATLAS Collaboration, Charged-particle multiplicities in *pp* interactionsmeasured with the ATLAS detector at the LHC, New J. Phys. **13**, 053033 (2011).
[60] A. Salzburger on behalf of the ATLAS Collaboration, Optimisation of the ATLAS Track Reconstruction Software for Run-2, J. Phys.: Conf. Ser. **664**, 072042 (2015).
[61] ATLAS Collaboration, The Optimization of ATLAS Track Reconstruction in DenseEnvironments ATL-PHYS-PUB-2015-006, 2015, http://cdsweb.cern.ch/record/2002609
[62] S. Agostinelli *et al.* (GEANT4 Collaboration), GEANT4: A simulation toolkit, Nucl. Instrum. Methods Phys. Res., Sect. A **506**, 250 (2003).
[63] ATLAS Collaboration, The ATLAS Simulation Infrastructure, Eur. Phys. J. C **70**, 823 (2010).
[64] X. N. Wang and M. Gyulassy, HIJING: A Monte Carlo model for multiple jet production in pp, p A and A A collisions, Phys. Rev. D **44**, 3501 (1991).
[65] T. Sjöstrand, S. Mrenna, and P. Z. Skands, A Brief Introduction to PYTHIA 8.1, Comput. Phys. Commun. **178**, 852 (2008).
[66] ATLAS Collaboration, ATLAS tunes of PYTHIA6 and PYTHIA8 for MC11, ATL-PHYS-PUB-2011-009, 2011, http://cds.cern.ch/record/1363300
[67] A. Sherstnev and R. S. Thorne, Parton Distributions for LO Generators, Eur. Phys. J. C **55**, 553 (2008).
[68] ATLAS Collaboration, Charged-particle distributions in $\sqrt{s} =$ 13 TeV *pp* interactions measured with the ATLAS detector at the LHC, Phys. Lett. B **758**, 67 (2016).
[69] ATLAS Collaboration, Measurement of the distributions of event-by-event flow harmonics in lead-lead collisions at $\sqrt{s_{\rm NN}} =$ 2.76 TeV with the ATLAS detector at the LHC, J. High Energy Phys. 11 (2013) 183.
[70] ATLAS Collaboration, Measurement of the correlation between flow harmonics of different order in lead-lead collisions at $\sqrt{s_{NN}} = 2.76$ TeV with the ATLAS detector, Phys. Rev. C **92**, 034903 (2015).
[71] A. Adare *et al.*, PHENIX Collaboration, Dihadron azimuthal correlations in Au+Au collisions at $\sqrt{s_{NN}} = 200$-GeV, Phys. Rev. C **78**, 014901 (2008).
[72] N. N. Ajitanand *et al.*, Decomposition of harmonic and jet contributions toparticle-pair correlations at ultra-relativistic energies, Phys. Rev. C **72**, 011902 (2005).
[73] ATLAS Collaboration, Measurement of the centrality dependence of thecharged-particle pseudorapidity distribution in proton–lead collisions at $\sqrt{s_{\rm NN}} = 5.02$ TeV with the ATLAS detector, Eur. Phys. J. C **76**, 199 (2016).
[74] K. Dusling, W. Li, and B. Schenke, Novel collective phenomena in high-energy proton-protonand proton-nucleus collisions, Int. J. Mod. Phys. E **25**, 1630002 (2016).
[75] E. Avsar, C. Flensburg, Y. Hatta, and T. Ueda, Eccentricity and elliptic flow in proton-proton collisionsfrom parton evolution, Phys. Lett. B **702**, 394 (2011).
[76] K. Welsh, J. Singer, and U. W. Heinz, Initial state fluctuations in collisions between light andheavy ions, Phys. Rev. C **94**, 024919 (2016).
[77] ATLAS Collaboration, Measurement of event-plane correlations in $\sqrt{s_{NN}} = 2.76$ TeV lead-lead collisions with the ATLAS detector, Phys. Rev. C **90**, 024905 (2014).
[78] Z. Qiu and U. Heinz, Hydrodynamic event-plane correlations in Pb+Pb collisions at $\sqrt{s} = 2.76A$ TeV, Phys. Lett. B **717**, 261 (2012).
[79] D. Teaney and L. Yan, Non-linear flow response and reaction plane correlations, Nucl. Phys. A **904-905**, 365c (2013).
[80] D. Teaney and L. Yan, Event-plane correlations and hydrodynamic simulations ofheavy ion collisions, Phys. Rev. C **90**, 024902 (2014).
[81] L. Yan and J. Y. Ollitrault, $\nu_4, \nu_5, \nu_6, \nu_7$: nonlinear hydrodynamicresponse versus LHC data, Phys. Lett. B **744**, 82 (2015).
[82] J. Qian, U. W. Heinz, and J. Liu, Mode-coupling effects in anisotropic flow in heavy-ioncollisions, Phys. Rev. C **93**, 064901 (2016).
[83] ATLAS Collaboration, ATLAS Computing Acknowledgements 2016-2017, ATL-GEN-PUB-2016-002, 2016, http://cds.cern.ch/record/2202407

M. Aaboud,[137d] G. Aad,[88] B. Abbott,[115] J. Abdallah,[8] O. Abdinov,[12] B. Abeloos,[119] O. S. AbouZeid,[139] N. L. Abraham,[151] H. Abramowicz,[155] H. Abreu,[154] R. Abreu,[118] Y. Abulaiti,[148a,148b] B. S. Acharya,[167a,167b,a] S. Adachi,[157] L. Adamczyk,[41a]

D. L. Adams,[27] J. Adelman,[110] S. Adomeit,[102] T. Adye,[133] A. A. Affolder,[139] T. Agatonovic-Jovin,[14] J. A. Aguilar-Saavedra,[128a,128f] S. P. Ahlen,[24] F. Ahmadov,[68,b] G. Aielli,[135a,135b] H. Akerstedt,[148a,148b] T. P. A. Åkesson,[84] A. V. Akimov,[98] G. L. Alberghi,[22a,22b] J. Albert,[172] S. Albrand,[58] M. J. Alconada Verzini,[74] M. Aleksa,[32] I. N. Aleksandrov,[68] C. Alexa,[28b] G. Alexander,[155] T. Alexopoulos,[10] M. Alhroob,[115] B. Ali,[130] M. Aliev,[76a,76b] G. Alimonti,[94a] J. Alison,[33] S. P. Alkire,[38] B. M. M. Allbrooke,[151] B. W. Allen,[118] P. P. Allport,[19] A. Aloisio,[106a,106b] A. Alonso,[39] F. Alonso,[74] C. Alpigiani,[140] A. A. Alshehri,[56] M. Alstaty,[88] B. Alvarez Gonzalez,[32] D. Álvarez Piqueras,[170] M. G. Alviggi,[106a,106b] B. T. Amadio,[16] Y. Amaral Coutinho,[26a] C. Amelung,[25] D. Amidei,[92] S. P. Amor Dos Santos,[128a,128c] A. Amorim,[128a,128b] S. Amoroso,[32] G. Amundsen,[25] C. Anastopoulos,[141] L. S. Ancu,[52] N. Andari,[19] T. Andeen,[11] C. F. Anders,[60b] J. K. Anders,[77] K. J. Anderson,[33] A. Andreazza,[94a,94b] V. Andrei,[60a] S. Angelidakis,[9] I. Angelozzi,[109] A. Angerami,[38] F. Anghinolfi,[32] A. V. Anisenkov,[111,c] N. Anjos,[13] A. Annovi,[126a,126b] C. Antel,[60a] M. Antonelli,[50] A. Antonov,[100,*] D. J. Antrim,[166] F. Anulli,[134a] M. Aoki,[69] L. Aperio Bella,[19] G. Arabidze,[93] Y. Arai,[69] J. P. Araque,[128a] A. T. H. Arce,[48] F. A. Arduh,[74] J-F. Arguin,[97] S. Argyropoulos,[66] M. Arik,[20a] A. J. Armbruster,[145] L. J. Armitage,[79] O. Arnaez,[32] H. Arnold,[51] M. Arratia,[30] O. Arslan,[23] A. Artamonov,[99] G. Artoni,[122] S. Artz,[86] S. Asai,[157] N. Asbah,[45] A. Ashkenazi,[155] B. Åsman,[148a,148b] L. Asquith,[151] K. Assamagan,[27] R. Astalos,[146a] M. Atkinson,[169] N. B. Atlay,[143] K. Augsten,[130] G. Avolio,[32] B. Axen,[16] M. K. Ayoub,[119] G. Azuelos,[97,d] M. A. Baak,[32] A. E. Baas,[60a] M. J. Baca,[19] H. Bachacou,[138] K. Bachas,[76a,76b] M. Backes,[122] M. Backhaus,[32] P. Bagiacchi,[134a,134b] P. Bagnaia,[134a,134b] Y. Bai,[35a] J. T. Baines,[133] M. Bajic,[39] O. K. Baker,[179] E. M. Baldin,[111,c] P. Balek,[175] T. Balestri,[150] F. Balli,[138] W. K. Balunas,[124] E. Banas,[42] Sw. Banerjee,[176,e] A. A. E. Bannoura,[178] L. Barak,[32] E. L. Barberio,[91] D. Barberis,[53a,53b] M. Barbero,[88] T. Barillari,[103] M-S Barisits,[32] T. Barklow,[145] N. Barlow,[30] S. L. Barnes,[87] B. M. Barnett,[133] R. M. Barnett,[16] Z. Barnovska-Blenessy,[36a] A. Baroncelli,[136a] G. Barone,[25] A. J. Barr,[122] L. Barranco Navarro,[170] F. Barreiro,[85] J. Barreiro Guimarães da Costa,[35a] R. Bartoldus,[145] A. E. Barton,[75] P. Bartos,[146a] A. Basalaev,[125] A. Bassalat,[119,f] R. L. Bates,[56] S. J. Batista,[161] J. R. Batley,[30] M. Battaglia,[139] M. Bauce,[134a,134b] F. Bauer,[138] H. S. Bawa,[145,g] J. B. Beacham,[113] M. D. Beattie,[75] T. Beau,[83] P. H. Beauchemin,[165] P. Bechtle,[23] H. P. Beck,[18,h] K. Becker,[122] M. Becker,[86] M. Beckingham,[173] C. Becot,[112] A. J. Beddall,[20d] A. Beddall,[20b] V. A. Bednyakov,[68] M. Bedognetti,[109] C. P. Bee,[150] L. J. Beemster,[109] T. A. Beermann,[32] M. Begel,[27] J. K. Behr,[45] A. S. Bell,[81] G. Bella,[155] L. Bellagamba,[22a] A. Bellerive,[31] M. Bellomo,[89] K. Belotskiy,[100] O. Beltramello,[32] N. L. Belyaev,[100] O. Benary,[155,*] D. Benchekroun,[137a] M. Bender,[102] K. Bendtz,[148a,148b] N. Benekos,[10] Y. Benhammou,[155] E. Benhar Noccioli,[179] J. Benitez,[66] D. P. Benjamin,[48] J. R. Bensinger,[25] S. Bentvelsen,[109] L. Beresford,[122] M. Beretta,[50] D. Berge,[109] E. Bergeaas Kuutmann,[168] N. Berger,[5] J. Beringer,[16] S. Berlendis,[58] N. R. Bernard,[89] C. Bernius,[112] F. U. Bernlochner,[23] T. Berry,[80] P. Berta,[131] C. Bertella,[86] G. Bertoli,[148a,148b] F. Bertolucci,[126a,126b] I. A. Bertram,[75] C. Bertsche,[45] D. Bertsche,[115] G. J. Besjes,[39] O. Bessidskaia Bylund,[148a,148b] M. Bessner,[45] N. Besson,[138] C. Betancourt,[51] A. Bethani,[58] S. Bethke,[103] A. J. Bevan,[79] R. M. Bianchi,[127] M. Bianco,[32] O. Biebel,[102] D. Biedermann,[17] R. Bielski,[87] N. V. Biesuz,[126a,126b] M. Biglietti,[136a] J. Bilbao De Mendizabal,[52] T. R. V. Billoud,[97] H. Bilokon,[50] M. Bindi,[57] S. Binet,[119] A. Bingul,[20b] C. Bini,[134a,134b] S. Biondi,[22a,22b] T. Bisanz,[57] D. M. Bjergaard,[48] C. W. Black,[152] J. E. Black,[145] K. M. Black,[24] D. Blackburn,[140] R. E. Blair,[6] T. Blazek,[146a] I. Bloch,[45] C. Blocker,[25] A. Blue,[56] W. Blum,[86,*] U. Blumenschein,[57] S. Blunier,[34a] G. J. Bobbink,[109] V. S. Bobrovnikov,[111,c] S. S. Bocchetta,[84] A. Bocci,[48] C. Bock,[102] M. Boehler,[51] D. Boerner,[178] J. A. Bogaerts,[32] D. Bogavac,[102] A. G. Bogdanchikov,[111] C. Bohm,[148a] V. Boisvert,[80] P. Bokan,[14] T. Bold,[41a] A. S. Boldyrev,[167a,167c] M. Bomben,[83] M. Bona,[79] M. Boonekamp,[138] A. Borisov,[132] G. Borissov,[75] J. Bortfeldt,[32] D. Bortoletto,[122] V. Bortolotto,[62a,62b,62c] K. Bos,[109] D. Boscherini,[22a] M. Bosman,[13] J. D. Bossio Sola,[29] J. Boudreau,[127] J. Bouffard,[2] E. V. Bouhova-Thacker,[75] D. Boumediene,[37] C. Bourdarios,[119] S. K. Boutle,[56] A. Boveia,[32] J. Boyd,[32] I. R. Boyko,[68] J. Bracinik,[19] A. Brandt,[8] G. Brandt,[57] O. Brandt,[60a] U. Bratzler,[158] B. Brau,[89] J. E. Brau,[118] W. D. Breaden Madden,[56] K. Brendlinger,[124] A. J. Brennan,[91] L. Brenner,[109] R. Brenner,[168] S. Bressler,[175] T. M. Bristow,[49] D. Britton,[56] D. Britzger,[45] F. M. Brochu,[30] I. Brock,[23] R. Brock,[93] G. Brooijmans,[38] T. Brooks,[80] W. K. Brooks,[34b] J. Brosamer,[16] E. Brost,[110] J. H Broughton,[19] P. A. Bruckman de Renstrom,[42] D. Bruncko,[146b] R. Bruneliere,[51] A. Bruni,[22a] G. Bruni,[22a] L. S. Bruni,[109] BH Brunt,[30] M. Bruschi,[22a] N. Bruscino,[23] P. Bryant,[33] L. Bryngemark,[84] T. Buanes,[15] Q. Buat,[144] P. Buchholz,[143] A. G. Buckley,[56] I. A. Budagov,[68] F. Buehrer,[51] M. K. Bugge,[121] O. Bulekov,[100] D. Bullock,[8] H. Burckhart,[32] S. Burdin,[77] C. D. Burgard,[51] A. M. Burger,[5] B. Burghgrave,[110] K. Burka,[42] S. Burke,[133] I. Burmeister,[46] J. T. P. Burr,[122] E. Busato,[37] D. Büscher,[51] V. Büscher,[86] P. Bussey,[56] J. M. Butler,[24] C. M. Buttar,[56] J. M. Butterworth,[81] P. Butti,[109] W. Buttinger,[27] A. Buzatu,[56] A. R. Buzykaev,[111,c] S. Cabrera Urbán,[170] D. Caforio,[130] V. M. Cairo,[40a,40b] O. Cakir,[4a] N. Calace,[52] P. Calafiura,[16] A. Calandri,[88] G. Calderini,[83] P. Calfayan,[64] G. Callea,[40a,40b] L. P. Caloba,[26a] S. Calvente Lopez,[85] D. Calvet,[37] S. Calvet,[37] T. P. Calvet,[88] R. Camacho Toro,[33] S. Camarda,[32] P. Camarri,[135a,135b] D. Cameron,[121] R. Caminal Armadans,[169] C. Camincher,[58] S. Campana,[32] M. Campanelli,[81] A. Camplani,[94a,94b] A. Campoverde,[143] V. Canale,[106a,106b] A. Canepa,[163a] M. Cano Bret,[36c] J. Cantero,[116] T. Cao,[155] M. D. M. Capeans Garrido,[32] I. Caprini,[28b] M. Caprini,[28b] M. Capua,[40a,40b] R. M. Carbone,[38] R. Cardarelli,[135a] F. Cardillo,[51] I. Carli,[131] T. Carli,[32] G. Carlino,[106a] L. Carminati,[94a,94b] R. M. D. Carney,[148a,148b] S. Caron,[108] E. Carquin,[34b] G. D. Carrillo-Montoya,[32] J. R. Carter,[30] J. Carvalho,[128a,128c] D. Casadei,[19] M. P. Casado,[13,i] M. Casolino,[13] D. W. Casper,[166] E. Castaneda-Miranda,[147a] R. Castelijn,[109] A. Castelli,[109] V. Castillo Gimenez,[170] N. F. Castro,[128a,j] A. Catinaccio,[32] J. R. Catmore,[121] A. Cattai,[32] J. Caudron,[23] V. Cavaliere,[169] E. Cavallaro,[13] D. Cavalli,[94a] M. Cavalli-Sforza,[13] V. Cavasinni,[126a,126b] F. Ceradini,[136a,136b] L. Cerda Alberich,[170] A. S. Cerqueira,[26b] A. Cerri,[151] L. Cerrito,[135a,135b] F. Cerutti,[16] A. Cervelli,[18] S. A. Cetin,[20c] A. Chafaq,[137a] D. Chakraborty,[110] S. K. Chan,[59] Y. L. Chan,[62a] P. Chang,[169] J. D. Chapman,[30] D. G. Charlton,[19] A. Chatterjee,[52]

C. C. Chau,[161] C. A. Chavez Barajas,[151] S. Che,[113] S. Cheatham,[167a,167c] A. Chegwidden,[93] S. Chekanov,[6] S. V. Chekulaev,[163a] G. A. Chelkov,[68,k] M. A. Chelstowska,[92] C. Chen,[67] H. Chen,[27] S. Chen,[35b] S. Chen,[157] X. Chen,[35c] Y. Chen,[70] H. C. Cheng,[92] H. J Cheng,[35a] Y. Cheng,[33] A. Cheplakov,[68] E. Cheremushkina,[132] R. Cherkaoui El Moursli,[137e] V. Chernyatin,[27,*] E. Cheu,[7] L. Chevalier,[138] V. Chiarella,[50] G. Chiarelli,[126a,126b] G. Chiodini,[76a] A. S. Chisholm,[32] A. Chitan,[28b] M. V. Chizhov,[68] K. Choi,[64] A. R. Chomont,[37] S. Chouridou,[9] B. K. B. Chow,[102] V. Christodoulou,[81] D. Chromek-Burckhart,[32] J. Chudoba,[129] A. J. Chuinard,[90] J. J. Chwastowski,[42] L. Chytka,[117] G. Ciapetti,[134a,134b] A. K. Ciftci,[4a] D. Cinca,[46] V. Cindro,[78] I. A. Cioara,[23] C. Ciocca,[22a,22b] A. Ciocio,[16] F. Cirotto,[106a,106b] Z. H. Citron,[175] M. Citterio,[94a] M. Ciubancan,[28b] A. Clark,[52] B. L. Clark,[59] M. R. Clark,[38] P. J. Clark,[49] R. N. Clarke,[16] C. Clement,[148a,148b] Y. Coadou,[88] M. Cobal,[167a,167c] A. Coccaro,[52] J. Cochran,[67] L. Colasurdo,[108] B. Cole,[38] A. P. Colijn,[109] J. Collot,[58] T. Colombo,[166] P. Conde Muiño,[128a,128b] E. Coniavitis,[51] S. H. Connell,[147b] I. A. Connelly,[80] V. Consorti,[51] S. Constantinescu,[28b] G. Conti,[32] F. Conventi,[106a,l] M. Cooke,[16] B. D. Cooper,[81] A. M. Cooper-Sarkar,[122] F. Cormier,[171] K. J. R. Cormier,[161] T. Cornelissen,[178] M. Corradi,[134a,134b] F. Corriveau,[90,m] A. Cortes-Gonzalez,[32] G. Cortiana,[103] G. Costa,[94a] M. J. Costa,[170] D. Costanzo,[141] G. Cottin,[30] G. Cowan,[80] B. E. Cox,[87] K. Cranmer,[112] S. J. Crawley,[56] G. Cree,[31] S. Crépé-Renaudin,[58] F. Crescioli,[83] W. A. Cribbs,[148a,148b] M. Crispin Ortuzar,[122] M. Cristinziani,[23] V. Croft,[108] G. Crosetti,[40a,40b] A. Cueto,[85] T. Cuhadar Donszelmann,[141] J. Cummings,[179] M. Curatolo,[50] J. Cúth,[86] H. Czirr,[143] P. Czodrowski,[3] G. D'amen,[22a,22b] S. D'Auria,[56] M. D'Onofrio,[77] M. J. Da Cunha Sargedas De Sousa,[128a,128b] C. Da Via,[87] W. Dabrowski,[41a] T. Dado,[146a] T. Dai,[92] O. Dale,[15] F. Dallaire,[97] C. Dallapiccola,[89] M. Dam,[39] J. R. Dandoy,[33] N. P. Dang,[51] A. C. Daniells,[19] N. S. Dann,[87] M. Danninger,[171] M. Dano Hoffmann,[138] V. Dao,[51] G. Darbo,[53a] S. Darmora,[8] J. Dassoulas,[3] A. Dattagupta,[118] W. Davey,[23] C. David,[172] T. Davidek,[131] M. Davies,[155] P. Davison,[81] E. Dawe,[91] I. Dawson,[141] K. De,[8] R. de Asmundis,[106a] A. De Benedetti,[115] S. De Castro,[22a,22b] S. De Cecco,[83] N. De Groot,[108] P. de Jong,[109] H. De la Torre,[93] F. De Lorenzi,[67] A. De Maria,[57] D. De Pedis,[134a] A. De Salvo,[134a] U. De Sanctis,[151] A. De Santo,[151] J. B. De Vivie De Regie,[119] W. J. Dearnaley,[75] R. Debbe,[27] C. Debenedetti,[139] D. V. Dedovich,[68] N. Dehghanian,[3] I. Deigaard,[109] M. Del Gaudio,[40a,40b] J. Del Peso,[85] T. Del Prete,[126a,126b] D. Delgove,[119] F. Deliot,[138] C. M. Delitzsch,[52] A. Dell'Acqua,[32] L. Dell'Asta,[24] M. Dell'Orso,[126a,126b] M. Della Pietra,[106a,l] D. della Volpe,[52] M. Delmastro,[5] P. A. Delsart,[58] D. A. DeMarco,[161] S. Demers,[179] M. Demichev,[68] A. Demilly,[83] S. P. Denisov,[132] D. Denysiuk,[138] D. Derendarz,[42] J. E. Derkaoui,[137d] F. Derue,[83] P. Dervan,[77] K. Desch,[23] C. Deterre,[45] K. Dette,[46] P. O. Deviveiros,[32] A. Dewhurst,[133] S. Dhaliwal,[25] A. Di Ciaccio,[135a,135b] L. Di Ciaccio,[5] W. K. Di Clemente,[124] C. Di Donato,[106a,106b] A. Di Girolamo,[32] B. Di Girolamo,[32] B. Di Micco,[136a,136b] R. Di Nardo,[32] K. F. Di Petrillo,[59] A. Di Simone,[51] R. Di Sipio,[161] D. Di Valentino,[31] C. Diaconu,[88] M. Diamond,[161] F. A. Dias,[49] M. A. Diaz,[34a] E. B. Diehl,[92] J. Dietrich,[17] S. Díez Cornell,[45] A. Dimitrievska,[14] J. Dingfelder,[23] P. Dita,[28b] S. Dita,[28b] F. Dittus,[32] F. Djama,[88] T. Djobava,[54b] J. I. Djuvsland,[60a] M. A. B. do Vale,[26c] D. Dobos,[32] M. Dobre,[28b] C. Doglioni,[84] J. Dolejsi,[131] Z. Dolezal,[131] M. Donadelli,[26d] S. Donati,[126a,126b] P. Dondero,[123a,123b] J. Donini,[37] J. Dopke,[133] A. Doria,[106a] M. T. Dova,[74] A. T. Doyle,[56] E. Drechsler,[57] M. Dris,[10] Y. Du,[36b] J. Duarte-Campderros,[155] E. Duchovni,[175] G. Duckeck,[102] O. A. Ducu,[97,n] D. Duda,[109] A. Dudarev,[32] A. Chr. Dudder,[86] E. M. Duffield,[16] L. Duflot,[119] M. Dührssen,[32] M. Dumancic,[175] A. K. Duncan,[56] M. Dunford,[60a] H. Duran Yildiz,[4a] M. Düren,[55] A. Durglishvili,[54b] D. Duschinger,[47] B. Dutta,[45] M. Dyndal,[45] C. Eckardt,[45] K. M. Ecker,[103] R. C. Edgar,[92] N. C. Edwards,[49] T. Eifert,[32] G. Eigen,[15] K. Einsweiler,[16] T. Ekelof,[168] M. El Kacimi,[137c] V. Ellajosyula,[88] M. Ellert,[168] S. Elles,[5] F. Ellinghaus,[178] A. A. Elliot,[172] N. Ellis,[32] J. Elmsheuser,[27] M. Elsing,[32] D. Emeliyanov,[133] Y. Enari,[157] O. C. Endner,[86] J. S. Ennis,[173] J. Erdmann,[46] A. Ereditato,[18] G. Ernis,[178] J. Ernst,[2] M. Ernst,[27] S. Errede,[169] E. Ertel,[86] M. Escalier,[119] H. Esch,[46] C. Escobar,[127] B. Esposito,[50] A. I. Etienvre,[138] E. Etzion,[155] H. Evans,[64] A. Ezhilov,[125] M. Ezzi,[137e] F. Fabbri,[22a,22b] L. Fabbri,[22a,22b] G. Facini,[33] R. M. Fakhrutdinov,[132] S. Falciano,[134a] R. J. Falla,[81] J. Faltova,[32] Y. Fang,[35a] M. Fanti,[94a,94b] A. Farbin,[8] A. Farilla,[136a] C. Farina,[127] E. M. Farina,[123a,123b] T. Farooque,[13] S. Farrell,[16] S. M. Farrington,[173] P. Farthouat,[32] F. Fassi,[137e] P. Fassnacht,[32] D. Fassouliotis,[9] M. Faucci Giannelli,[80] A. Favareto,[53a,53b] W. J. Fawcett,[122] L. Fayard,[119] O. L. Fedin,[125,o] W. Fedorko,[171] S. Feigl,[121] L. Feligioni,[88] C. Feng,[36b] E. J. Feng,[32] H. Feng,[92] A. B. Fenyuk,[132] L. Feremenga,[8] P. Fernandez Martinez,[170] S. Fernandez Perez,[13] J. Ferrando,[45] A. Ferrari,[168] P. Ferrari,[109] R. Ferrari,[123a] D. E. Ferreira de Lima,[60b] A. Ferrer,[170] D. Ferrere,[52] C. Ferretti,[92] F. Fiedler,[86] A. Filipčič,[78] M. Filipuzzi,[45] F. Filthaut,[108] M. Fincke-Keeler,[172] K. D. Finelli,[152] M. C. N. Fiolhais,[128a,128c] L. Fiorini,[170] A. Fischer,[2] C. Fischer,[13] J. Fischer,[178] W. C. Fisher,[93] N. Flaschel,[45] I. Fleck,[143] P. Fleischmann,[92] G. T. Fletcher,[141] R. R. M. Fletcher,[124] T. Flick,[178] B. M. Flierl,[102] L. R. Flores Castillo,[62a] M. J. Flowerdew,[103] G. T. Forcolin,[87] A. Formica,[138] A. Forti,[87] A. G. Foster,[19] D. Fournier,[119] H. Fox,[75] S. Fracchia,[13] P. Francavilla,[83] M. Franchini,[22a,22b] D. Francis,[32] L. Franconi,[121] M. Franklin,[59] M. Frate,[166] M. Fraternali,[123a,123b] D. Freeborn,[81] S. M. Fressard-Batraneanu,[32] F. Friedrich,[47] D. Froidevaux,[32] J. A. Frost,[122] C. Fukunaga,[158] E. Fullana Torregrosa,[86] T. Fusayasu,[104] J. Fuster,[170] C. Gabaldon,[58] O. Gabizon,[154] A. Gabrielli,[22a,22b] A. Gabrielli,[16] G. P. Gach,[41a] S. Gadatsch,[32] G. Gagliardi,[53a,53b] L. G. Gagnon,[97] P. Gagnon,[64] C. Galea,[108] B. Galhardo,[128a,128c] E. J. Gallas,[122] B. J. Gallop,[133] P. Gallus,[130] G. Galster,[39] K. K. Gan,[113] S. Ganguly,[37] J. Gao,[36a] Y. Gao,[49] Y. S. Gao,[145,g] F. M. Garay Walls,[49] C. García,[170] J. E. García Navarro,[170] M. Garcia-Sciveres,[16] R. W. Gardner,[33] N. Garelli,[145] V. Garonne,[121] A. Gascon Bravo,[45] K. Gasnikova,[45] C. Gatti,[50] A. Gaudiello,[53a,53b] G. Gaudio,[123a] L. Gauthier,[97] I. L. Gavrilenko,[98] C. Gay,[171] G. Gaycken,[23] E. N. Gazis,[10] Z. Gecse,[171] C. N. P. Gee,[133] Ch. Geich-Gimbel,[23] M. Geisen,[86] M. P. Geisler,[60a] K. Gellerstedt,[148a,148b] C. Gemme,[53a] M. H. Genest,[58] C. Geng,[36a,p] S. Gentile,[134a,134b] C. Gentsos,[156] S. George,[80] D. Gerbaudo,[13] A. Gershon,[155] S. Ghasemi,[143] M. Ghneimat,[23] B. Giacobbe,[22a] S. Giagu,[134a,134b] P. Giannetti,[126a,126b] S. M. Gibson,[80] M. Gignac,[171] M. Gilchriese,[16] T. P. S. Gillam,[30] D. Gillberg,[31] G. Gilles,[178] D. M. Gingrich,[3,d] N. Giokaris,[9]

M. P. Giordani,[167a,167c] F. M. Giorgi,[22a] P. F. Giraud,[138] P. Giromini,[59] D. Giugni,[94a] F. Giuli,[122] C. Giuliani,[103] M. Giulini,[60b] B. K. Gjelsten,[121] S. Gkaitatzis,[156] I. Gkialas,[156] E. L. Gkougkousis,[119] L. K. Gladilin,[101] C. Glasman,[85] J. Glatzer,[13] P. C. F. Glaysher,[49] A. Glazov,[45] M. Goblirsch-Kolb,[25] J. Godlewski,[42] S. Goldfarb,[91] T. Golling,[52] D. Golubkov,[132] A. Gomes,[128a,128b,128d] R. Gonçalo,[128a] J. Goncalves Pinto Firmino Da Costa,[138] G. Gonella,[51] L. Gonella,[19] A. Gongadze,[68] S. González de la Hoz,[170] S. Gonzalez-Sevilla,[52] L. Goossens,[32] P. A. Gorbounov,[99] H. A. Gordon,[27] I. Gorelov,[107] B. Gorini,[32] E. Gorini,[76a,76b] A. Gorišek,[78] A. T. Goshaw,[48] C. Gössling,[46] M. I. Gostkin,[68] C. R. Goudet,[119] D. Goujdami,[137c] A. G. Goussiou,[140] N. Govender,[147b,q] E. Gozani,[154] L. Graber,[57] I. Grabowska-Bold,[41a] P. O. J. Gradin,[58] P. Grafström,[22a,22b] J. Gramling,[52] E. Gramstad,[121] S. Grancagnolo,[17] V. Gratchev,[125] P. M. Gravila,[28e] H. M. Gray,[32] E. Graziani,[136a] Z. D. Greenwood,[82,r] C. Grefe,[23] K. Gregersen,[81] I. M. Gregor,[45] P. Grenier,[145] K. Grevtsov,[5] J. Griffiths,[8] A. A. Grillo,[139] K. Grimm,[75] S. Grinstein,[13,s] Ph. Gris,[37] J.-F. Grivaz,[119] S. Groh,[86] E. Gross,[175] J. Grosse-Knetter,[57] G. C. Grossi,[82] Z. J. Grout,[81] L. Guan,[92] W. Guan,[176] J. Guenther,[65] F. Guescini,[52] D. Guest,[166] O. Gueta,[155] B. Gui,[113] E. Guido,[53a,53b] T. Guillemin,[5] S. Guindon,[2] U. Gul,[56] C. Gumpert,[32] J. Guo,[36c] W. Guo,[92] Y. Guo,[36a,p] R. Gupta,[43] S. Gupta,[122] G. Gustavino,[134a,134b] P. Gutierrez,[115] N. G. Gutierrez Ortiz,[81] C. Gutschow,[81] C. Guyot,[138] C. Gwenlan,[122] C. B. Gwilliam,[77] A. Haas,[112] C. Haber,[16] H. K. Hadavand,[8] N. Haddad,[137e] A. Hadef,[88] S. Hageböck,[23] M. Hagihara,[164] H. Hakobyan,[180,*] M. Haleem,[45] J. Haley,[116] G. Halladjian,[93] G. D. Hallewell,[88] K. Hamacher,[178] P. Hamal,[117] K. Hamano,[172] A. Hamilton,[147a] G. N. Hamity,[141] P. G. Hamnett,[45] L. Han,[36a] K. Hanagaki,[69,t] K. Hanawa,[157] M. Hance,[139] B. Haney,[124] P. Hanke,[60a] R. Hanna,[138] J. B. Hansen,[39] J. D. Hansen,[39] M. C. Hansen,[23] P. H. Hansen,[39] K. Hara,[164] A. S. Hard,[176] T. Harenberg,[178] F. Hariri,[119] S. Harkusha,[95] R. D. Harrington,[49] P. F. Harrison,[173] F. Hartjes,[109] N. M. Hartmann,[102] M. Hasegawa,[70] Y. Hasegawa,[142] A. Hasib,[115] S. Hassani,[138] S. Haug,[18] R. Hauser,[93] L. Hauswald,[47] M. Havranek,[129] C. M. Hawkes,[19] R. J. Hawkings,[32] D. Hayakawa,[159] D. Hayden,[93] C. P. Hays,[122] J. M. Hays,[79] H. S. Hayward,[77] S. J. Haywood,[133] S. J. Head,[19] T. Heck,[86] V. Hedberg,[84] L. Heelan,[8] S. Heim,[124] T. Heim,[16] B. Heinemann,[45] J. J. Heinrich,[102] L. Heinrich,[112] C. Heinz,[55] J. Hejbal,[129] L. Helary,[32] S. Hellman,[148a,148b] C. Helsens,[32] J. Henderson,[122] R. C. W. Henderson,[75] Y. Heng,[176] S. Henkelmann,[171] A. M. Henriques Correia,[32] S. Henrot-Versille,[119] G. H. Herbert,[17] H. Herde,[25] V. Herget,[177] Y. Hernández Jiménez,[147c] G. Herten,[51] R. Hertenberger,[102] L. Hervas,[32] G. G. Hesketh,[81] N. P. Hessey,[109] J. W. Hetherly,[43] E. Higón-Rodriguez,[170] E. Hill,[172] J. C. Hill,[30] K. H. Hiller,[45] S. J. Hillier,[19] I. Hinchliffe,[16] E. Hines,[124] M. Hirose,[51] D. Hirschbuehl,[178] J. Hobbs,[150] N. Hod,[163a] M. C. Hodgkinson,[141] P. Hodgson,[141] A. Hoecker,[32] M. R. Hoeferkamp,[107] F. Hoenig,[102] D. Hohn,[23] T. R. Holmes,[16] M. Homann,[46] T. Honda,[69] T. M. Hong,[127] B. H. Hooberman,[169] W. H. Hopkins,[118] Y. Horii,[105] A. J. Horton,[144] J-Y. Hostachy,[58] S. Hou,[153] A. Hoummada,[137a] J. Howarth,[45] J. Hoya,[74] M. Hrabovsky,[117] I. Hristova,[17] J. Hrivnac,[119] T. Hryn'ova,[5] A. Hrynevich,[96] P. J. Hsu,[63] S.-C. Hsu,[140] Q. Hu,[36a] S. Hu,[36c] Y. Huang,[45] Z. Hubacek,[130] F. Hubaut,[88] F. Huegging,[23] T. B. Huffman,[122] E. W. Hughes,[38] G. Hughes,[75] M. Huhtinen,[32] P. Huo,[150] N. Huseynov,[68,b] J. Huston,[93] J. Huth,[59] G. Iacobucci,[52] G. Iakovidis,[27] I. Ibragimov,[143] L. Iconomidou-Fayard,[119] E. Ideal,[179] Z. Idrissi,[137e] P. Iengo,[32] O. Igonkina,[109,u] T. Iizawa,[174] Y. Ikegami,[69] M. Ikeno,[69] Y. Ilchenko,[11,v] D. Iliadis,[156] N. Ilic,[145] G. Introzzi,[123a,123b] P. Ioannou,[9,*] M. Iodice,[136a] K. Iordanidou,[38] V. Ippolito,[59] N. Ishijima,[120] M. Ishino,[157] M. Ishitsuka,[159] C. Issever,[122] S. Istin,[20a] F. Ito,[164] J. M. Iturbe Ponce,[87] R. Iuppa,[162a,162b] H. Iwasaki,[69] J. M. Izen,[44] V. Izzo,[106a] S. Jabbar,[3] B. Jackson,[124] P. Jackson,[1] V. Jain,[2] K. B. Jakobi,[86] K. Jakobs,[51] S. Jakobsen,[32] T. Jakoubek,[129] D. O. Jamin,[116] D. K. Jana,[82] R. Jansky,[65] J. Janssen,[23] M. Janus,[57] P. A. Janus,[41a] G. Jarlskog,[84] N. Javadov,[68,b] T. Javůrek,[51] F. Jeanneau,[138] L. Jeanty,[16] J. Jejelava,[54a,w] G.-Y. Jeng,[152] P. Jenni,[51,x] C. Jeske,[173] S. Jézéquel,[5] H. Ji,[176] J. Jia,[150] H. Jiang,[67] Y. Jiang,[36a] Z. Jiang,[145] S. Jiggins,[81] J. Jimenez Pena,[170] S. Jin,[35a] A. Jinaru,[28b] O. Jinnouchi,[159] H. Jivan,[147c] P. Johansson,[141] K. A. Johns,[7] W. J. Johnson,[140] K. Jon-And,[148a,148b] G. Jones,[173] R. W. L. Jones,[75] S. Jones,[7] T. J. Jones,[77] J. Jongmanns,[60a] P. M. Jorge,[128a,128b] J. Jovicevic,[163a] X. Ju,[176] A. Juste Rozas,[13,s] M. K. Köhler,[175] A. Kaczmarska,[42] M. Kado,[119] H. Kagan,[113] M. Kagan,[145] S. J. Kahn,[88] T. Kaji,[174] E. Kajomovitz,[48] C. W. Kalderon,[122] A. Kaluza,[86] S. Kama,[43] A. Kamenshchikov,[132] N. Kanaya,[157] S. Kaneti,[30] L. Kanjir,[78] V. A. Kantserov,[100] J. Kanzaki,[69] B. Kaplan,[112] L. S. Kaplan,[176] A. Kapliy,[33] D. Kar,[147c] K. Karakostas,[10] A. Karamaoun,[3] N. Karastathis,[10] M. J. Kareem,[57] E. Karentzos,[10] M. Karnevskiy,[86] S. N. Karpov,[68] Z. M. Karpova,[68] K. Karthik,[112] V. Kartvelishvili,[75] A. N. Karyukhin,[132] K. Kasahara,[164] L. Kashif,[176] R. D. Kass,[113] A. Kastanas,[149] Y. Kataoka,[157] C. Kato,[157] A. Katre,[52] J. Katzy,[45] K. Kawade,[105] K. Kawagoe,[73] T. Kawamoto,[157] G. Kawamura,[57] V. F. Kazanin,[111,c] R. Keeler,[172] R. Kehoe,[43] J. S. Keller,[45] J. J. Kempster,[80] H. Keoshkerian,[161] O. Kepka,[129] B. P. Kerševan,[78] S. Kersten,[178] R. A. Keyes,[90] M. Khader,[169] F. Khalil-zada,[12] A. Khanov,[116] A. G. Kharlamov,[111,c] T. Kharlamova,[111] T. J. Khoo,[52] V. Khovanskiy,[99] E. Khramov,[68] J. Khubua,[54b,y] S. Kido,[70] C. R. Kilby,[80] H. Y. Kim,[8] S. H. Kim,[164] Y. K. Kim,[33] N. Kimura,[156] O. M. Kind,[17] B. T. King,[77] M. King,[170] J. Kirk,[133] A. E. Kiryunin,[103] T. Kishimoto,[157] D. Kisielewska,[41a] F. Kiss,[51] K. Kiuchi,[164] O. Kivernyk,[138] E. Kladiva,[146b] M. H. Klein,[38] M. Klein,[77] U. Klein,[77] K. Kleinknecht,[86] P. Klimek,[110] A. Klimentov,[27] R. Klingenberg,[46] T. Klioutchnikova,[32] E.-E. Kluge,[60a] P. Kluit,[109] S. Kluth,[103] J. Knapik,[42] E. Kneringer,[65] E. B. F. G. Knoops,[88] A. Knue,[56] A. Kobayashi,[157] D. Kobayashi,[159] T. Kobayashi,[157] M. Kobel,[47] M. Kocian,[145] P. Kodys,[131] N. M. Koehler,[103] T. Koffas,[31] E. Koffeman,[109] T. Koi,[145] H. Kolanoski,[17] M. Kolb,[60b] I. Koletsou,[5] A. A. Komar,[98,*] Y. Komori,[157] T. Kondo,[69] N. Kondrashova,[36c] K. Köneke,[51] A. C. König,[108] T. Kono,[69,z] R. Konoplich,[112,aa] N. Konstantinidis,[81] R. Kopeliansky,[64] S. Koperny,[41a] A. K. Kopp,[51] K. Korcyl,[42] K. Kordas,[156] A. Korn,[81] A. A. Korol,[111,c] I. Korolkov,[13] E. V. Korolkova,[141] O. Kortner,[103] S. Kortner,[103] T. Kosek,[131] V. V. Kostyukhin,[23] A. Kotwal,[48] A. Koulouris,[10] A. Kourkoumeli-Charalampidi,[123a,123b] C. Kourkoumelis,[9] V. Kouskoura,[27] A. B. Kowalewska,[42] R. Kowalewski,[172] T. Z. Kowalski,[41a] C. Kozakai,[157] W. Kozanecki,[138] A. S. Kozhin,[132] V. A. Kramarenko,[101] G. Kramberger,[78]

D. Krasnopevtsev,[100] M. W. Krasny,[83] A. Krasznahorkay,[32] A. Kravchenko,[27] M. Kretz,[60c] J. Kretzschmar,[77] K. Kreutzfeldt,[55] P. Krieger,[161] K. Krizka,[33] K. Kroeninger,[46] H. Kroha,[103] J. Kroll,[124] J. Kroseberg,[23] J. Krstic,[14] U. Kruchonak,[68] H. Krüger,[23] N. Krumnack,[67] M. C. Kruse,[48] M. Kruskal,[24] T. Kubota,[91] H. Kucuk,[81] S. Kuday,[4b] J. T. Kuechler,[178] S. Kuehn,[51] A. Kugel,[60c] F. Kuger,[177] T. Kuhl,[45] V. Kukhtin,[68] R. Kukla,[138] Y. Kulchitsky,[95] S. Kuleshov,[34b] M. Kuna,[134a,134b] T. Kunigo,[71] A. Kupco,[129] H. Kurashige,[70] L. L. Kurchaninov,[163a] Y. A. Kurochkin,[95] M. G. Kurth,[44] V. Kus,[129] E. S. Kuwertz,[172] M. Kuze,[159] J. Kvita,[117] T. Kwan,[172] D. Kyriazopoulos,[141] A. La Rosa,[103] J. L. La Rosa Navarro,[26d] L. La Rotonda,[40a,40b] C. Lacasta,[170] F. Lacava,[134a,134b] J. Lacey,[31] H. Lacker,[17] D. Lacour,[83] E. Ladygin,[68] R. Lafaye,[5] B. Laforge,[83] T. Lagouri,[179] S. Lai,[57] S. Lammers,[64] W. Lampl,[7] E. Lançon,[138] U. Landgraf,[51] M. P. J. Landon,[79] M. C. Lanfermann,[52] V. S. Lang,[60a] J. C. Lange,[13] A. J. Lankford,[166] F. Lanni,[27] K. Lantzsch,[23] A. Lanza,[123a] S. Laplace,[83] C. Lapoire,[32] J. F. Laporte,[138] T. Lari,[94a] F. Lasagni Manghi,[22a,22b] M. Lassnig,[32] P. Laurelli,[50] W. Lavrijsen,[16] A. T. Law,[139] P. Laycock,[77] T. Lazovich,[59] M. Lazzaroni,[94a,94b] B. Le,[91] O. Le Dortz,[83] E. Le Guirriec,[88] E. P. Le Quilleuc,[138] M. LeBlanc,[172] T. LeCompte,[6] F. Ledroit-Guillon,[58] C. A. Lee,[27] S. C. Lee,[153] L. Lee,[1] B. Lefebvre,[90] G. Lefebvre,[83] M. Lefebvre,[172] F. Legger,[102] C. Leggett,[16] A. Lehan,[77] G. Lehmann Miotto,[32] X. Lei,[7] W. A. Leight,[31] A. G. Leister,[179] M. A. L. Leite,[26d] R. Leitner,[131] D. Lellouch,[175] B. Lemmer,[57] K. J. C. Leney,[81] T. Lenz,[23] B. Lenzi,[32] R. Leone,[7] S. Leone,[126a,126b] C. Leonidopoulos,[49] S. Leontsinis,[10] G. Lerner,[151] C. Leroy,[97] A. A. J. Lesage,[138] C. G. Lester,[30] M. Levchenko,[125] J. Levêque,[5] D. Levin,[92] L. J. Levinson,[175] M. Levy,[19] D. Lewis,[79] M. Leyton,[44] B. Li,[36a,p] C. Li,[36a] H. Li,[150] L. Li,[48] L. Li,[36c] Q. Li,[35a] S. Li,[48] X. Li,[87] Y. Li,[143] Z. Liang,[35a] B. Liberti,[135a] A. Liblong,[161] P. Lichard,[32] K. Lie,[169] J. Liebal,[23] W. Liebig,[15] A. Limosani,[152] S. C. Lin,[153,ab] T. H. Lin,[86] B. E. Lindquist,[150] A. E. Lionti,[52] E. Lipeles,[124] A. Lipniacka,[15] M. Lisovyi,[60b] T. M. Liss,[169] A. Lister,[171] A. M. Litke,[139] B. Liu,[153,ac] D. Liu,[153] H. Liu,[92] H. Liu,[27] J. Liu,[36b] J. B. Liu,[36a] K. Liu,[88] L. Liu,[169] M. Liu,[36a] Y. L. Liu,[36a] Y. Liu,[36a] M. Livan,[123a,123b] A. Lleres,[58] J. Llorente Merino,[35a] S. L. Lloyd,[79] F. Lo Sterzo,[153] E. M. Lobodzinska,[45] P. Loch,[7] F. K. Loebinger,[87] K. M. Loew,[25] A. Loginov,[179,*] T. Lohse,[17] K. Lohwasser,[45] M. Lokajicek,[129] B. A. Long,[24] J. D. Long,[169] R. E. Long,[75] L. Longo,[76a,76b] K. A. Looper,[113] J. A. López,[34b] D. Lopez Mateos,[59] B. Lopez Paredes,[141] I. Lopez Paz,[13] A. Lopez Solis,[83] J. Lorenz,[102] N. Lorenzo Martinez,[64] M. Losada,[21] P. J. Lösel,[102] X. Lou,[35a] A. Lounis,[119] J. Love,[6] P. A. Love,[75] H. Lu,[62a] N. Lu,[92] H. J. Lubatti,[140] C. Luci,[134a,134b] A. Lucotte,[58] C. Luedtke,[51] F. Luehring,[64] W. Lukas,[65] L. Luminari,[134a] O. Lundberg,[148a,148b] B. Lund-Jensen,[149] P. M. Luzi,[83] D. Lynn,[27] R. Lysak,[129] E. Lytken,[84] V. Lyubushkin,[68] H. Ma,[27] L. L. Ma,[36b] Y. Ma,[36b] G. Maccarrone,[50] A. Macchiolo,[103] C. M. Macdonald,[141] B. Maček,[78] J. Machado Miguens,[124,128b] D. Madaffari,[88] R. Madar,[37] H. J. Maddocks,[168] W. F. Mader,[47] A. Madsen,[45] J. Maeda,[70] S. Maeland,[15] T. Maeno,[27] A. Maevskiy,[101] E. Magradze,[57] J. Mahlstedt,[109] C. Maiani,[119] C. Maidantchik,[26a] A. A. Maier,[103] T. Maier,[102] A. Maio,[128a,128b,128d] S. Majewski,[118] Y. Makida,[69] N. Makovec,[119] B. Malaescu,[83] Pa. Malecki,[42] V. P. Maleev,[125] F. Malek,[58] U. Mallik,[66] D. Malon,[6] C. Malone,[30] S. Maltezos,[10] S. Malyukov,[32] J. Mamuzic,[170] G. Mancini,[50] L. Mandelli,[94a] I. Mandić,[78] J. Maneira,[128a,128b] L. Manhaes de Andrade Filho,[26b] J. Manjarres Ramos,[163b] A. Mann,[102] A. Manousos,[32] B. Mansoulie,[138] J. D. Mansour,[35a] R. Mantifel,[90] M. Mantoani,[57] S. Manzoni,[94a,94b] L. Mapelli,[32] G. Marceca,[29] L. March,[52] G. Marchiori,[83] M. Marcisovsky,[129] M. Marjanovic,[14] D. E. Marley,[92] F. Marroquim,[26a] S. P. Marsden,[87] Z. Marshall,[16] S. Marti-Garcia,[170] B. Martin,[93] T. A. Martin,[173] V. J. Martin,[49] B. Martin dit Latour,[15] M. Martinez,[13,s] V. I. Martinez Outschoorn,[169] S. Martin-Haugh,[133] V. S. Martoiu,[28b] A. C. Martyniuk,[81] A. Marzin,[32] L. Masetti,[86] T. Mashimo,[157] R. Mashinistov,[98] J. Masik,[87] A. L. Maslennikov,[111,c] I. Massa,[22a,22b] L. Massa,[22a,22b] P. Mastrandrea,[5] A. Mastroberardino,[40a,40b] T. Masubuchi,[157] P. Mättig,[178] J. Mattmann,[86] J. Maurer,[28b] S. J. Maxfield,[77] D. A. Maximov,[111,c] R. Mazini,[153] I. Maznas,[156] S. M. Mazza,[94a,94b] N. C. Mc Fadden,[107] G. Mc Goldrick,[161] S. P. Mc Kee,[92] A. McCarn,[92] R. L. McCarthy,[150] T. G. McCarthy,[103] L. I. McClymont,[81] E. F. McDonald,[91] J. A. Mcfayden,[81] G. Mchedlidze,[57] S. J. McMahon,[133] R. A. McPherson,[172,m] M. Medinnis,[45] S. Meehan,[140] S. Mehlhase,[102] A. Mehta,[77] K. Meier,[60a] C. Meineck,[102] B. Meirose,[44] D. Melini,[170] B. R. Mellado Garcia,[147c] M. Melo,[146a] F. Meloni,[18] L. Meng,[77] X. Meng,[92] A. Mengarelli,[22a,22b] S. Menke,[103] E. Meoni,[165] S. Mergelmeyer,[17] P. Mermod,[52] L. Merola,[106a,106b] C. Meroni,[94a] F. S. Merritt,[33] A. Messina,[134a,134b] J. Metcalfe,[6] A. S. Mete,[166] C. Meyer,[86] C. Meyer,[124] J-P. Meyer,[138] J. Meyer,[109] H. Meyer Zu Theenhausen,[60a] F. Miano,[151] R. P. Middleton,[133] S. Miglioranzi,[53a,53b] L. Mijović,[49] G. Mikenberg,[175] M. Mikestikova,[129] M. Mikuž,[78] M. Milesi,[91] A. Milic,[27] D. W. Miller,[33] C. Mills,[49] A. Milov,[175] D. A. Milstead,[148a,148b] A. A. Minaenko,[132] Y. Minami,[157] I. A. Minashvili,[68] A. I. Mincer,[112] B. Mindur,[41a] M. Mineev,[68] Y. Minegishi,[157] Y. Ming,[176] L. M. Mir,[13] K. P. Mistry,[124] T. Mitani,[174] J. Mitrevski,[102] V. A. Mitsou,[170] A. Miucci,[18] P. S. Miyagawa,[141] A. Mizukami,[69] J. U. Mjörnmark,[84] M. Mlynarikova,[131] T. Moa,[148a,148b] K. Mochizuki,[97] P. Mogg,[51] S. Mohapatra,[38] S. Molander,[148a,148b] R. Moles-Valls,[23] R. Monden,[71] M. C. Mondragon,[93] K. Mönig,[45] J. Monk,[39] E. Monnier,[88] A. Montalbano,[150] J. Montejo Berlingen,[32] F. Monticelli,[74] S. Monzani,[94a,94b] R. W. Moore,[3] N. Morange,[119] D. Moreno,[21] M. Moreno Llácer,[57] P. Morettini,[53a] S. Morgenstern,[32] D. Mori,[144] T. Mori,[157] M. Morii,[59] M. Morinaga,[157] V. Morisbak,[121] S. Moritz,[86] A. K. Morley,[152] G. Mornacchi,[32] J. D. Morris,[79] S. S. Mortensen,[39] L. Morvaj,[150] P. Moschovakos,[10] M. Mosidze,[54b] H. J. Moss,[141] J. Moss,[145,ad] K. Motohashi,[159] R. Mount,[145] E. Mountricha,[27] E. J. W. Moyse,[89] S. Muanza,[88] R. D. Mudd,[19] F. Mueller,[103] J. Mueller,[127] R. S. P. Mueller,[102] T. Mueller,[30] D. Muenstermann,[75] P. Mullen,[56] G. A. Mullier,[18] F. J. Munoz Sanchez,[87] J. A. Murillo Quijada,[19] W. J. Murray,[173,133] H. Musheghyan,[57] M. Muškinja,[78] A. G. Myagkov,[132,ae] M. Myska,[130] B. P. Nachman,[16] O. Nackenhorst,[52] K. Nagai,[122] R. Nagai,[69,z] K. Nagano,[69] Y. Nagasaka,[61] K. Nagata,[164] M. Nagel,[51] E. Nagy,[88] A. M. Nairz,[32] Y. Nakahama,[105] K. Nakamura,[69] T. Nakamura,[157] I. Nakano,[114] R. F. Naranjo Garcia,[45] R. Narayan,[11] D. I. Narrias Villar,[60a] I. Naryshkin,[125] T. Naumann,[45] G. Navarro,[21] R. Nayyar,[7] H. A. Neal,[92]

P. Yu. Nechaeva,[98] T. J. Neep,[87] A. Negri,[123a,123b] M. Negrini,[22a] S. Nektarijevic,[108] C. Nellist,[119] A. Nelson,[166] S. Nemecek,[129] P. Nemethy,[112] A. A. Nepomuceno,[26a] M. Nessi,[32,af] M. S. Neubauer,[169] M. Neumann,[178] R. M. Neves,[112] P. Nevski,[27] P. R. Newman,[19] D. H. Nguyen,[6] T. Nguyen Manh,[97] R. B. Nickerson,[122] R. Nicolaidou,[138] J. Nielsen,[139] V. Nikolaenko,[132,ae] I. Nikolic-Audit,[83] K. Nikolopoulos,[19] J. K. Nilsen,[121] P. Nilsson,[27] Y. Ninomiya,[157] A. Nisati,[134a] R. Nisius,[103] T. Nobe,[157] M. Nomachi,[120] I. Nomidis,[31] T. Nooney,[79] S. Norberg,[115] M. Nordberg,[32] N. Norjoharuddeen,[122] O. Novgorodova,[47] S. Nowak,[103] M. Nozaki,[69] L. Nozka,[117] K. Ntekas,[166] E. Nurse,[81] F. Nuti,[91] F. O'grady,[7] D. C. O'Neil,[144] A. A. O'Rourke,[45] V. O'Shea,[56] F. G. Oakham,[31,d] H. Oberlack,[103] T. Obermann,[23] J. Ocariz,[83] A. Ochi,[70] I. Ochoa,[38] J. P. Ochoa-Ricoux,[34a] S. Oda,[73] S. Odaka,[69] H. Ogren,[64] A. Oh,[87] S. H. Oh,[48] C. C. Ohm,[16] H. Ohman,[168] H. Oide,[53a,53b] H. Okawa,[164] Y. Okumura,[157] T. Okuyama,[69] A. Olariu,[28b] L. F. Oleiro Seabra,[128a] S. A. Olivares Pino,[49] D. Oliveira Damazio,[27] A. Olszewski,[42] J. Olszowska,[42] A. Onofre,[128a,128e] K. Onogi,[105] P. U. E. Onyisi,[11,v] M. J. Oreglia,[33] Y. Oren,[155] D. Orestano,[136a,136b] N. Orlando,[62b] R. S. Orr,[161] B. Osculati,[53a,53b,*] R. Ospanov,[87] G. Otero y Garzon,[29] H. Otono,[73] M. Ouchrif,[137d] F. Ould-Saada,[121] A. Ouraou,[138] K. P. Oussoren,[109] Q. Ouyang,[35a] M. Owen,[56] R. E. Owen,[19] V. E. Ozcan,[20a] N. Ozturk,[8] K. Pachal,[144] A. Pacheco Pages,[13] L. Pacheco Rodriguez,[138] C. Padilla Aranda,[13] M. Pagáčová,[51] S. Pagan Griso,[16] M. Paganini,[179] F. Paige,[27] P. Pais,[89] K. Pajchel,[121] G. Palacino,[64] S. Palazzo,[40a,40b] S. Palestini,[32] M. Palka,[41b] D. Pallin,[37] E. St. Panagiotopoulou,[10] C. E. Pandini,[83] J. G. Panduro Vazquez,[80] P. Pani,[148a,148b] S. Panitkin,[27] D. Pantea,[28b] L. Paolozzi,[52] Th. D. Papadopoulou,[10] K. Papageorgiou,[156] A. Paramonov,[6] D. Paredes Hernandez,[179] A. J. Parker,[75] M. A. Parker,[30] K. A. Parker,[141] F. Parodi,[53a,53b] J. A. Parsons,[38] U. Parzefall,[51] V. R. Pascuzzi,[161] E. Pasqualucci,[134a] S. Passaggio,[53a] Fr. Pastore,[80] G. Pásztor,[31,ag] S. Pataraia,[178] J. R. Pater,[87] T. Pauly,[32] J. Pearce,[172] B. Pearson,[115] L. E. Pedersen,[39] M. Pedersen,[121] S. Pedraza Lopez,[170] R. Pedro,[128a,128b] S. V. Peleganchuk,[111,c] O. Penc,[129] C. Peng,[35a] H. Peng,[36a] J. Penwell,[64] B. S. Peralva,[26b] M. M. Perego,[138] D. V. Perepelitsa,[27] E. Perez Codina,[163a] L. Perini,[94a,94b] H. Pernegger,[32] S. Perrella,[106a,106b] R. Peschke,[45] V. D. Peshekhonov,[68] K. Peters,[45] R. F. Y. Peters,[87] B. A. Petersen,[32] T. C. Petersen,[39] E. Petit,[58] A. Petridis,[1] C. Petridou,[156] P. Petroff,[119] E. Petrolo,[134a] M. Petrov,[122] F. Petrucci,[136a,136b] N. E. Pettersson,[89] A. Peyaud,[138] R. Pezoa,[34b] P. W. Phillips,[133] G. Piacquadio,[145,ah] E. Pianori,[173] A. Picazio,[89] E. Piccaro,[79] M. Piccinini,[22a,22b] M. A. Pickering,[122] R. Piegaia,[29] J. E. Pilcher,[33] A. D. Pilkington,[87] A. W. J. Pin,[87] M. Pinamonti,[167a,167c,ai] J. L. Pinfold,[3] A. Pingel,[39] S. Pires,[83] H. Pirumov,[45] M. Pitt,[175] L. Plazak,[146a] M.-A. Pleier,[27] V. Pleskot,[86] E. Plotnikova,[68] D. Pluth,[67] R. Poettgen,[148a,148b] L. Poggioli,[119] D. Pohl,[23] G. Polesello,[123a] A. Poley,[45] A. Policicchio,[40a,40b] R. Polifka,[161] A. Polini,[22a] C. S. Pollard,[56] V. Polychronakos,[27] K. Pommès,[32] L. Pontecorvo,[134a] B. G. Pope,[93] G. A. Popeneciu,[28c] A. Poppleton,[32] S. Pospisil,[130] K. Potamianos,[16] I. N. Potrap,[68] C. J. Potter,[30] C. T. Potter,[118] G. Poulard,[32] J. Poveda,[32] V. Pozdnyakov,[68] M. E. Pozo Astigarraga,[32] P. Pralavorio,[88] A. Pranko,[16] S. Prell,[67] D. Price,[87] L. E. Price,[6] M. Primavera,[76a] S. Prince,[90] K. Prokofiev,[62c] F. Prokoshin,[34b] S. Protopopescu,[27] J. Proudfoot,[6] M. Przybycien,[41a] D. Puddu,[136a,136b] M. Purohit,[27,aj] P. Puzo,[119] J. Qian,[92] G. Qin,[56] Y. Qin,[87] A. Quadt,[57] W. B. Quayle,[167a,167b] M. Queitsch-Maitland,[45] D. Quilty,[56] S. Raddum,[121] V. Radeka,[27] V. Radescu,[122] S. K. Radhakrishnan,[150] P. Radloff,[118] P. Rados,[91] F. Ragusa,[94a,94b] G. Rahal,[181] J. A. Raine,[87] S. Rajagopalan,[27] M. Rammensee,[32] C. Rangel-Smith,[168] M. G. Ratti,[94a,94b] D. M. Rauch,[45] F. Rauscher,[102] S. Rave,[86] T. Ravenscroft,[56] I. Ravinovich,[175] M. Raymond,[32] A. L. Read,[121] N. P. Readioff,[77] M. Reale,[76a,76b] D. M. Rebuzzi,[123a,123b] A. Redelbach,[177] G. Redlinger,[27] R. Reece,[139] R. G. Reed,[147c] K. Reeves,[44] L. Rehnisch,[17] J. Reichert,[124] A. Reiss,[86] C. Rembser,[32] H. Ren,[35a] M. Rescigno,[134a] S. Resconi,[94a] O. L. Rezanova,[111,c] P. Reznicek,[131] R. Rezvani,[97] R. Richter,[103] S. Richter,[81] E. Richter-Was,[41b] O. Ricken,[23] M. Ridel,[83] P. Rieck,[103] C. J. Riegel,[178] J. Rieger,[57] O. Rifki,[115] M. Rijssenbeek,[150] A. Rimoldi,[123a,123b] M. Rimoldi,[18] L. Rinaldi,[22a] B. Ristić,[52] E. Ritsch,[32] I. Riu,[13] F. Rizatdinova,[116] E. Rizvi,[79] C. Rizzi,[13] S. H. Robertson,[90,m] A. Robichaud-Veronneau,[90] D. Robinson,[30] J. E. M. Robinson,[45] A. Robson,[56] C. Roda,[126a,126b] Y. Rodina,[88,ak] A. Rodriguez Perez,[13] D. Rodriguez Rodriguez,[170] S. Roe,[32] C. S. Rogan,[59] O. Røhne,[121] J. Roloff,[59] A. Romaniouk,[100] M. Romano,[22a,22b] S. M. Romano Saez,[37] E. Romero Adam,[170] N. Rompotis,[140] M. Ronzani,[51] L. Roos,[83] E. Ros,[170] S. Rosati,[134a] K. Rosbach,[51] P. Rose,[139] N.-A. Rosien,[57] V. Rossetti,[148a,148b] E. Rossi,[106a,106b] L. P. Rossi,[53a] J. H. N. Rosten,[30] R. Rosten,[140] M. Rotaru,[28b] I. Roth,[175] J. Rothberg,[140] D. Rousseau,[119] A. Rozanov,[88] Y. Rozen,[154] X. Ruan,[147c] F. Rubbo,[145] M. S. Rudolph,[161] F. Rühr,[51] A. Ruiz-Martinez,[31] Z. Rurikova,[51] N. A. Rusakovich,[68] A. Ruschke,[102] H. L. Russell,[140] J. P. Rutherfoord,[7] N. Ruthmann,[32] Y. F. Ryabov,[125] M. Rybar,[169] G. Rybkin,[119] S. Ryu,[6] A. Ryzhov,[132] G. F. Rzehorz,[57] A. F. Saavedra,[152] G. Sabato,[109] S. Sacerdoti,[29] H. F-W. Sadrozinski,[139] R. Sadykov,[68] F. Safai Tehrani,[134a] P. Saha,[110] M. Sahinsoy,[60a] M. Saimpert,[138] T. Saito,[157] H. Sakamoto,[157] Y. Sakurai,[174] G. Salamanna,[136a,136b] A. Salamon,[135a,135b] J. E. Salazar Loyola,[34b] D. Salek,[109] P. H. Sales De Bruin,[140] D. Salihagic,[103] A. Salnikov,[145] J. Salt,[170] D. Salvatore,[40a,40b] F. Salvatore,[151] A. Salvucci,[62a,62b,62c] A. Salzburger,[32] D. Sammel,[51] D. Sampsonidis,[156] J. Sánchez,[170] V. Sanchez Martinez,[170] A. Sanchez Pineda,[106a,106b] H. Sandaker,[121] R. L. Sandbach,[79] M. Sandhoff,[178] C. Sandoval,[21] D. P. C. Sankey,[133] M. Sannino,[53a,53b] A. Sansoni,[50] C. Santoni,[37] R. Santonico,[135a,135b] H. Santos,[128a] I. Santoyo Castillo,[151] K. Sapp,[127] A. Sapronov,[68] J. G. Saraiva,[128a,128d] B. Sarrazin,[23] O. Sasaki,[69] K. Sato,[164] E. Sauvan,[5] G. Savage,[80] P. Savard,[161,d] N. Savic,[103] C. Sawyer,[133] L. Sawyer,[82,r] J. Saxon,[33] C. Sbarra,[22a] A. Sbrizzi,[22a,22b] T. Scanlon,[81] D. A. Scannicchio,[166] M. Scarcella,[152] V. Scarfone,[40a,40b] J. Schaarschmidt,[175] P. Schacht,[103] B. M. Schachtner,[102] D. Schaefer,[32] L. Schaefer,[124] R. Schaefer,[45] J. Schaeffer,[86] S. Schaepe,[23] S. Schaetzel,[60b] U. Schäfer,[86] A. C. Schaffer,[119] D. Schaile,[102] R. D. Schamberger,[150] V. Scharf,[60a] V. A. Schegelsky,[125] D. Scheirich,[131] M. Schernau,[166] C. Schiavi,[53a,53b] S. Schier,[139] C. Schillo,[51] M. Schioppa,[40a,40b] S. Schlenker,[32] K. R. Schmidt-Sommerfeld,[103] K. Schmieden,[32] C. Schmitt,[86] S. Schmitt,[45] S. Schmitz,[86] B. Schneider,[163a] U. Schnoor,[51] L. Schoeffel,[138] A. Schoening,[60b] B. D. Schoenrock,[93] E. Schopf,[23] M. Schott,[86]

J. F. P. Schouwenberg,[108] J. Schovancova,[8] S. Schramm,[52] M. Schreyer,[177] N. Schuh,[86] A. Schulte,[86] M. J. Schultens,[23] H.-C. Schultz-Coulon,[60a] H. Schulz,[17] M. Schumacher,[51] B. A. Schumm,[139] Ph. Schune,[138] A. Schwartzman,[145] T. A. Schwarz,[92] H. Schweiger,[87] Ph. Schwemling,[138] R. Schwienhorst,[93] J. Schwindling,[138] T. Schwindt,[23] G. Sciolla,[25] F. Scuri,[126a,126b] F. Scutti,[91] J. Searcy,[92] P. Seema,[23] S. C. Seidel,[107] A. Seiden,[139] F. Seifert,[130] J. M. Seixas,[26a] G. Sekhniaidze,[106a] K. Sekhon,[92] S. J. Sekula,[43] D. M. Seliverstov,[125,*] N. Semprini-Cesari,[22a,22b] C. Serfon,[121] L. Serin,[119] L. Serkin,[167a,167b] M. Sessa,[136a,136b] R. Seuster,[172] H. Severini,[115] T. Sfiligoj,[78] F. Sforza,[32] A. Sfyrla,[52] E. Shabalina,[57] N. W. Shaikh,[148a,148b] L. Y. Shan,[35a] R. Shang,[169] J. T. Shank,[24] M. Shapiro,[16] P. B. Shatalov,[99] K. Shaw,[167a,167b] S. M. Shaw,[87] A. Shcherbakova,[148a,148b] C. Y. Shehu,[151] P. Sherwood,[81] L. Shi,[153,al] S. Shimizu,[70] C. O. Shimmin,[166] M. Shimojima,[104] S. Shirabe,[73] M. Shiyakova,[68,am] A. Shmeleva,[98] D. Shoaleh Saadi,[97] M. J. Shochet,[33] S. Shojaii,[94a,94b] D. R. Shope,[115] S. Shrestha,[113] E. Shulga,[100] M. A. Shupe,[7] P. Sicho,[129] A. M. Sickles,[169] P. E. Sidebo,[149] E. Sideras Haddad,[147c] O. Sidiropoulou,[177] D. Sidorov,[116] A. Sidoti,[22a,22b] F. Siegert,[47] Dj. Sijacki,[14] J. Silva,[128a,128d] S. B. Silverstein,[148a] V. Simak,[130] Lj. Simic,[14] S. Simion,[119] E. Simioni,[86] B. Simmons,[81] D. Simon,[37] M. Simon,[86] P. Sinervo,[161] N. B. Sinev,[118] M. Sioli,[22a,22b] G. Siragusa,[177] S. Yu. Sivoklokov,[101] J. Sjölin,[148a,148b] M. B. Skinner,[75] H. P. Skottowe,[59] P. Skubic,[115] M. Slater,[19] T. Slavicek,[130] M. Slawinska,[109] K. Sliwa,[165] R. Slovak,[131] V. Smakhtin,[175] B. H. Smart,[5] L. Smestad,[15] J. Smiesko,[146a] S. Yu. Smirnov,[100] Y. Smirnov,[100] L. N. Smirnova,[101,an] O. Smirnova,[84] J. W. Smith,[57] M. N. K. Smith,[38] R. W. Smith,[38] M. Smizanska,[75] K. Smolek,[130] A. A. Snesarev,[98] I. M. Snyder,[118] S. Snyder,[27] R. Sobie,[172,m] F. Socher,[47] A. Soffer,[155] D. A. Soh,[153] G. Sokhrannyi,[78] C. A. Solans Sanchez,[32] M. Solar,[130] E. Yu. Soldatov,[100] U. Soldevila,[170] A. A. Solodkov,[132] A. Soloshenko,[68] O. V. Solovyanov,[132] V. Solovyev,[125] P. Sommer,[51] H. Son,[165] H. Y. Song,[36a,ao] A. Sood,[16] A. Sopczak,[130] V. Sopko,[130] V. Sorin,[13] D. Sosa,[60b] C. L. Sotiropoulou,[126a,126b] R. Soualah,[167a,167c] A. M. Soukharev,[111,c] D. South,[45] B. C. Sowden,[80] S. Spagnolo,[76a,76b] M. Spalla,[126a,126b] M. Spangenberg,[173] F. Spanò,[80] D. Sperlich,[17] F. Spettel,[103] R. Spighi,[22a] G. Spigo,[32] L. A. Spiller,[91] M. Spousta,[131] R. D. St. Denis,[56,*] A. Stabile,[94a] R. Stamen,[60a] S. Stamm,[17] E. Stanecka,[42] R. W. Stanek,[6] C. Stanescu,[136a] M. Stanescu-Bellu,[45] M. M. Stanitzki,[45] S. Stapnes,[121] E. A. Starchenko,[132] G. H. Stark,[33] J. Stark,[58] P. Staroba,[129] P. Starovoitov,[60a] S. Stärz,[32] R. Staszewski,[42] P. Steinberg,[27] B. Stelzer,[144] H. J. Stelzer,[32] O. Stelzer-Chilton,[163a] H. Stenzel,[55] G. A. Stewart,[56] J. A. Stillings,[23] M. C. Stockton,[90] M. Stoebe,[90] G. Stoicea,[28b] P. Stolte,[57] S. Stonjek,[103] A. R. Stradling,[8] A. Straessner,[47] M. E. Stramaglia,[18] J. Strandberg,[149] S. Strandberg,[148a,148b] A. Strandlie,[121] M. Strauss,[115] P. Strizenec,[146b] R. Ströhmer,[177] D. M. Strom,[118] R. Stroynowski,[43] A. Strubig,[108] S. A. Stucci,[27] B. Stugu,[15] N. A. Styles,[45] D. Su,[145] J. Su,[127] S. Suchek,[60a] Y. Sugaya,[120] M. Suk,[130] V. V. Sulin,[98] S. Sultansoy,[4c] T. Sumida,[71] S. Sun,[59] X. Sun,[35a] J. E. Sundermann,[51] K. Suruliz,[151] C. J. E. Suster,[152] M. R. Sutton,[151] S. Suzuki,[69] M. Svatos,[129] M. Swiatlowski,[33] S. P. Swift,[2] I. Sykora,[146a] T. Sykora,[131] D. Ta,[51] K. Tackmann,[45] J. Taenzer,[155] A. Taffard,[166] R. Tafirout,[163a] N. Taiblum,[155] H. Takai,[27] R. Takashima,[72] T. Takeshita,[142] Y. Takubo,[69] M. Talby,[88] A. A. Talyshev,[111,c] J. Tanaka,[157] M. Tanaka,[159] R. Tanaka,[119] S. Tanaka,[69] R. Tanioka,[70] B. B. Tannenwald,[113] S. Tapia Araya,[34b] S. Tapprogge,[86] S. Tarem,[154] G. F. Tartarelli,[94a] P. Tas,[131] M. Tasevsky,[129] T. Tashiro,[71] E. Tassi,[40a,40b] A. Tavares Delgado,[128a,128b] Y. Tayalati,[137e] A. C. Taylor,[107] G. N. Taylor,[91] P. T. E. Taylor,[91] W. Taylor,[163b] F. A. Teischinger,[32] P. Teixeira-Dias,[80] K. K. Temming,[51] D. Temple,[144] H. Ten Kate,[32] P. K. Teng,[153] J. J. Teoh,[120] F. Tepel,[178] S. Terada,[69] K. Terashi,[157] J. Terron,[85] S. Terzo,[13] M. Testa,[50] R. J. Teuscher,[161,m] T. Theveneaux-Pelzer,[88] J. P. Thomas,[19] J. Thomas-Wilsker,[80] P. D. Thompson,[19] A. S. Thompson,[56] L. A. Thomsen,[179] E. Thomson,[124] M. J. Tibbetts,[16] R. E. Ticse Torres,[88] V. O. Tikhomirov,[98,ap] Yu. A. Tikhonov,[111,c] S. Timoshenko,[100] P. Tipton,[179] S. Tisserant,[88] K. Todome,[159] T. Todorov,[5,*] S. Todorova-Nova,[131] J. Tojo,[73] S. Tokár,[146a] K. Tokushuku,[69] E. Tolley,[59] L. Tomlinson,[87] M. Tomoto,[105] L. Tompkins,[145,aq] K. Toms,[107] B. Tong,[59] P. Tornambe,[51] E. Torrence,[118] H. Torres,[144] E. Torró Pastor,[140] J. Toth,[88,ar] F. Touchard,[88] D. R. Tovey,[141] T. Trefzger,[177] A. Tricoli,[27] I. M. Trigger,[163a] S. Trincaz-Duvoid,[83] M. F. Tripiana,[13] W. Trischuk,[161] B. Trocmé,[58] A. Trofymov,[45] C. Troncon,[94a] M. Trottier-McDonald,[16] M. Trovatelli,[172] L. Truong,[167a,167c] M. Trzebinski,[42] A. Trzupek,[42] J. C-L. Tseng,[122] P. V. Tsiareshka,[95] G. Tsipolitis,[10] N. Tsirintanis,[9] S. Tsiskaridze,[13] V. Tsiskaridze,[51] E. G. Tskhadadze,[54a] K. M. Tsui,[62a] I. I. Tsukerman,[99] V. Tsulaia,[16] S. Tsuno,[69] D. Tsybychev,[150] Y. Tu,[62b] A. Tudorache,[28b] V. Tudorache,[28b] T. T. Tulbure,[28a] A. N. Tuna,[59] S. A. Tupputi,[22a,22b] S. Turchikhin,[68] D. Turgeman,[175] I. Turk Cakir,[4b] R. Turra,[94a,94b] P. M. Tuts,[38] G. Ucchielli,[22a,22b] I. Ueda,[157] M. Ughetto,[148a,148b] F. Ukegawa,[164] G. Unal,[32] A. Undrus,[27] G. Unel,[166] F. C. Ungaro,[91] Y. Unno,[69] C. Unverdorben,[102] J. Urban,[146b] P. Urquijo,[91] P. Urrejola,[86] G. Usai,[8] J. Usui,[69] L. Vacavant,[88] V. Vacek,[130] B. Vachon,[90] C. Valderanis,[102] E. Valdes Santurio,[148a,148b] N. Valencic,[109] S. Valentinetti,[22a,22b] A. Valero,[170] L. Valery,[13] S. Valkar,[131] J. A. Valls Ferrer,[170] W. Van Den Wollenberg,[109] P. C. Van Der Deijl,[109] H. van der Graaf,[109] N. van Eldik,[154] P. van Gemmeren,[6] J. Van Nieuwkoop,[144] I. van Vulpen,[109] M. C. van Woerden,[109] M. Vanadia,[134a,134b] W. Vandelli,[32] R. Vanguri,[124] A. Vaniachine,[160] P. Vankov,[109] G. Vardanyan,[180] R. Vari,[134a] E. W. Varnes,[7] T. Varol,[43] D. Varouchas,[83] A. Vartapetian,[8] K. E. Varvell,[152] J. G. Vasquez,[179] G. A. Vasquez,[34b] F. Vazeille,[37] T. Vazquez Schroeder,[90] J. Veatch,[57] V. Veeraraghavan,[7] L. M. Veloce,[161] F. Veloso,[128a,128c] S. Veneziano,[134a] A. Ventura,[76a,76b] M. Venturi,[172] N. Venturi,[161] A. Venturini,[25] V. Vercesi,[123a] M. Verducci,[134a,134b] W. Verkerke,[109] J. C. Vermeulen,[109] A. Vest,[47,as] M. C. Vetterli,[144,d] O. Viazlo,[84] I. Vichou,[169,*] T. Vickey,[141] O. E. Vickey Boeriu,[141] G. H. A. Viehhauser,[122] S. Viel,[16] L. Vigani,[122] M. Villa,[22a,22b] M. Villaplana Perez,[94a,94b] E. Vilucchi,[50] M. G. Vincter,[31] V. B. Vinogradov,[68] C. Vittori,[22a,22b] I. Vivarelli,[151] S. Vlachos,[10] M. Vlasak,[130] M. Vogel,[178] P. Vokac,[130] G. Volpi,[126a,126b] M. Volpi,[91] H. von der Schmitt,[103] E. von Toerne,[23] V. Vorobel,[131] K. Vorobev,[100] M. Vos,[170] R. Voss,[32] J. H. Vossebeld,[77] N. Vranjes,[14] M. Vranjes Milosavljevic,[14] V. Vrba,[129] M. Vreeswijk,[109] R. Vuillermet,[32] I. Vukotic,[33] P. Wagner,[23] W. Wagner,[178] H. Wahlberg,[74] S. Wahrmund,[47] J. Wakabayashi,[105] J. Walder,[75]

R. Walker,[102] W. Walkowiak,[143] V. Wallangen,[148a,148b] C. Wang,[35b] C. Wang,[36b,88] F. Wang,[176] H. Wang,[16] H. Wang,[43] J. Wang,[45] J. Wang,[152] K. Wang,[90] R. Wang,[6] S. M. Wang,[153] T. Wang,[38] W. Wang,[36a] C. Wanotayaroj,[118] A. Warburton,[90] C. P. Ward,[30] D. R. Wardrope,[81] A. Washbrook,[49] P. M. Watkins,[19] A. T. Watson,[19] M. F. Watson,[19] G. Watts,[140] S. Watts,[87] B. M. Waugh,[81] S. Webb,[86] M. S. Weber,[18] S. W. Weber,[177] S. A. Weber,[31] J. S. Webster,[6] A. R. Weidberg,[122] B. Weinert,[64] J. Weingarten,[57] C. Weiser,[51] H. Weits,[109] P. S. Wells,[32] T. Wenaus,[27] T. Wengler,[32] S. Wenig,[32] N. Wermes,[23] M. D. Werner,[67] P. Werner,[32] M. Wessels,[60a] J. Wetter,[165] K. Whalen,[118] N. L. Whallon,[140] A. M. Wharton,[75] A. White,[8] M. J. White,[1] R. White,[34b] D. Whiteson,[166] F. J. Wickens,[133] W. Wiedenmann,[176] M. Wielers,[133] C. Wiglesworth,[39] L. A. M. Wiik-Fuchs,[23] A. Wildauer,[103] F. Wilk,[87] H. G. Wilkens,[32] H. H. Williams,[124] S. Williams,[109] C. Willis,[93] S. Willocq,[89] J. A. Wilson,[19] I. Wingerter-Seez,[5] F. Winklmeier,[118] O. J. Winston,[151] B. T. Winter,[23] M. Wittgen,[145] T. M. H. Wolf,[109] R. Wolff,[88] M. W. Wolter,[42] H. Wolters,[128a,128c] S. D. Worm,[133] B. K. Wosiek,[42] J. Wotschack,[32] M. J. Woudstra,[87] K. W. Wozniak,[42] M. Wu,[58] M. Wu,[33] S. L. Wu,[176] X. Wu,[52] Y. Wu,[92] T. R. Wyatt,[87] B. M. Wynne,[49] S. Xella,[39] Z. Xi,[92] D. Xu,[35a] L. Xu,[27] B. Yabsley,[152] S. Yacoob,[147a] D. Yamaguchi,[159] Y. Yamaguchi,[120] A. Yamamoto,[69] S. Yamamoto,[157] T. Yamanaka,[157] K. Yamauchi,[105] Y. Yamazaki,[70] Z. Yan,[24] H. Yang,[36c] H. Yang,[176] Y. Yang,[153] Z. Yang,[15] W-M. Yao,[16] Y. C. Yap,[83] Y. Yasu,[69] E. Yatsenko,[5] K. H. Yau Wong,[23] J. Ye,[43] S. Ye,[27] I. Yeletskikh,[68] E. Yildirim,[86] K. Yorita,[174] R. Yoshida,[6] K. Yoshihara,[124] C. Young,[145] C. J. S. Young,[32] S. Youssef,[24] D. R. Yu,[16] J. Yu,[8] J. M. Yu,[92] J. Yu,[67] L. Yuan,[70] S. P. Y. Yuen,[23] I. Yusuff,[30,at] B. Zabinski,[42] R. Zaidan,[66] A. M. Zaitsev,[132,ae] N. Zakharchuk,[45] J. Zalieckas,[15] A. Zaman,[150] S. Zambito,[59] L. Zanello,[134a,134b] D. Zanzi,[91] C. Zeitnitz,[178] M. Zeman,[130] A. Zemla,[41a] J. C. Zeng,[169] Q. Zeng,[145] O. Zenin,[132] T. Ženiš,[146a] D. Zerwas,[119] D. Zhang,[92] F. Zhang,[176] G. Zhang,[36a,ao] H. Zhang,[35b] J. Zhang,[6] L. Zhang,[51] L. Zhang,[36a] M. Zhang,[169] R. Zhang,[23] R. Zhang,[36a,au] X. Zhang,[36b] Z. Zhang,[119] X. Zhao,[43] Y. Zhao,[36b] Z. Zhao,[36a] A. Zhemchugov,[68] J. Zhong,[122] B. Zhou,[92] C. Zhou,[176] L. Zhou,[38] L. Zhou,[43] M. Zhou,[35a] M. Zhou,[150] N. Zhou,[35c] C. G. Zhu,[36b] H. Zhu,[35a] J. Zhu,[92] Y. Zhu,[36a] X. Zhuang,[35a] K. Zhukov,[98] A. Zibell,[177] D. Zieminska,[64] N. I. Zimine,[68] C. Zimmermann,[86] S. Zimmermann,[51] Z. Zinonos,[57] M. Zinser,[86] M. Ziolkowski,[143] L. Živković,[14] G. Zobernig,[176] A. Zoccoli,[22a,22b] M. zur Nedden,[17] and L. Zwalinski[32]

(ATLAS Collaboration)

[1]*Department of Physics, University of Adelaide, Adelaide, Australia*
[2]*Physics Department, SUNY Albany, Albany, New York, USA*
[3]*Department of Physics, University of Alberta, Edmonton, Alberta, Canada*
[4a]*Department of Physics, Ankara University, Ankara, Turkey*
[4b]*Istanbul Aydin University, Istanbul, Turkey*
[4c]*Division of Physics, TOBB University of Economics and Technology, Ankara, Turkey*
[5]*LAPP, CNRS/IN2P3 and Université Savoie Mont Blanc, Annecy-le-Vieux, France*
[6]*High Energy Physics Division, Argonne National Laboratory, Argonne, Illinois, USA*
[7]*Department of Physics, University of Arizona, Tucson, Arizona, USA*
[8]*Department of Physics, The University of Texas at Arlington, Arlington, Texas, USA*
[9]*Physics Department, University of Athens, Athens, Greece*
[10]*Physics Department, National Technical University of Athens, Zografou, Greece*
[11]*Department of Physics, The University of Texas at Austin, Austin, Texas, USA*
[12]*Institute of Physics, Azerbaijan Academy of Sciences, Baku, Azerbaijan*
[13]*Institut de Física d'Altes Energies (IFAE), The Barcelona Institute of Science and Technology, Barcelona, Spain*
[14]*Institute of Physics, University of Belgrade, Belgrade, Serbia*
[15]*Department for Physics and Technology, University of Bergen, Bergen, Norway*
[16]*Physics Division, Lawrence Berkeley National Laboratory and University of California, Berkeley, California, USA*
[17]*Department of Physics, Humboldt University, Berlin, Germany*
[18]*Albert Einstein Center for Fundamental Physics and Laboratory for High Energy Physics, University of Bern, Bern, Switzerland*
[19]*School of Physics and Astronomy, University of Birmingham, Birmingham, United Kingdom*
[20a]*Department of Physics, Bogazici University, Istanbul, Turkey*
[20b]*Department of Physics Engineering, Gaziantep University, Gaziantep, Turkey*
[20c]*Istanbul Bilgi University, Faculty of Engineering and Natural Sciences, Istanbul, Turkey;*
[20d]*Bahcesehir University, Faculty of Engineering and Natural Sciences, Istanbul, Turkey*
[21]*Centro de Investigaciones, Universidad Antonio Narino, Bogota, Colombia*
[22a]*INFN Sezione di Bologna, Bologna, Italy*
[22b]*Dipartimento di Fisica e Astronomia, Università di Bologna, Bologna, Italy*
[23]*Physikalisches Institut, University of Bonn, Bonn, Germany*
[24]*Department of Physics, Boston University, Boston, Massachusetts, USA*
[25]*Department of Physics, Brandeis University, Waltham, Massachusetts, USA*
[26a]*Universidade Federal do Rio De Janeiro COPPE/EE/IF, Rio de Janeiro, Sao Paulo, Brazil*
[26b]*Electrical Circuits Department, Federal University of Juiz de Fora (UFJF), Juiz de Fora, Sao Paulo, Brazil*

[26c]*Federal University of Sao Joao del Rei (UFSJ), Sao Joao del Rei, Sao Paulo, Brazil*
[26d]*Instituto de Fisica, Universidade de Sao Paulo, Sao Paulo, Brazil*
[27]*Physics Department, Brookhaven National Laboratory, Upton, New York, USA*
[28a]*Transilvania University of Brasov, Brasov, Romania*
[28b]*National Institute of Physics and Nuclear Engineering, Bucharest, Romania*
[28c]*National Institute for Research and Development of Isotopic and Molecular Technologies, Physics Department, Cluj Napoca, Romania*
[28d]*University Politehnica Bucharest, Bucharest, Romania*
[28e]*West University in Timisoara, Timisoara, Romania*
[29]*Departamento de Física, Universidad de Buenos Aires, Buenos Aires, Argentina*
[30]*Cavendish Laboratory, University of Cambridge, Cambridge, United Kingdom*
[31]*Department of Physics, Carleton University, Ottawa, Ontario, Canada*
[32]*CERN, Geneva, Switzerland*
[33]*Enrico Fermi Institute, University of Chicago, Chicago, Illinois, USA*
[34a]*Departamento de Física, Pontificia Universidad Católica de Chile, Santiago, Chile*
[34b]*Departamento de Física, Universidad Técnica Federico Santa María, Valparaíso, Chile*
[35a]*Institute of High Energy Physics, Chinese Academy of Sciences, Beijing, China*
[35b]*Department of Physics, Nanjing University, Jiangsu, China*
[35c]*Physics Department, Tsinghua University, Beijing 100084, China*
[36a]*Department of Modern Physics, University of Science and Technology of China, Anhui, China*
[36b]*School of Physics, Shandong University, Shandong, China*
[36c]*Department of Physics and Astronomy, Shanghai Key Laboratory for Particle Physics and Cosmology, Shanghai Jiao Tong University, Shanghai; (also affiliated with PKU-CHEP), China*
[37]*Laboratoire de Physique Corpusculaire, Clermont Université and Université Blaise Pascal and CNRS/IN2P3, Clermont-Ferrand, France*
[38]*Nevis Laboratory, Columbia University, Irvington, New York, USA*
[39]*Niels Bohr Institute, University of Copenhagen, Kobenhavn, Denmark*
[40a]*INFN Gruppo Collegato di Cosenza, Laboratori Nazionali di Frascati, Italy*
[40b]*Dipartimento di Fisica, Università della Calabria, Rende, Italy*
[41a]*AGH University of Science and Technology, Faculty of Physics and Applied Computer Science, Krakow, Poland*
[41b]*Marian Smoluchowski Institute of Physics, Jagiellonian University, Krakow, Poland*
[42]*Institute of Nuclear Physics Polish Academy of Sciences, Krakow, Poland*
[43]*Physics Department, Southern Methodist University, Dallas, Texas, USA*
[44]*Physics Department, University of Texas at Dallas, Richardson, Texas, USA*
[45]*DESY, Hamburg and Zeuthen, Germany*
[46]*Lehrstuhl für Experimentelle Physik IV, Technische Universität Dortmund, Dortmund, Germany*
[47]*Institut für Kern- und Teilchenphysik, Technische Universität Dresden, Dresden, Germany*
[48]*Department of Physics, Duke University, Durham, North Carolina, USA*
[49]*SUPA - School of Physics and Astronomy, University of Edinburgh, Edinburgh, United Kingdom*
[50]*INFN Laboratori Nazionali di Frascati, Frascati, Italy*
[51]*Fakultät für Mathematik und Physik, Albert-Ludwigs-Universität, Freiburg, Germany*
[52]*Section de Physique, Université de Genève, Geneva, Switzerland*
[53a]*INFN Sezione di Genova, Genova, Italy*
[53b]*Dipartimento di Fisica, Università di Genova, Genova, Italy*
[54a]*E. Andronikashvili Institute of Physics, Iv. Javakhishvili Tbilisi State University, Tbilisi, Georgia*
[54b]*High Energy Physics Institute, Tbilisi State University, Tbilisi, Georgia*
[55]*II Physikalisches Institut, Justus-Liebig-Universität Giessen, Giessen, Germany*
[56]*SUPA - School of Physics and Astronomy, University of Glasgow, Glasgow, United Kingdom*
[57]*II Physikalisches Institut, Georg-August-Universität, Göttingen, Germany*
[58]*Laboratoire de Physique Subatomique et de Cosmologie, Université Grenoble-Alpes, CNRS/IN2P3, Grenoble, France*
[59]*Laboratory for Particle Physics and Cosmology, Harvard University, Cambridge, Massachusetts, USA*
[60a]*Kirchhoff-Institut für Physik, Ruprecht-Karls-Universität Heidelberg, Heidelberg, Germany*
[60b]*Physikalisches Institut, Ruprecht-Karls-Universität Heidelberg, Heidelberg, Germany*
[60c]*ZITI Institut für technische Informatik, Ruprecht-Karls-Universität Heidelberg, Mannheim, Germany*
[61]*Faculty of Applied Information Science, Hiroshima Institute of Technology, Hiroshima, Japan*
[62a]*Department of Physics, The Chinese University of Hong Kong, Shatin, New Territories, Hong Kong, China*
[62b]*Department of Physics, The University of Hong Kong, Hong Kong, China*
[62c]*Department of Physics and Institute for Advanced Study, The Hong Kong University of Science and Technology, Clear Water Bay, Kowloon, Hong Kong, China*
[63]*Department of Physics, National Tsing Hua University, Taiwan, Taiwan*
[64]*Department of Physics, Indiana University, Bloomington, Indiana, USA*

[65]*Institut für Astro- und Teilchenphysik, Leopold-Franzens-Universität, Innsbruck, Austria*
[66]*University of Iowa, Iowa City, Iowa, USA*
[67]*Department of Physics and Astronomy, Iowa State University, Ames, Iowa, USA*
[68]*Joint Institute for Nuclear Research, JINR Dubna, Dubna, Russia*
[69]*KEK, High Energy Accelerator Research Organization, Tsukuba, Japan*
[70]*Graduate School of Science, Kobe University, Kobe, Japan*
[71]*Faculty of Science, Kyoto University, Kyoto, Japan*
[72]*Kyoto University of Education, Kyoto, Japan*
[73]*Department of Physics, Kyushu University, Fukuoka, Japan*
[74]*Instituto de Física La Plata, Universidad Nacional de La Plata and CONICET, La Plata, Argentina*
[75]*Physics Department, Lancaster University, Lancaster, United Kingdom*
[76a]*INFN Sezione di Lecce, Lecce, Italy*
[76b]*Dipartimento di Matematica e Fisica, Università del Salento, Lecce, Italy*
[77]*Oliver Lodge Laboratory, University of Liverpool, Liverpool, United Kingdom*
[78]*Department of Physics, Jožef Stefan Institute and University of Ljubljana, Ljubljana, Slovenia*
[79]*School of Physics and Astronomy, Queen Mary University of London, London, United Kingdom*
[80]*Department of Physics, Royal Holloway University of London, Surrey, United Kingdom*
[81]*Department of Physics and Astronomy, University College London, London, United Kingdom*
[82]*Louisiana Tech University, Ruston, Louisiana, USA*
[83]*Laboratoire de Physique Nucléaire et de Hautes Energies, UPMC and Université Paris-Diderot and CNRS/IN2P3, Paris, France*
[84]*Fysiska Institutionen, Lunds Universitet, Lund, Sweden*
[85]*Departamento de Fisica Teorica C-15, Universidad Autonoma de Madrid, Madrid, Spain*
[86]*Institut für Physik, Universität Mainz, Mainz, Germany*
[87]*School of Physics and Astronomy, University of Manchester, Manchester, United Kingdom*
[88]*CPPM, Aix-Marseille Université and CNRS/IN2P3, Marseille, France*
[89]*Department of Physics, University of Massachusetts, Amherst, Massachusetts, USA*
[90]*Department of Physics, McGill University, Montreal, Quebec, Canada*
[91]*School of Physics, University of Melbourne, Victoria, Australia*
[92]*Department of Physics, The University of Michigan, Ann Arbor, Michigan, USA*
[93]*Department of Physics and Astronomy, Michigan State University, East Lansing, Michigan, USA*
[94a]*INFN Sezione di Milano, Milano, Italy*
[94b]*Dipartimento di Fisica, Università di Milano, Milano, Italy*
[95]*B. I. Stepanov Institute of Physics, National Academy of Sciences of Belarus, Minsk, Republic of Belarus*
[96]*National Scientific and Educational Centre for Particle and High Energy Physics, Minsk, Republic of Belarus*
[97]*Group of Particle Physics, University of Montreal, Montreal, Quebec, Canada*
[98]*P. N. Lebedev Physical Institute of the Russian Academy of Sciences, Moscow, Russia*
[99]*Institute for Theoretical and Experimental Physics (ITEP), Moscow, Russia*
[100]*National Research Nuclear University MEPhI, Moscow, Russia*
[101]*D. V. Skobeltsyn Institute of Nuclear Physics, M. V. Lomonosov Moscow State University, Moscow, Russia*
[102]*Fakultät für Physik, Ludwig-Maximilians-Universität München, München, Germany*
[103]*Max-Planck-Institut für Physik (Werner-Heisenberg-Institut), München, Germany*
[104]*Nagasaki Institute of Applied Science, Nagasaki, Japan*
[105]*Graduate School of Science and Kobayashi-Maskawa Institute, Nagoya University, Nagoya, Japan*
[106a]*INFN Sezione di Napoli, Napoli, Italy*
[106b]*Dipartimento di Fisica, Università di Napoli, Napoli, Italy*
[107]*Department of Physics and Astronomy, University of New Mexico, Albuquerque, New Mexico, USA*
[108]*Institute for Mathematics, Astrophysics and Particle Physics, Radboud University Nijmegen/Nikhef, Nijmegen, Netherlands*
[109]*Nikhef National Institute for Subatomic Physics and University of Amsterdam, Amsterdam, Netherlands*
[110]*Department of Physics, Northern Illinois University, DeKalb, Illinois, USA*
[111]*Budker Institute of Nuclear Physics, SB RAS, Novosibirsk, Russia*
[112]*Department of Physics, New York University, New York, New York, USA*
[113]*Ohio State University, Columbus, Ohio, USA*
[114]*Faculty of Science, Okayama University, Okayama, Japan*
[115]*Homer L. Dodge Department of Physics and Astronomy, University of Oklahoma, Norman, Oklahoma, USA*
[116]*Department of Physics, Oklahoma State University, Stillwater, Oklahoma, USA*
[117]*Palacký University, RCPTM, Olomouc, Czech Republic*
[118]*Center for High Energy Physics, University of Oregon, Eugene, Oregon, USA*
[119]*LAL, Univ. Paris-Sud, CNRS/IN2P3, Université Paris-Saclay, Orsay, France*
[120]*Graduate School of Science, Osaka University, Osaka, Japan*

[121]*Department of Physics, University of Oslo, Oslo, Norway*
[122]*Department of Physics, Oxford University, Oxford, United Kingdom*
[123a]*INFN Sezione di Pavia, Pavia, Italy*
[123b]*Dipartimento di Fisica, Università di Pavia, Pavia, Italy*
[124]*Department of Physics, University of Pennsylvania, Philadelphia, Pennsylvania, USA*
[125]*National Research Centre "Kurchatov Institute" B. P. Konstantinov Petersburg Nuclear Physics Institute, St. Petersburg, Russia*
[126a]*INFN Sezione di Pisa, Pisa, Italy*
[126b]*Dipartimento di Fisica E. Fermi, Università di Pisa, Pisa, Italy*
[127]*Department of Physics and Astronomy, University of Pittsburgh, Pittsburgh, Pennsylvania, USA*
[128a]*Laboratório de Instrumentação e Física Experimental de Partículas - LIP, Lisboa, Portugal*
[128b]*Faculdade de Ciências, Universidade de Lisboa, Lisboa, Portugal*
[128c]*Department of Physics, University of Coimbra, Coimbra, Portugal*
[128d]*Centro de Física Nuclear da Universidade de Lisboa, Lisboa, Portugal*
[128e]*Departamento de Fisica, Universidade do Minho, Braga, Portugal*
[128f]*Departamento de Fisica Teorica y del Cosmos and CAFPE, Universidad de Granada, Granada (Spain), Portugal*
[128g]*Dep Fisica and CEFITEC of Faculdade de Ciencias e Tecnologia, Universidade Nova de Lisboa, Caparica, Portugal*
[129]*Institute of Physics, Academy of Sciences of the Czech Republic, Praha, Czech Republic*
[130]*Czech Technical University in Prague, Praha, Czech Republic*
[131]*Faculty of Mathematics and Physics, Charles University in Prague, Praha, Czech Republic*
[132]*State Research Center Institute for High Energy Physics (Protvino), NRC KI, Russia*
[133]*Particle Physics Department, Rutherford Appleton Laboratory, Didcot, United Kingdom*
[134a]*INFN Sezione di Roma, Roma, Italy*
[134b]*Dipartimento di Fisica, Sapienza Università di Roma, Roma, Italy*
[135a]*INFN Sezione di Roma Tor Vergata, Roma, Italy*
[135b]*Dipartimento di Fisica, Università di Roma Tor Vergata, Roma, Italy*
[136a]*INFN Sezione di Roma Tre, Roma, Italy*
[136b]*Dipartimento di Matematica e Fisica, Università Roma Tre, Roma, Italy*
[137a]*Faculté des Sciences Ain Chock, Réseau Universitaire de Physique des Hautes Energies - Université Hassan II, Casablanca, Morocco*
[137b]*Centre National de l'Energie des Sciences Techniques Nucleaires, Rabat, Morocco*
[137c]*Faculté des Sciences Semlalia, Université Cadi Ayyad, LPHEA-Marrakech, Morocco*
[137d]*Faculté des Sciences, Université Mohamed Premier and LPTPM, Oujda, Morocco*
[137e]*Faculté des Sciences, Université Mohammed V, Rabat, Morocco*
[138]*DSM/IRFU (Institut de Recherches sur les Lois Fondamentales de l'Univers), CEA Saclay (Commissariat à l'Energie Atomique et aux Energies Alternatives), Gif-sur-Yvette, France*
[139]*Santa Cruz Institute for Particle Physics, University of California Santa Cruz, Santa Cruz, California, USA*
[140]*Department of Physics, University of Washington, Seattle, Washington, USA*
[141]*Department of Physics and Astronomy, University of Sheffield, Sheffield, United Kingdom*
[142]*Department of Physics, Shinshu University, Nagano, Japan*
[143]*Fachbereich Physik, Universität Siegen, Siegen, Germany*
[144]*Department of Physics, Simon Fraser University, Burnaby, British Columbia, Canada*
[145]*SLAC National Accelerator Laboratory, Stanford, California, USA*
[146a]*Faculty of Mathematics, Physics & Informatics, Comenius University, Bratislava, Slovak Republic*
[146b]*Department of Subnuclear Physics, Institute of Experimental Physics of the Slovak Academy of Sciences, Kosice, Slovak Republic*
[147a]*Department of Physics, University of Cape Town, Cape Town, South Africa*
[147b]*Department of Physics, University of Johannesburg, Johannesburg, South Africa*
[147c]*School of Physics, University of the Witwatersrand, Johannesburg, South Africa*
[148a]*Department of Physics, Stockholm University, Stockholm, Sweden*
[148b]*The Oskar Klein Centre, Stockholm, Sweden*
[149]*Physics Department, Royal Institute of Technology, Stockholm, Sweden*
[150]*Departments of Physics & Astronomy and Chemistry, Stony Brook University, Stony Brook New York, USA*
[151]*Department of Physics and Astronomy, University of Sussex, Brighton, United Kingdom*
[152]*School of Physics, University of Sydney, Sydney, Australia*
[153]*Institute of Physics, Academia Sinica, Taipei, Taiwan*
[154]*Department of Physics, Technion: Israel Institute of Technology, Haifa, Israel*
[155]*Raymond and Beverly Sackler School of Physics and Astronomy, Tel Aviv University, Tel Aviv, Israel*
[156]*Department of Physics, Aristotle University of Thessaloniki, Thessaloniki, Greece*
[157]*International Center for Elementary Particle Physics and Department of Physics, The University of Tokyo, Tokyo, Japan*
[158]*Graduate School of Science and Technology, Tokyo Metropolitan University, Tokyo, Japan*
[159]*Department of Physics, Tokyo Institute of Technology, Tokyo, Japan*

[160]*Tomsk State University, Tomsk, Russia*
[161]*Department of Physics, University of Toronto, Toronto, Ontario, Canada*
[162a]*INFN-TIFPA, Trento, Italy*
[162b]*University of Trento, Trento, Italy*
[163a]*TRIUMF, Vancouver, British Columbia, Ontario, Canada*
[163b]*Department of Physics and Astronomy, York University, Toronto, Ontario, Canada*
[164]*Faculty of Pure and Applied Sciences, and Center for Integrated Research in Fundamental Science and Engineering, University of Tsukuba, Tsukuba, Japan*
[165]*Department of Physics and Astronomy, Tufts University, Massachusetts, USA*
[166]*Department of Physics and Astronomy, University of California Irvine, Irvine, California, USA*
[167a]*INFN Gruppo Collegato di Udine, Sezione di Trieste, Udine, Italy*
[167b]*ICTP, Trieste, Italy*
[167c]*Dipartimento di Chimica, Fisica e Ambiente, Università di Udine, Udine, Italy*
[168]*Department of Physics and Astronomy, University of Uppsala, Uppsala, Sweden*
[169]*Department of Physics, University of Illinois, Urbana, Illinois, USA*
[170]*Instituto de Fisica Corpuscular (IFIC) and Departamento de Fisica Atomica, Molecular y Nuclear and Departamento de Ingeniería Electrónica and Instituto de Microelectrónica de Barcelona (IMB-CNM), University of Valencia and CSIC, Valencia, Spain*
[171]*Department of Physics, University of British Columbia, Vancouver, British Columbia, Canada*
[172]*Department of Physics and Astronomy, University of Victoria, Victoria, British Columbia, Canada*
[173]*Department of Physics, University of Warwick, Coventry, United Kingdom*
[174]*Waseda University, Tokyo, Japan*
[175]*Department of Particle Physics, The Weizmann Institute of Science, Rehovot, Israel*
[176]*Department of Physics, University of Wisconsin, Madison, Wisconsin, USA*
[177]*Fakultät für Physik und Astronomie, Julius-Maximilians-Universität, Würzburg, Germany*
[178]*Fakultät für Mathematik und Naturwissenschaften, Fachgruppe Physik, Bergische Universität Wuppertal, Wuppertal, Germany*
[179]*Department of Physics, Yale University, New Haven, Connecticut, USA*
[180]*Yerevan Physics Institute, Yerevan, Armenia*
[181]*Centre de Calcul de l'Institut National de Physique Nucléaire et de Physique des Particules (IN2P3), Villeurbanne, France*

[a]Also at Department of Physics, King's College London, London, United Kingdom.
[b]Also at Institute of Physics, Azerbaijan Academy of Sciences, Baku, Azerbaijan.
[c]Also at Novosibirsk State University, Novosibirsk, Russia.
[d]Also at TRIUMF, Vancouver, BC, Canada.
[e]Also at Department of Physics & Astronomy, University of Louisville, Louisville, KY, USA.
[f]Also at Physics Department, An-Najah National University, Nablus, Palestine.
[g]Also at Department of Physics, California State University, Fresno, CA, USA.
[h]Also at Department of Physics, University of Fribourg, Fribourg, Switzerland.
[i]Also at Departament de Fisica de la Universitat Autonoma de Barcelona, Barcelona, Spain.
[j]Also at Departamento de Fisica e Astronomia, Faculdade de Ciencias, Universidade do Porto, Portugal.
[k]Also at Tomsk State University, Tomsk, Russia.
[l]Also at Universita di Napoli Parthenope, Napoli, Italy.
[m]Also at Institute of Particle Physics (IPP), Victoria, BC, Canada.
[n]Also at National Institute of Physics and Nuclear Engineering, Bucharest, Romania.
[o]Also at Department of Physics, St. Petersburg State Polytechnical University, St. Petersburg, Russia.
[p]Also at Department of Physics, The University of Michigan, Ann Arbor, MI, USA.
[q]Also at Centre for High Performance Computing, CSIR Campus, Rosebank, Cape Town, South Africa.
[r]Also at Louisiana Tech University, Ruston, LA, USA.
[s]Also at Institucio Catalana de Recerca i Estudis Avancats, ICREA, Barcelona, Spain.
[t]Also at Graduate School of Science, Osaka University, Osaka, Japan.
[u]Also at Institute for Mathematics, Astrophysics and Particle Physics, Radboud University Nijmegen/Nikhef, Nijmegen, Netherlands.
[v]Also at Department of Physics, The University of Texas at Austin, Austin, TX, USA.
[w]Also at Institute of Theoretical Physics, Ilia State University, Tbilisi, Georgia.
[x]Also at CERN, Geneva, Switzerland.
[y]Also at Georgian Technical University (GTU),Tbilisi, Georgia.
[z]Also at Ochadai Academic Production, Ochanomizu University, Tokyo, Japan.
[aa]Also at Manhattan College, New York, NY, USA.
[ab]Also at Academia Sinica Grid Computing, Institute of Physics, Academia Sinica, Taipei, Taiwan.
[ac]Also at School of Physics, Shandong University, Shandong, China.
[ad]Also at Department of Physics, California State University, Sacramento, CA, USA.
[ae]Also at Moscow Institute of Physics and Technology State University, Dolgoprudny, Russia.

[af]Also at Section de Physique, Université de Genève, Geneva, Switzerland.
[ag]Also at Eotvos Lorand University, Budapest, Hungary.
[ah]Also at Departments of Physics & Astronomy and Chemistry, Stony Brook University, Stony Brook, NY, USA.
[ai]Also at International School for Advanced Studies (SISSA), Trieste, Italy.
[aj]Also at Department of Physics and Astronomy, University of South Carolina, Columbia SC, USA.
[ak]Also at Institut de Física d'Altes Energies (IFAE), The Barcelona Institute of Science and Technology, Barcelona, Spain.
[al]Also at School of Physics and Engineering, Sun Yat-sen University, Guangzhou, China.
[am]Also at Institute for Nuclear Research and Nuclear Energy (INRNE) of the Bulgarian Academy of Sciences, Sofia, Bulgaria.
[an]Also at Faculty of Physics, M.V.Lomonosov Moscow State University, Moscow, Russia.
[ao]Also at Institute of Physics, Academia Sinica, Taipei, Taiwan.
[ap]Also at National Research Nuclear University MEPhI, Moscow, Russia.
[aq]Also at Department of Physics, Stanford University, Stanford, CA, USA.
[ar]Also at Institute for Particle and Nuclear Physics, Wigner Research Centre for Physics, Budapest, Hungary.
[as]Also at Flensburg University of Applied Sciences, Flensburg, Germany.
[at]Also at University of Malaya, Department of Physics, Kuala Lumpur, Malaysia.
[au]Also at CPPM, Aix-Marseille Université and CNRS/IN2P3, Marseille, France.
[*]Deceased.